H_∞ Performance Limitations for Problems with Sensor Time Delays

by

Darrell Gaudette

A thesis
presented to the University of Waterloo
in fulfillment of the
thesis requirement for the degree of
Master of Applied Science
in
Electrical and Computer Engineering

Waterloo, Ontario, Canada, 2008

I hereby declare that I am the sole author of this thesis. This is a true copy of the thesis, including any required final revisions, as accepted by my examiners.

I understand that my thesis may be made electronically available to the public.

Abstract

Motivated by ongoing research into automating radiotherapy, this thesis is concerned with linear feedback control and estimation problems where only a delayed output signal is measurable. Various discrete-time performance limitations are derived using tools from model-matching theory as well as the early H_∞ literature. It is shown that there exist performance limitations for both one-degree-of-freedom control and estimation problems, but the nature of the limitations differs depending on whether the plant is stable or unstable. Some continuous-time performance limitations are also found, with more complete results in the case where the plant is unstable. Extensions of the various performance limitation to two-degree-of-freedom control are also studied.

Acknowledgements

I would like to thank my supervisor, Prof. Dan Davison, for all his help. I would also like to thank, Prof. Daniel Miller and Prof. David Wang for their comments.

Dedication

To my father, for all he did for me. I will never forget you.

Contents

List of Tables

List of Figures

Chapter 1

Introduction

1.1 Motivation: A Radiotherapy Problem

This work was motivated by an ongoing research project into automating external beam radiotherapy treatment. External beam radiotherapy is the most common form of radiotherapy, and is used to treat many forms of cancer. Currently, the treatment is carried out by applying a beam of high-energy radiation onto the tumour from various angles over numerous treatment sessions, based on a complicated treatment planning procedure. External beam radiotherapy is carried out on an adjustable machine, as shown in Figures 1.1 and 1.2. The patient is placed on the table, and the radiation is emitted from within the adjustable arm. A multi-leaf collimator, as shown in Figure 1.3, is placed between the radiation source and the patient, inside the arm of the radiotherapy machine. The collimator consists of two sets of heavy metal plates (or leaves), placed on each side, that block the radiation from passing. By adjusting the position of these leaves, an opening is created in the middle through which the radiation is allowed to pass. To deliver treatment, the leaves are adjusted to create the shape required. The interested reader is encouraged to see [25] and [22] for further details on the physics behind radiotherapy.

For various reasons (patient movement/shifting, internal tumour movement, breathing, positioning bias), a safety margin around the tumour must be employed to ensure the tumour receives the prescribed radiation dose. Unfortunately, this safety margin leads to radiation hitting healthy tissue, which can lead to side effects, and is detrimental to the cancer treatment. Minimizing the amount of healthy tissue irradiated during radiotherapy treatment is a useful goal, and one that researchers are working on today.

The idea of "automating" radiotherapy is simple from a theoretical control perspective. If one can locate and track the tumour, then using a simple feedback control scheme, the radiation beam can be moved via the multi-leaf collimator to the current tumour location. There are several potential benefits of automating radiotherapy:

- Reduction of patient setup time due to the ability to correct an initial position bias.

Figure 1.1: A picture of an external beam radiotherapy machine [19].

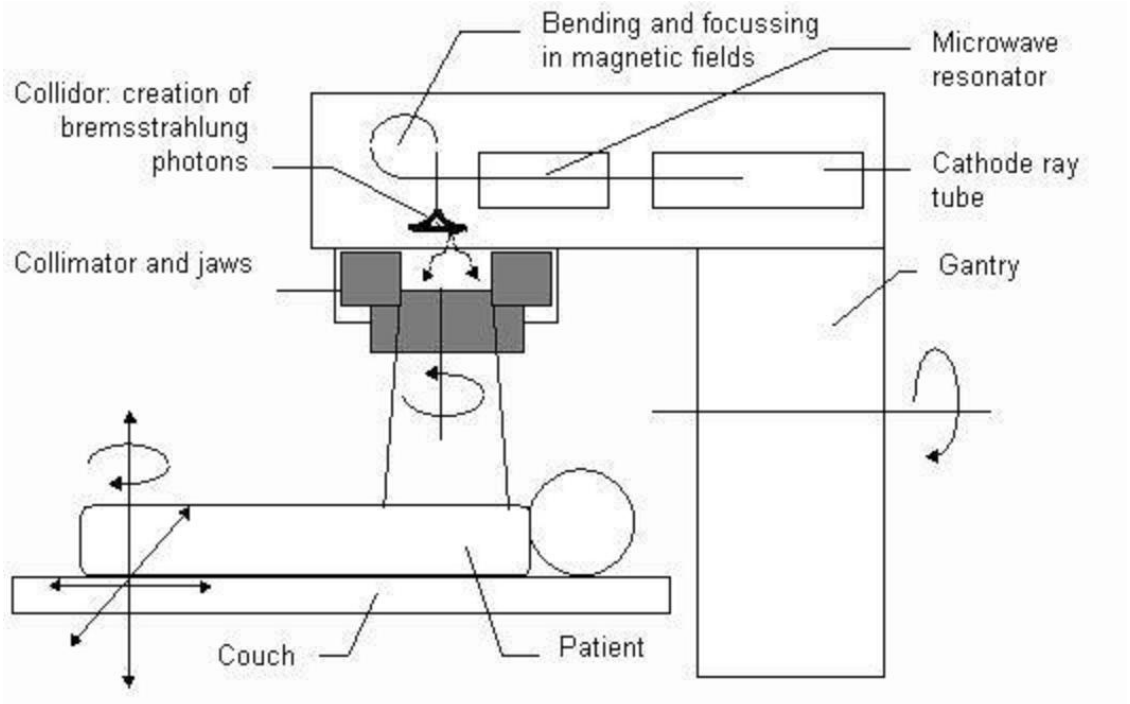

Figure 1.2: A few key components of a radiotherapy machine [31].

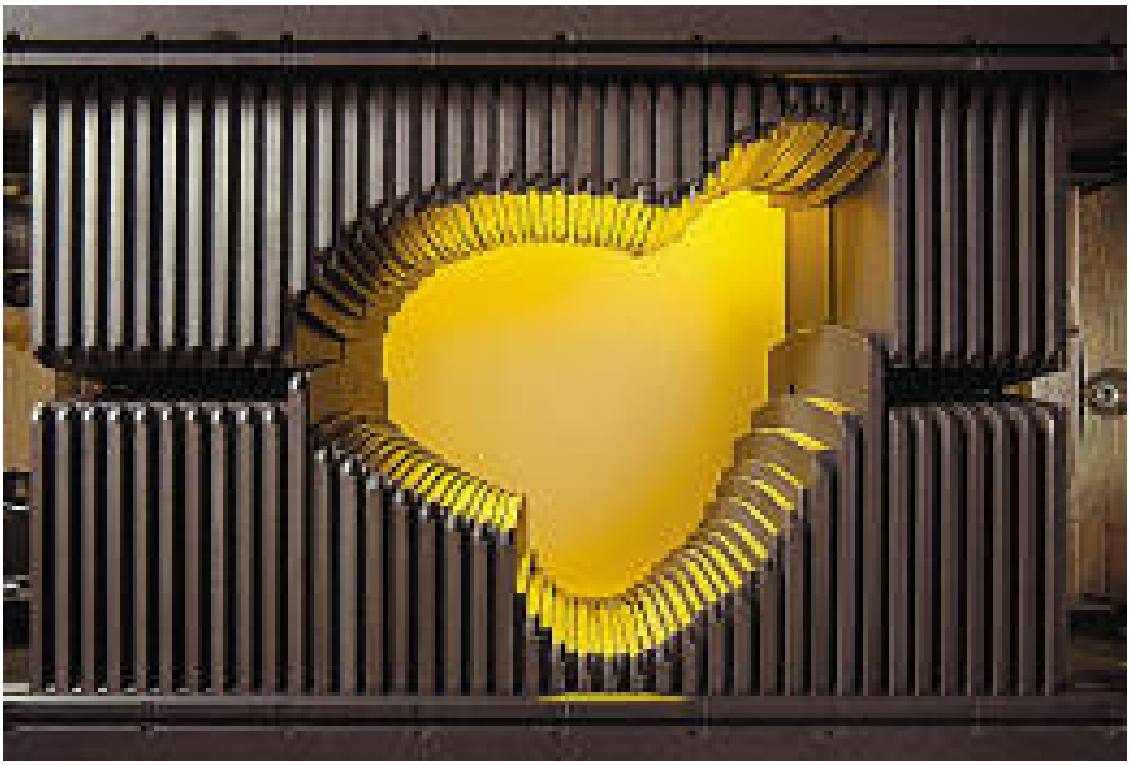

Figure 1.3: A picture of a multi-leaf collimator [20].

- The ability to treat tumours in areas that are highly sensitive to movement (for example, a lung tumour).
- Reduction of the amount of healthy tissue exposed to radiation if the patient shifts position.
- The ability to create and deliver more complicated dose profiles from a single beam position. This can also lead to shorter treatment times due to a possible reduction in the required number of beam positions (which takes time to set up).

Unfortunately, implementing this sort of automatic feedback control is challenging. Just locating the exact position of the tumour while it is undergoing radiation treatment is an extremely difficult problem. However, previous researchers [7, 8] did arrive at a control scheme for the problem, as depicted in Figure 1.4. Their proposed control scheme can be divided into two basic components: an estimation block, where the tumour location is determined, and a feedback control block, where the beam location is determined and implemented via the multi-leaf collimator. These blocks are described in more detail later on.

An important aspect of the design in Figure 1.4 are the two time-delay blocks. Due to the horrible image quality created by the powerful radiotherapy beam, various advanced image processing algorithms need to be used. These algorithms introduce a time delay of approximately $0.5s$ after the output but before the feedback, and therefore act as a

"sensor time delay". In this thesis, we characterize the effect that a sensor time delay has on performance for both the estimation problem at the top of Figure 1.4 and the control problem at the bottom of that same figure.

1.2 What are Performance Limitations?

The best way to illustrate the impact and usefulness of a performance limitations is with a simple example. The Pointlessly Unstable Elevator Co. wants to be the first company to market unstable elevators. They propose using the simple one-degree-of-freedom (1-DOF) control setup depicted in Figure 1.5, with the plant, P, having stable dynamics except for one real open right half plane (ORHP) pole, p, at $s = 0.5$. The plant also has an integrator, resulting in zero steady-state error for a unit step input under a stabilizing feedback controller. Assume there is an overall system requirement that the rise time, t_r, be 2 seconds. The Pointlessly Unstable Elevator Co. is wondering what happens to the overshoot, y_{os}, for their elevator.

Figure 1.6 shows a typical step response for a closed-loop stable system. For our example, particular attention should be paid to the overshoot and rise time as depicted in Figure 1.6. Definitions based on Figure 1.6 are as follows: the absolute overshoot is

$$y_{os} \equiv \sup_t \{y(t) - 1\}, \tag{1.1}$$

the relative overshoot is

$$y_{osrel} \equiv y_{os} \cdot 100\%, \tag{1.2}$$

and the rise time is (note that this is a non-standard definition of rise time)

$$t_r \equiv \sup_\delta \left\{ \delta : y(t) \leq \frac{t}{\delta} \ \ \forall t \in [0, \delta] \right\}. \tag{1.3}$$

Then, from [28], for any closed-loop stable system, the following relationship between rise time, the location of a single ORHP pole, and overshoot holds:

$$y_{os} \geq \frac{p \cdot t_r}{2}. \tag{1.4}$$

It should be noted that (1.4) is not a tight bound, but it can still provide useful information to a designer. Substituting in the numbers for the example, it can quickly be determined from (1.4) that the overshoot must be greater than 50%! If (1.4) was used at an early stage of the design, the designer would quickly realize that a rise time requirement of 2 seconds is practically incompatible with a plant that has an ORHP pole at $s = 0.5$. The designer would then be able to do something, for example, install a better actuator to allow for a much faster rise time or move the ORHP pole further left, in order to obtain reasonable overshoot performance. This is one use of a performance limitation since physical changes to the system, made to improve performance, are still possible. However, performance limitations can also be used at a later stage of design, when plant

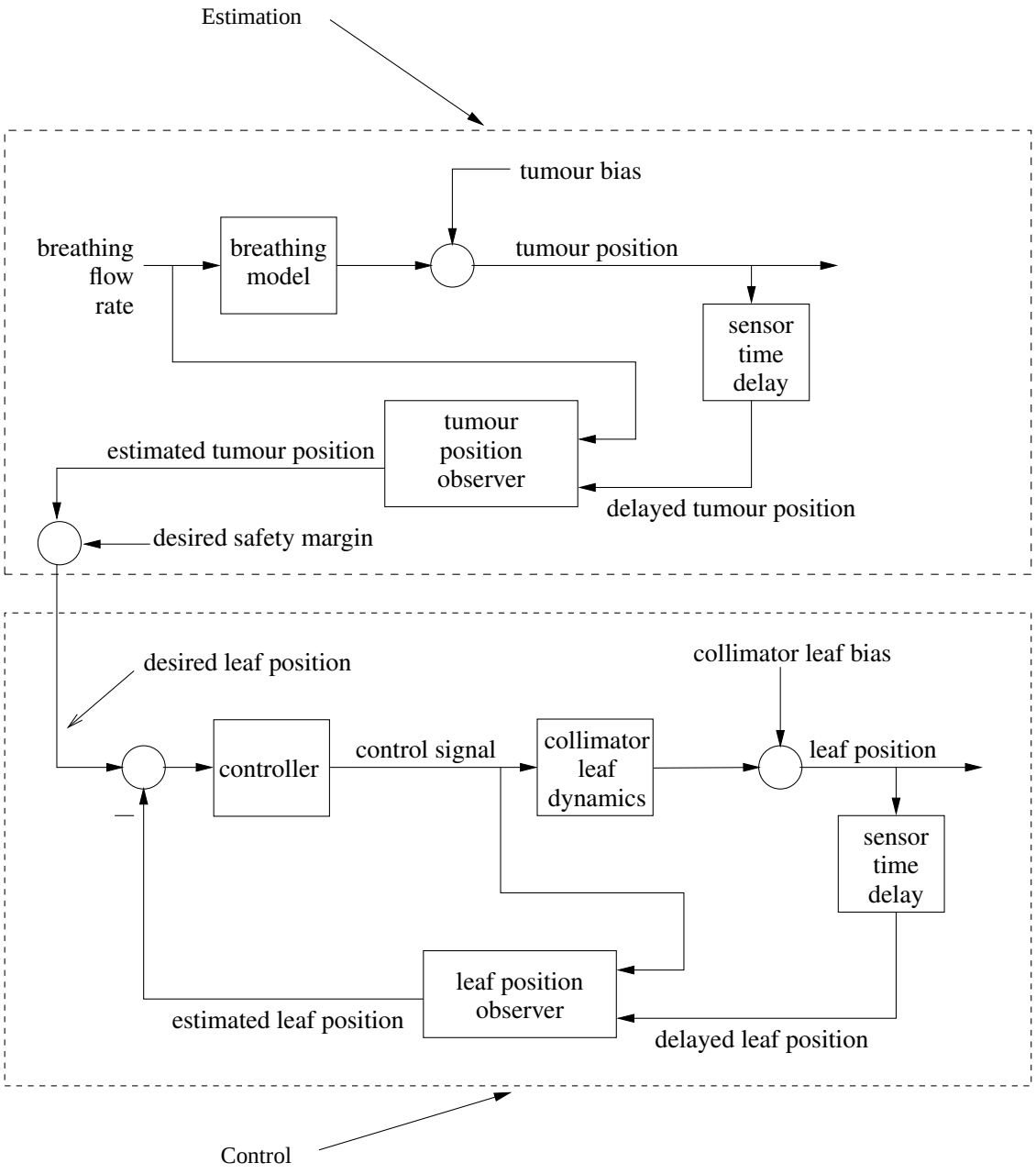

Figure 1.4: The essential components of the radiotherapy tumor-tracking control scheme proposed in [7, 8].

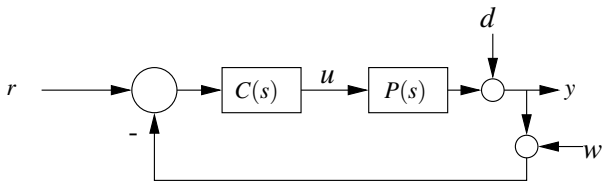

Figure 1.5: A 1-DOF feedback setup.

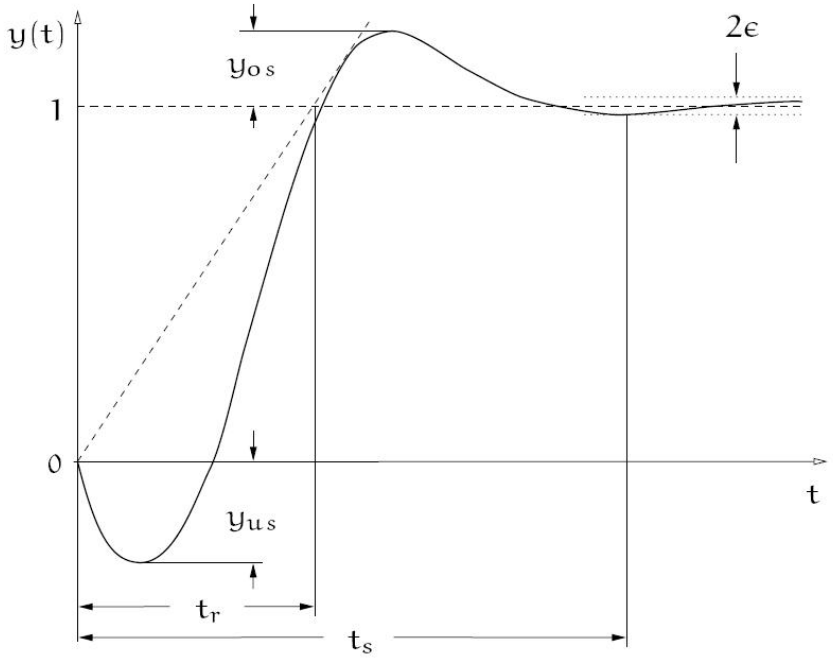

Figure 1.6: A step response showing the overshoot, undershoot, and rise time definitions, from [28].

modifications are not possible. For this example, using (1.4), the controller designer would quickly understand that no matter what he tries to do, his system is going to have far too much overshoot for an elevator; the designer would then have to ponder the use of a two-degree-of-freedom (2-DOF) and/or a nonlinear controller.

It should also be noted that a more complicated relationship for a closed-loop stable system can be found, also from [28]:

$$y_{os} \geq \frac{(p \cdot t_r - 1) \cdot e^{p \cdot t_r} + 1}{p \cdot t_r}. \tag{1.5}$$

This is also not a tight bound, but it is tighter than (1.4). Substituting the numbers for our example into (1.5) proves that the overshoot must be greater than 100%! While (1.4) suggested that the required design specifications produce significant overshoot, (1.5) shows that the required specs leads to at least twice as much overshoot. So, why would someone use (1.4) over (1.5)? The answer lies in the simplicty of (1.4), which allows for a simple

hand calculation, creating a simple-to-use-and-remember "rule of thumb". On the other hand, (1.5), while still manageable, is more difficult to use and remember than (1.4). For the example used, knowledge that the overshoot must be at least 50%, as obtained from (1.4), is probably enough for the designer to rethink his physical design.

The above example demonstrates the dueling requirements of performance limitations. On one hand, it is very desirable to have simple relationships that produce easy-to-use rules. On the other hand, it is also desirable to have tight bounds to provide more precise results. These two requirements, like many other aspects of control, often involve trade offs, either towards simplicity or tightness. The example also demonstrates the desirability of using performance limitations at an early stage of design. If the Pointlessly Unstable Elevator Co. control engineer were simply handed the plant, as designed by the mechanical engineering department, then the only use of (1.4)-(1.5) is to let the control engineer explain to his boss why the elevator has over 100% overshoot. When the pointlessly unstable elevator, starting at the first floor, goes all the way up to the third floor before returning to the second floor, the control engineer will have proof justifying that this is the best possible overshoot performance for the given elevator. However, had the Pointlessly Unstable Elevator Co. used performance limitations at an earlier stage, they could potentially have redesigned the elevator, perhaps moving the pole further to the left, say to $s = 0.005$ instead of $s = 0.5$. Then the Pointlessly Unstable Elevator Co. elevator could potentially have negligible overshoot.

There are other well-known performance limitations. For example, given a plant with one real ORHP pole at $s = p$ and one real ORHP zero at $s = q$ (with $p < q$), and using (1.1) as the definition of overshoot, then, from [28], any stabilizing controller results in a closed-loop system that satisfies

$$y_{os} \geq \frac{p}{q-p}. \tag{1.6}$$

Similarly, and also from [28], if $q > p$, and defining the absolute undershoot, y_{us}, as shown in Figure 1.6 to be:

$$y_{us} \equiv \sup_t \{-y(t)\}, \tag{1.7}$$

then for any stabilizing controller, the closed-loop system satisfies

$$y_{us} \geq \frac{q}{p-q}. \tag{1.8}$$

Performance limitations can also be applied in the frequency domain. Define the sensitivity function, $S(j\omega)$, for the feedback control setup shown in Figure 1.5 as,

$$S(j\omega) \equiv \frac{1}{1+P(j\omega)C(j\omega)}. \tag{1.9}$$

Then, as first developed by Bode in [2], but taken from [17], assuming that $L(s) \equiv P(s)C(s)$ has relative degree of at least two and that the closed-loop system is stable,

$$\int_0^\infty \ln|S(j\omega)|d\omega \geq 0, \tag{1.10}$$

and, moreover, given a plant with ORHP poles at $\{p_1, p_2, ..., p_{n_p}\}$,

$$\frac{1}{\pi}\int_0^\infty \ln|S(j\omega)|d\omega \geq \sum_{i=1}^{n_p} p_i. \tag{1.11}$$

These two results, (1.10) and (1.11), are the basis behind the well-known "Bode waterbed effect" [17, 28]: if $|S(j\omega)|$ is made small ($|S(j\omega)| < 1$) over a certain frequency range, then it must necessarily become large ($|S(j\omega)| > 1$) over some other frequency range. Since $|S(j\omega)|$ also encompasses disturbance rejection and sensitivity to plant perturbations (as is shown in the next section), it is desirable to keep this small ($|S(j\omega)| << 1$). However, (1.10) ensures that for any plant, keeping the sensitivity function small for all frequencies is impossible, and some sort of design tradeoff must occur. For an unstable plant, (1.11) simply makes the "Bode waterbed effect" more pronounced.

This section provided a few examples of various forms of performance limitations, but many more exist. An interested reader is encouraged to read [17] for a quick survey of numerous results. For a more in-depth treatment, [28] is recommended, as it has many more results along with proofs. Also of note is that [28] tackles performance limitations for estimation problems as well as for feedback control problems. This thesis deals with performance limitations associated with a sensor time delay for both feedback control and estimation problems. The next section briefly introduces these two problems, as well as the performance metrics and tools that are used in the remainder of this thesis.

1.3 Basic Problem Setup

In this section we define the norms and performance metrics that are used in the remainder of this thesis. First, an introduction and definition of the H_∞-norm is presented, followed by formal definitions of the various performance metrics that are used in subsequent chapters. Finally, three important questions are posed, with answers provided throughout Chapters 2-5.

What is the H_∞ norm and why is it useful? Answering the first part of the question first, given a continuous-time single-input single-output (SISO), linear, time-invariant, causal, proper and rational transfer function G, its H_∞ norm, denoted $\|G\|_\infty$, is defined as [10, 16]:

$$\|G\|_\infty \equiv \sup_\omega |G(j\omega)|. \tag{1.12}$$

Similarly, given a discrete-time SISO, linear, time-invariant, causal, proper and rational transfer function F, its H_∞ norm, denoted $\|F\|_\infty$, is defined as [10, 16]:

$$\|F\|_\infty \equiv \sup_\theta |F(e^{j\theta})|. \tag{1.13}$$

In essence, the H_∞ norm describes the largest gain of a system over all frequencies. Given a Bode plot of G, for example the plot shown in Figure 1.7, then $\|G\|_\infty$ is the highest peak on the plot.

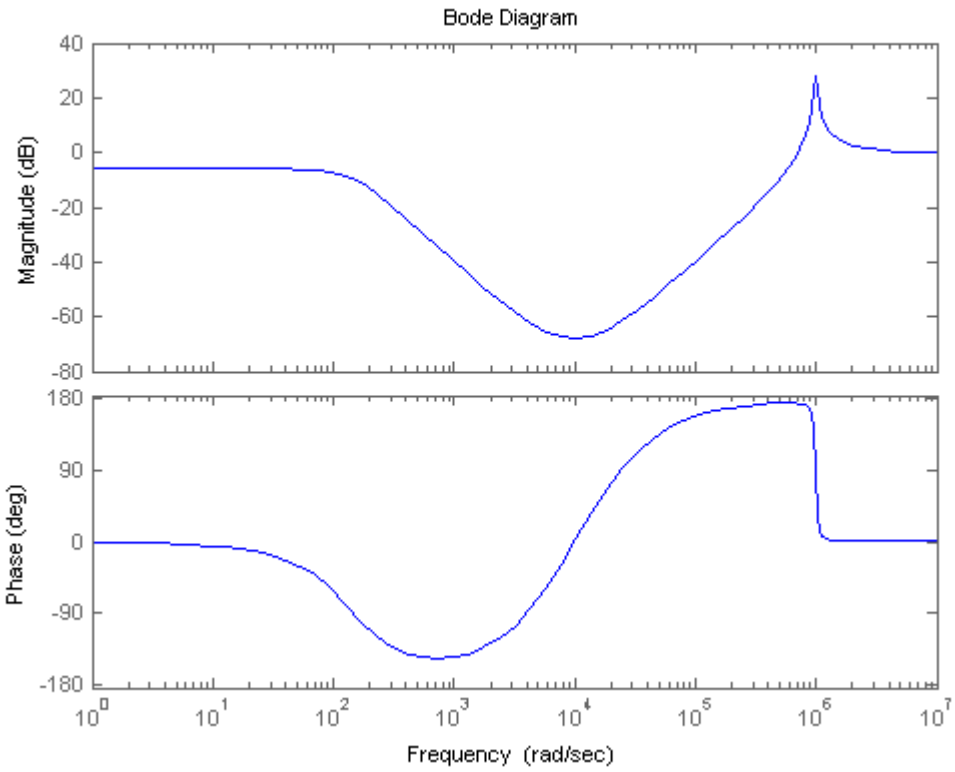

Figure 1.7: A Bode plot of T_{dy} for the plant $P(s) = \frac{(0.01s+1)^2}{(0.0001s+1)^4}$ with $C(s) = 1$.

It is sometimes convenient to switch between the continuous-time and discrete-time domains. As a result, the well-known bilinear transformation, [27],

$$z = \frac{1+s}{1-s}, \tag{1.14}$$

is used throughout this thesis. Equation (1.14) is a conformal mapping between the continuous-time s-plane and the discrete-time z-plane. This mapping maps the open right-half-plane (ORHP) to outside the unit disk, and the open left-half-plane (OLHP) to inside the unit disk, thereby preserving the stability of the system.

Due to a slight difference in the computation of a discrete-time norm compared to a continuous-time norm, the following convention is used. In most circumstances, the context should provide clarity as to whether a discrete-time or continuous-time norm is required, and no extra notation will be used. However, occasionally a distinction is noted between the continuous-time and discrete-time norm for added clarity by placing a superscript DT (for discrete-time) or CT (for continuous-time) on the unclear norm. As an example, given a continuous-time plant, $G(s)$, and using the bilinear transformation (1.14) to produce a discrete-time plant, $\hat{G}[z]$, the following notation for their respective norms will be used when required for additional clarity: $\|G\|_\infty^{CT}$ and $\|\hat{G}\|_\infty^{DT}$

Before answering why the H_∞-norm is useful for measuring system performance, a quick introduction of the performance metrics used throughout the remainder of this thesis is in order. A performance metric is an attempt to quantify system performance with a computable number. For this thesis, each performance metric is a weighted H_∞-norm of some relevant transfer function. This thesis primarily focuses on four transfer functions, which have slightly different forms between the control setup shown in Figure 1.8 (where r is the input, d is a disturbance, y is the output, w is the noise, y_m is the delayed output, C is the controller, P is the plant, and F is the delay), and the estimation problem shown in Figure 1.9 (where u is the input, d is the disturbance, y is the output, w is the noise, y_d is the delayed output, $\hat{y}$ is the estimated output, P is the plant, F is the delay, and G_1 and G_2 combine to form the estimator). For the presentation of these results, a discrete-time plant will be assumed. For continuous-time results, replace the discrete-time complex variable z with the continuous-time complex variable s. For the feedback control setup in Figure 1.8, the four aspects of performance and corresponding transfer functions are:

- the *tracking* of the system represented as

$$T_{re}[z] \equiv \frac{E[z]}{R[z]} \tag{1.15}$$

  where $e \equiv r - y$

- the *sensitivity with respect to perturbations in P* of the control system, represented as

$$S[z] \equiv \frac{\partial T_{ry}[z]}{\partial P[z]} \frac{P[z]}{T_{ry}[z]} \tag{1.16}$$

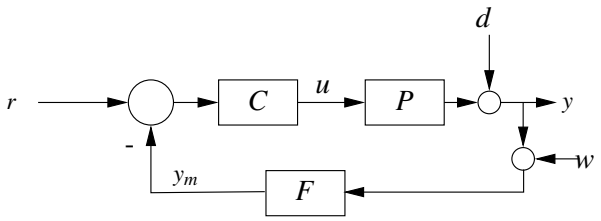

Figure 1.8: A block diagram of the feedback control problem with a sensor time delay.

- the *disturbance rejection* of the system represented as

$$T_{dy}[z] \equiv \frac{Y[z]}{D[z]} \tag{1.17}$$

- and the *sensor noise rejection* of the system represented as

$$T_{we}[z] \equiv \frac{E[z]}{W[z]}. \tag{1.18}$$

For the estimation problem of Figure 1.9, the tracking performance is dropped (for reasons explained in Chapter 3). The three transfer functions of interest are then:

- the *sensitivity of the estimator with respect to perturbations in P* represented as

$$S[z] \equiv \frac{\partial T_{y\hat{y}}[z]}{\partial P[z]} \frac{P[z]}{T_{y\hat{y}}[z]} \tag{1.19}$$

- the *disturbance rejection of the estimator* represented as

$$T_{de}[z] \equiv \frac{E[z]}{D[z]} \tag{1.20}$$

  (where $e \equiv \hat{y} - y$), and

- the *sensor noise rejection of the estimator* represented as

$$T_{we}[z] \equiv \frac{E[z]}{W[z]}. \tag{1.21}$$

It should also be noted that the notational overlap between the feedback control setup of Figure 1.8 and the estimation problem of Figure 1.9 should not be a problem. The context of the chapter or theorem should make it clear what problem is being addressed.

Now, why is the H_∞-norm a useful measure of performance? It is in essence a measure of the worst performance of a system. Given a Bode plot of a transfer function, the H_∞-norm is the highest gain achieved on the Bode plot. But that in and of itself is not necessarily significant, as the "peak" could be outside of relevant frequencies. For example, using the setup of Figure 1.8 and given a plant, $P(s) = \frac{(0.01s+1)^2}{(0.0001s+1)^4}$, and controller,

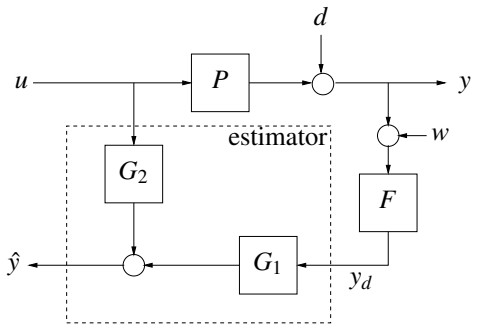

Figure 1.9: A block diagram of the estimation problem with a sensor time delay.

$C(s) = 1$, what is $\|T_{dy}\|_\infty$? Figure 1.7 shows the Bode plot of T_{dy}, and from that $\|T_{dy}\|_\infty$ is 25.125 (28 dB). At first glance, this makes it appear that $\|T_{dy}(s)\|_\infty$ is quite poor and that the system has poor disturbance rejection properties. However, if the maximum frequency of the disturbance, d, was known to be 10 rad/s, then the H_∞ norm alone is not telling the entire story since the peak occurs at a very high frequency.

For this reason, instead of looking at solely the H_∞-norm, for example, $\|T_{dy}\|_\infty$, it is better to look at a weighted H_∞-norm. For the disturbance example above, a weighting function would be employed to weight frequencies below 10 rad/s heavily, while virtually ignoring frequencies above 10 rad/s. Letting $W(s) = \frac{1}{1+0.1s}$, and plotting the Bode plot of $W(s)T_{dy}(s)$, as shown in Figure 1.10, a different picture emerges. Instead of a large peak at very high frequency, the highest point is now at a low frequency, but with a much lower gain of 0.5 (-6dB). The norm of interest, $\|WT_{dy}\|_\infty$ now makes more sense than before, as it is providing more useful information. The fact that $T_{dy}(s)$ has a large peak at high frequencies does not matter for this particular example, and the weighting function, $W(s)$, filters that extraneous information out. The weighted H_∞-norm is thus a useful norm for system performance. It can be shifted to weight any frequency range that is relevant to a particular problem, and it can thus quantify the worst performance of a system at frequencies of interest, a very useful piece of information to know. For simplicity, $\|W\|_\infty = 1$ is normally used to prevent artificial scaling of the result by the weighting function and to allow for easier comparison of results. This assumption is not strictly required, but is made throughout this thesis.

The performance metrics that are used throughout this thesis are presented in the following table. The feedback control column refers to the problem shown in Figure 1.8, and the estimation column refers to the problem shown in Figure 1.9.

	Feedback Control	Estimation
Weighted tracking	$\|W_1 T_{re}\|_\infty$	
Weighted sensitivity to perturbations of P	$\|W_2 S\|_\infty$	$\|W_5 S\|_\infty$
Weighted disturbance rejection	$\|W_3 T_{dy}\|_\infty$	$\|W_6 T_{de}\|_\infty$
Weighted noise rejection	$\|W_4 T_{we}\|_\infty$	$\|W_7 T_{we}\|_\infty$

Table 1.1: The various performance metrics used.

In Table 1.1, W_1, W_2, W_3, W_4, W_5, W_6 and W_7 are stable, minimum phase, proper

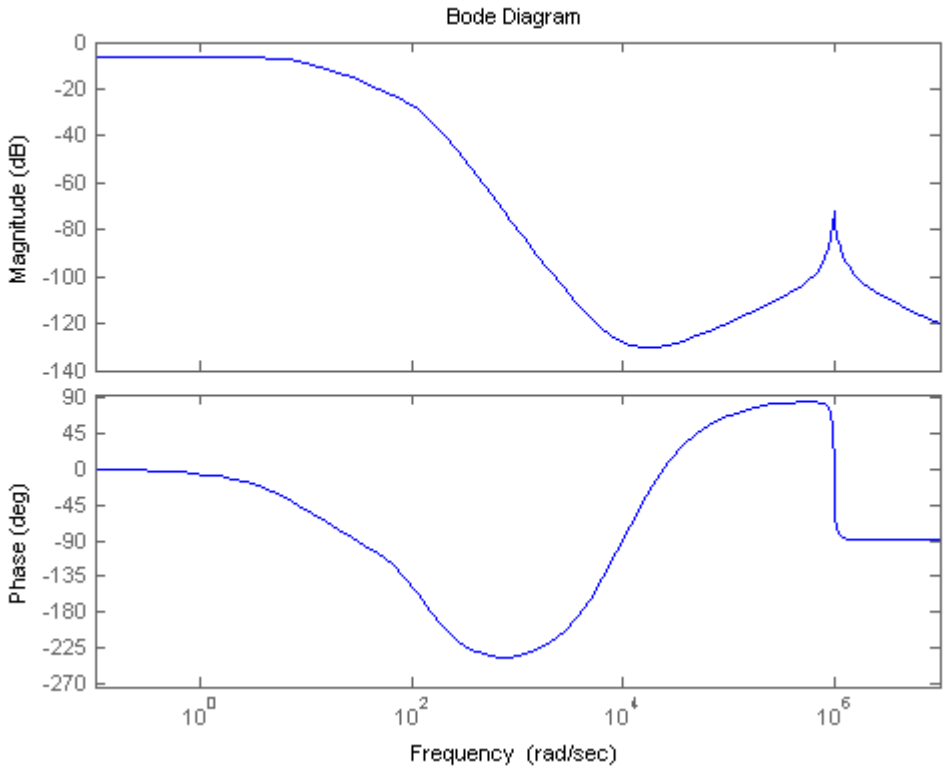

Figure 1.10: A Bode plot of WT_{dy} for the same P and C as Figure 1.7 with $W(s) = \frac{1}{1+0.1s}$.

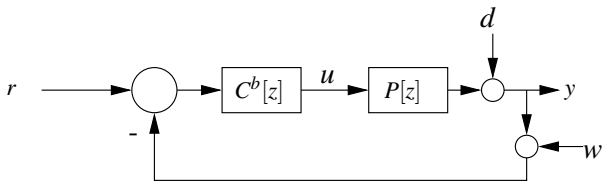

Figure 1.11: A 1-DOF, discrete-time feedback setup with no sensor time delay (C^b will be used as a "baseline" controller in future chapters).

(biproper in the discrete-time case) weighting functions with $\|W_i\|_\infty = 1,\ i = 1,\ldots,7$. It should be noted that the assumption that the weighting functions be stable and minimum phase can be made without a loss of generality. Since only the magnitude of the weighting function matters, for a continuous-time weighting function, any RHP poles and zeros can be replaced with the LHP mirror image, resulting in the exact same magnitude response. The reader is encouraged to read [35] for further details on this, as well as the importance and reasoning behind looking at a weighted H_∞-norm.

This thesis addresses three questions. The first two apply to both the estimation and control problems, while the third applies to only the control problem. These questions are as follows:

Q1: For each performance metric in Table 1.1, is there a fundamental performance limitation due to the sensor time delay, and if so, what is it?

Q2: If a fundamental performance limitation exists, does system performance get worse as the delay, n, increases, and if so, does the performance get arbitrarily poor?

Q3: If a stabilizing controller is designed for the no-delay system of Figure 1.11, can a new controller for the time delay system of Figure 1.8 be found so that the tracking performance of the original no-delay system is recovered?

It should also be noted that results that isolate the sensor time delay are desired (i.e., plant independent results). While completely independent results are not always possible, results that use a minimal amount of knowledge of the plant are desired. For example, knowledge of the open-loop stability of the plant or the location of one RHP pole are sufficient information to use most of the performance metrics in this thesis. These results ideally allow the user to fully comprehend the performance degradation that one can expect to be caused solely by the sensor time delay, allowing design decisions to be made at an earlier stage.

1.4 Organization of the Thesis

The organization of this thesis generally follows the chronological order of the research, with a few minor deviations for clarity. The thesis starts with this introduction, followed

by a look at performance limitations associated with a standard feedback control setup in the presence of a sensor time delay for both stable and unstable discrete-time plants. Chapter 3 looks at performance limitations associated with a standard estimation problem, again, with a sensor time delay, again for discrete-time plants. Chapter 4 looks at performance limitations for both the control and estimation problems for continuous-time systems, which turns out to be more challenging; as a result, only partial results are available for continuous-time systems. Chapter 5 briefly details some preliminary work for further extensions. Finally, some conclusions and summaries of the most important results are provided.

Chapter 2

Discrete-Time SISO Control

2.1 Overview

The motivation for this research is the radiotherapy control problem detailed in Section 1.1. This chapter concerns itself with the feedback control loop at the bottom of Figure 1.4. This loop can essentially be viewed as a standard 1-DOF feedback control loop, as depicted in Figure 1.11, with a sensor time delay, $F[z] = \frac{1}{z^n}$ added, as shown in Figure 1.8.

The answers to Q1-Q3 that were posed at the end of Section 1.3 are answered in the remainder of this chapter. The next section provides some important background material: the well-known Youla Parameterization, standard model-matching theory, and an early H_∞ result from [35]. After that, Q1-Q3 from Section 1.3 are answered, first for a stable plant, and then for an unstable plant. Examples for both the stable plant case and the unstable plant case highlight the various results at the end of their respective sections.

Unless specifically noted otherwise, all systems in this chapter are taken as discrete-time, SISO linear time invariant, causal, with proper and rational transfer functions, except in Section 2.2.1, where the input-output nature will always be specified for additional clarity (i.e., SISO or multi-input multi-output (MIMO)).

2.2 Background Results

2.2.1 Youla (Q) Parameterization

An early question in modern control theory was: which plants can be stabilized by feedback control? The answer, determined with remarkable completeness, was published by Youla et al in [33, 34]. This result allows the computation of all stabilizing controllers for a given plant, and specifies that any plant without an unstable (i.e., outside the unit circle) pole/zero cancellation can be stabilized by feedback control. This parameterization is remarkably simple, especially for a stable plant. By parameterizing all stabilizing

controllers with a single variable, normally denoted as Q, entire new fields of control were able to open up, including H_∞ control. The coprime factorization and Youla parameterization results give below have been taken from [32], with only minor notational changes. The results are presented without proofs, so the interested reader is encouraged to consult [32] for the various proofs. We deal with discrete-time systems, but a similar result applies to continuous-time systems.

Before stating the Youla parameterization results, we need to look at an important tool, namely coprime factorization. To start, let $\mathcal{S}$ denote the set of all *stable* transfer function matrices. The full coprime factorization result is given in the following lemma:

Lemma 2.1 [32] Given a MIMO system $P[z]$, there exist N, $\tilde{N}$, M, $\tilde{M}$, X, $\tilde{X}$, Y, and $\tilde{Y} \in \mathcal{S}$ such that:

$$P[z] = N[z]M^{-1}[z] = \tilde{M}[z]\tilde{N}^{-1}[z] \tag{2.1}$$

and

$$\begin{bmatrix} Y[z] & X[z] \\ -\tilde{N}[z] & \tilde{M}[z] \end{bmatrix} \begin{bmatrix} M[z] & -\tilde{X}[z] \\ N[z] & \tilde{Y}[z] \end{bmatrix} = \begin{bmatrix} I & 0 \\ 0 & I \end{bmatrix}. \tag{2.2}$$

□

Lemma 2.1 brings about the terms "left coprime factorization" comprised of $N[z]$, $M[z]$, $X[z]$, and $Y[x]$, and "right coprime factorization" comprised of $\tilde{N}[z]$, $\tilde{M}[z]$, $\tilde{X}[z]$, and $\tilde{Y}[z]$. Due to the commutation property of scalars, their is no need to distinguish between left and right coprime factorizations for SISO systems as there is for MIMO systems. Since most of this thesis deals with SISO systems, a simpler form of (2.1)-(2.2) for SISO systems is presented in the following corollary:

Corollary 2.1 Given a SISO system $P[z]$, then there exist N,M,X, and $Y \in \mathcal{S}$ such that:

$$P[z] = \frac{N[z]}{M[z]} \tag{2.3}$$

and

$$N[z]X[z] + M[z]Y[z] = 1. \tag{2.4}$$

□

Their are numerous methods for calculating the various terms in Lemma 2.1. For SISO systems only requiring $N[z]$,$M[z]$,$X[z]$, and $Y[x]$, Euclid's formula may be used, as shown in [10]. However, Euclid's formula is cumbersome to use for more complicated systems, and fails entirely for MIMO systems. As such, a state-space based approach is preferred for computing $N[z]$, $\tilde{N}[z]$, $M[z]$, $\tilde{M}[z]$, $X[z]$, $\tilde{X}[z]$, $Y[z]$, and $\tilde{Y}[z]$ for the MIMO case, and $N[z]$, $M[z]$, $X[z]$, and $Y[x]$ for the SISO case. This algorithm is presented in the following lemma:

Lemma 2.2 [32] Given a MIMO or SISO system $P[z]$ with state-space representation A,B,C, and D such that $P[z] = C(zI - A)^{-1}B + D$, with (A,B) stabilizable and (A,C) detectable, select any matrices K and F such that $A_0 \equiv A - BK$ and $\tilde{A}_0 \equiv A - FC$ are both stable (i.e., all eigenvalues have magnitude less than one). Then, a coprime factorization satisfying (2.1) - (2.2) can be found by setting $N[z]$, $\tilde{N}[z]$, $M[z]$, $\tilde{M}[z]$, $X[z]$, $\tilde{X}[z]$, $Y[z]$, and $\tilde{Y}[z]$ as follows:

$$\begin{aligned}
N[z] &= (C - DK)(zI - A_0)^{-1}B + D && (2.5)\\
D[z] &= I - K(zI - A_0)^{-1}B && (2.6)\\
X[z] &= K(zI - \tilde{A}_0)^{-1}F && (2.7)\\
Y[z] &= I + K(zI - \tilde{A}_0)^{-1}(B - FD) && (2.8)\\
\tilde{N}[z] &= C(zI - \tilde{A}_0)^{-1}(B - FD) + D && (2.9)\\
\tilde{M}[z] &= I - C(zI - \tilde{A}_0)^{-1}F && (2.10)\\
\tilde{X}[z] &= K(zI - A_0)^{-1}F && (2.11)\\
\tilde{Y}[z] &= I + (C - DK)(zI - A_0)^{-1}F. && (2.12)
\end{aligned}$$

For SISO systems, only (2.5) - (2.8) need to be used. □

For stable plants, it is unnecessary to use Lemma 2.2, as the following simplification can be used:

Corollary 2.2 Given a system $P \in \mathcal{S}$, then the following coprime factorization can be used:

$$\begin{aligned}
N[z] &= \tilde{N}[z] = P[z] && (2.13)\\
M[z] &= \tilde{M}[z] = I && (2.14)\\
X[z] &= \tilde{X}[z] = 0 && (2.15)\\
Y[z] &= \tilde{Y}[z] = I. && (2.16)
\end{aligned}$$

□

The above results are now used to present the well-known Youla Parameterization, which parameterizes the set of all stabilizing controllers with a single variable, often denoted by Q, hence the term "Q-parameterization". The result, again taken from [32], is presented in the following lemma:

Lemma 2.3 [32] Given any MIMO system P, with a coprime factorization given by Lemma 2.1, for the feedback setup shown in Figure 1.11, the set of all stabilizing controllers, $C[z]$, is given by:

$$\left\{(Y[z] - Q[z]\tilde{N}[z])^{-1}(X[z] + Q[z]\tilde{M}[z]) : Q \in \mathcal{S}, Y - Q\tilde{N} \neq 0\right\} \quad (2.17)$$

$$\text{or} \quad \left\{(\tilde{X}[z] + M[z]Q[z])(\tilde{Y}[z] - N[z]Q[z])^{-1} : Q \in \mathcal{S}, \tilde{Y} - NQ \neq 0\right\}. \quad (2.18)$$

□

Lemma 2.3 can be simplified for SISO systems as shown in the following corollary:

Corollary 2.3 Given a SISO system P, with a coprime factorization given by Corollary 2.1, for the feedback setup shown in Figure 1.11, the set of all stabilizing controllers, $C[z]$, is given by:

$$\left\{ \frac{X[z]+M[z]Q[z]}{Y[z]-N[z]Q[z]} : Q \in \mathcal{S}, Y - NQ \neq 0 \right\}. \tag{2.19}$$

□

Furthermore, if the plant is stable, the coprime factorization can be found using Corollary 2.2, resulting in a simpler Youla parameterization for both MIMO and SISO plants, as given by the following corollaries:

Corollary 2.4 Given a MIMO system $P \in \mathcal{S}$, with a coprime factorization given by Lemma 2.1, for the feedback setup shown in Figure 1.11, the set of all stabilizing controllers, $C[z]$, is given by:

$$\left\{ (I - Q[z]P[z])^{-1}(Q[z]) : Q \in \mathcal{S}, I - QP \neq 0 \right\} \tag{2.20}$$

$$\text{or} \quad \left\{ (Q[z])(I - P[z]Q[z])^{-1} : Q \in \mathcal{S}, I - PQ \neq 0 \right\}. \tag{2.21}$$

□

Corollary 2.5 Given SISO system $P \in \mathcal{S}$, with a coprime factorization given by Corollary 2.1, for the feedback setup shown in Figure 1.11, the set of all stabilizing controllers, $C[z]$, is given by:

$$\left\{ \frac{Q[z]}{1-P[z]Q[z]} : Q \in \mathcal{S}, 1 - PQ \neq 0 \right\}. \tag{2.22}$$

□

It should be noted that in (2.17)-(2.22), the extra restrictions on Q (e.g., $1 - PQ \neq 0$ in (2.22)) beyond stability are satisfied if the plant is strictly proper (this can be verified by noting the relative degree of the various coprime terms for strictly proper plants). In almost all cases in this thesis, Youla parameterization is carried out on a plant augmented with a sensor time delay. As a result, even for a biproper plant, when augmented with the sensor time delay, $\frac{1}{z^n}$, the resulting system is strictly proper for $n \geq 1$. As such, these additional constraints can be ignored when dealing with a discrete-time delayed system.

Finally, there exists a Youla parameterization for two-degree-of-freedom (2-DOF) systems, but that is presented in the 2-DOF section later on in this thesis.

2.2.2 SISO Model Matching

In deriving various H_∞ performance limitations, the problem often reduces to a so-called model-matching problem. This section details the SISO model-matching problem, and is mainly taken from [10]. A MIMO version also exists, but it is dealt with in a later chapter for simplicity. The result is stated for continuous time, but with use of the bilinear transformation (1.14), it can be used for discrete time as well.

Given two transfer functions, $T_1(s)$ and $T_2(s)$, which are both stable, rational and proper, with $T_2(s)$ also having no zeros on the imaginary axis, the model-matching problem is to find a stable $Q(s)$ that minimizes $\|T_1 - T_2Q\|_\infty$. In essence, the problem is to find Q to minimize the error between two "models", T_1 and T_2Q. Define $\widehat{\mathcal{S}}$ to be the set of all not-necessarily-proper transfer functions with poles in the OLHP. The model-matching problem is denoted as

$$\gamma_{opt} \equiv \min_{Q \in \widehat{\mathcal{S}}} \|T_1 - T_2Q\|_\infty, \tag{2.23}$$

where γ_{opt} denotes the minimum error between the two models. It should also be noted that Q is not required to be proper; however, from [35], a procedure for finding a stable and proper Q_p can be found to make $\|T_1 - T_2Q_p\|_\infty$ arbitrarily close to γ_{opt}, so the lack of properness is not a critical problem, i.e.,

$$\inf_{Q_p \in \mathcal{S}} \|T_1 - T_2Q_p\|_\infty = \min_{Q \in \widehat{\mathcal{S}}} \|T_1 - T_2Q\|_\infty.$$

There are two solution techniques for the model-matching problem, one involving use of Nevanlinna-Pick (NP) interpolation theory, and the other using a state-space solution. Both techniques are presented here without proof, as the NP problem provides more insight into the problem, while the state-space solution works better for computations. For derivations of these solutions, the reader is encouraged to see [14, 30]. Details about how to solve the NP interpolation problem are not provided here, so the interested reader is encouraged to see [10] for a brief explanation and [1] for more details.

First, consider the NP solution to the model-matching problem. This is presented as a simple algorithm to be followed, in order to find both the optimal Q and the minimum error γ_{opt} [10]. Note the critical role that is played by the non-minimum phase zeros of T_2 in the model matching problem solution. The algorithm is as follows:

1. Find the RHP zeros of T_2, denoted by $\{z_i : 1 = 1, 2, ..., m\}$ where m is the number of RHP zeros.

2. Define
$$b_i \equiv T_1(z_i), i = 1, 2, ..., m.$$

3. Create the following two matrices:
$$A \equiv \left[\frac{1}{z_i + \overline{z}_j}\right], \quad B \equiv \left[\frac{b_i \overline{b}_j}{z_i + \overline{z}_j}\right].$$

4. The best achievable value of $\|T_1 - T_2 Q\|_\infty$ is

$$\gamma_{opt} \equiv \lambda_{max}\left[A^{-\frac{1}{2}} B A^{-\frac{1}{2}}\right],$$

where λ_{max} denotes the maximum eigenvalue.

5. Solve the NP problem, with a solution given by the all-pass transfer function G, with the following data (see [10, 1] for details):

$$\begin{array}{ccc} z_1 & \cdots & z_m \\ \gamma_{opt}^{-1} b_1 & \cdots & \gamma_{opt}^{-1} b_m. \end{array}$$

6. Set

$$Q = \frac{T_1 - \gamma_{opt} G}{T_2}.$$

Now for the state-space based solution to the problem, which is also presented as an algorithm for the computation of γ_{opt} and Q [10]:

1. Factor T_2 as the product of an all pass factor, T_{ap}, and a minimum-phase factor T_{mp}, i.e.,

$$T_2 = T_{ap} T_{mp}.$$

2. Define

$$R = \frac{T_1}{T_{ap}}.$$

3. Factor R as $R = R_1 + R_2$ where R_1 is strictly proper and with all poles in the RHP and R_2 has all poles in the OLHP (i.e., R_2 is stable).

4. Find a minimal state-space realization of R_1,

$$R_1(s) = \left[\begin{array}{c|c} A & B \\ \hline C & 0 \end{array}\right].$$

5. Solve the Lyaponov equations:

$$\begin{array}{rcl} AL_c + L_c A' & = & BB' \\ A'L_o + L_o A & = & C'C. \end{array}$$

6. Find the maximum eigenvalue of $L_c L_o$, with corresponding eigenvector w. Denote the maximum eigenvalue as λ^2.

7. Define:

$$\begin{aligned} f(s) &= \left[\begin{array}{c|c} A & w \\ \hline C & 0 \end{array}\right], \\ g(s) &= \left[\begin{array}{c|c} -A' & \lambda^{-1}L_o w \\ \hline B' & 0 \end{array}\right], \\ X(s) &= R(s) - \frac{\lambda f(s)}{g(s)}. \end{aligned} \tag{2.24}$$

8. Finally, set $\gamma_{opt} = \lambda$ and $Q = \frac{X(s)}{T_{mp}(s)}$.

To solve a discrete-time model-matching problem, convert the problem to continuous-time using the bilinear transformation (1.14) and solve the resulting continuous-time problem. Once solved, convert the optimal Q back to discrete time, again using the bilinear transformation. For example, for the discrete-time model-matching problem with $T_1[z] = \frac{z}{z+0.5}$ and $T_2[z] = \frac{1}{z^n}$, use the bilinear transformation (1.14) to get the continuous-time model-matching problem with $T_1[z] = \frac{2(s+2)}{s+3}$ and $T_2[z] = \left(\frac{s-1}{s+1}\right)^n$. Note that the particular problem of a discrete-time delay $\frac{1}{z^n}$ gets mapped to n ORHP zeros at $s = 1$ for $n \geq 1$. It should also be noted that a discrete-time transfer function $T_2[z]$ with relative degree ρ will have ρ non-minimum phase zeros after conversion to continuous-time, $\tilde{T}_2(s)$, via the bilinear transformation (1.14).

2.2.3 Francis-Zames Bound

Throughout the thesis, the following result is used when dealing with unstable plants. It is a continuous-time, SISO result, so its use for discrete-time systems requires the bilinear transformation (1.14), but that process is described as the result is used later on. The result is a minor modification to a result from [35], and is presented below:

Lemma 2.4 Let $\tilde{\mathcal{S}}$ denote the set of stable and proper *continuous-time* transfer functions. Let $\tilde{R}(s)$ be a proper, rational transfer function satisfying the interpolation conditions

$$\tilde{R}(\tilde{p}_i) = 1 \ (i = 1, \ldots, m) \tag{2.25}$$

$$\tilde{R}(\tilde{z}_j) = 0 \ (j = 1, \ldots, n), \tag{2.26}$$

where the $\tilde{p}_i$ and $\tilde{z}_j$ are (possibly repeated) complex numbers with positive real parts. Note that there may be other complex numbers a not equal to p_i or z_j where $\tilde{R}(a) = 1$ or $\tilde{R}(a) = 0$.

Then, for any $\tilde{W} \in \tilde{\mathcal{S}}$,

$$\|\tilde{W}\tilde{R}\|_\infty \geq \max_{i=1,2,..,m} \left| \tilde{W}(\tilde{p}_i) \prod_{j=1}^{n} \left(\frac{\bar{\tilde{z}}_j + \tilde{p}_i}{\tilde{z}_j - \tilde{p}_i} \right) \right|. \tag{2.27}$$

□

Proof: A simple proof proceeds by defining the Blaschke product

$$\tilde{B}(s) = \prod_{j=1}^{n} \left(\frac{\tilde{z}_j - s}{\bar{\tilde{z}}_j + s} \right)$$

and factoring $\tilde{R}(s)$ as $\tilde{R}(s) = B(s)\hat{R}(s)$, where $\hat{R} \in \tilde{\mathcal{S}}$. Then,

$$\begin{aligned} \|\tilde{W}\tilde{R}\|_\infty &= \|\tilde{W}B\hat{R}\|_\infty \\ &= \|\tilde{W}\hat{R}\|_\infty \\ &\geq \max_i |\tilde{W}(\tilde{p}_i)\hat{R}(\tilde{p}_i)| \\ &= \max_i |\tilde{W}(\tilde{p}_i)B^{-1}(\tilde{p}_i)\tilde{R}(\tilde{p}_i)| \\ &= \max_i |\tilde{W}(\tilde{p}_i)B^{-1}(\tilde{p}_i)|, \end{aligned} \tag{2.28}$$

where the second equality holds because $B(s)$ is all-pass, the inequality follows from the Maximum Modulus Theorem, and the last equality holds since $\tilde{R}(\tilde{p}_i) = 1$. □

For a standard feedback control problem as shown in Figure 1.5, $\tilde{R}(s)$ can be thought of as the *complementary sensitivity function*, often denoted by $T(s)$, with $\tilde{p}_i$ and $\tilde{z}_i$ being the RHP poles and zeros of the plant. Lemma 2.4 will be used extensively when dealing with unstable plants for both continuous-time and discrete-time systems. ‘

2.3 Stable Plant Case

Here we focus on performance limitations arising in Figure 1.8 with a stable plant, P. Results for sensitivity to plant perturbations and tracking were originally derived in [9] using a parameterization-of-observers scheme. However, that approach does not allow for a result on disturbance rejection or for unstable plants (which is dealt with in the next section). Using Youla parameterization, as described in [18], overcomes these original difficulties, in addition to providing an alternative path to the results in [9]. This section answers the three questions posed at the end of Section 1.3 for the four metrics presented in the feedback control column of Table 1.1 with a stable plant.

It should also be noted that for the stable plant case, there is no fundamental limit on noise rejection, as the zero controller ($C[z] = 0$) rejects all noise injected at w in Figure 1.8. Obviously, this solution may not be ideal for other control objectives, but the noise rejection can be made arbitrarily good (i.e., there is no fundamental performance limitation for noise in the stable plant case). As a result, noise rejection is considered for only the unstable plant case, which is presented in Section 2.4.

2.3.1 Is there a fundamental performance limitation?

The following theorem shows that for disturbance rejection and sensitivity, there is a fundamental performance limitation imposed by the time delay. For tracking, there is no fundamental performance limitation, as will be shown in Section 2.3.3.

Theorem 2.1 Assume $P[z]$ is stable for the feedback control setup shown in Figure 1.8. For the sensor time delay $F[z] = \frac{1}{z^n}$ with $n \geq 1$, define

$$\begin{aligned}
\beta_n &\equiv \inf_{Q \in \mathcal{S}} \|W_2 - W_2 P F Q\|_\infty > 0 && (2.29)\\
\underline{\beta}_n &\equiv \inf_{Q \in \mathcal{S}} \|W_2 - F Q\|_\infty > 0 && (2.30)\\
\gamma_n &\equiv \inf_{Q \in \mathcal{S}} \|W_3 - W_3 P F Q\|_\infty > 0 && (2.31)\\
\underline{\gamma}_n &\equiv \inf_{Q \in \mathcal{S}} \|W_3 - F Q\|_\infty > 0. && (2.32)
\end{aligned}$$

Then, assuming closed-loop stability,

$$\begin{aligned}
\|W_2 S\|_\infty &\geq \beta_n \geq \underline{\beta}_n && (2.33)\\
\|W_3 T_{dy}\|_\infty &\geq \gamma_n \geq \underline{\gamma}_n. && (2.34)
\end{aligned}$$

□

Proof: From Equation (1.16),

$$\begin{aligned}
S[z] &= \frac{\partial T_{ry}[z]}{\partial P[z]} \frac{P[z]}{T_{ry}[z]}\\
&= \frac{\partial \frac{P[z]C[z]}{1+P[z]F[z]C[z]}}{\partial P[z]} \frac{P[z]}{\frac{P[z]C[z]}{1+P[z]F[z]C[z]}}\\
&= \frac{C[z]+P[z]F[z]C^2[z]-P[z]F[z]C^2[z]}{(1+P[z]F[z]C[z])^2} \frac{P[z]+P^2[z]F[z]C[z]}{P[z]C[z]}\\
&= \frac{C[z]}{(1+P[z]F[z]C[z])^2} \frac{1+P[z]F[z]C[z]}{C[z]}\\
&= \frac{1}{1+P[z]F[z]C[z]}, && (2.35)
\end{aligned}$$

and from (1.17),

$$\begin{aligned}
T_{dy}[z] &= \frac{Y[z]}{D[z]}\\
&= \frac{1}{1+P[z]F[z]C[z]}, && (2.36)
\end{aligned}$$

which is the same as for S, i.e., $T_{dy} = S$. Using the stable case of Youla Parameterization (2.22) for an augmented plant, $P[z]F[z]$, and substituting into (2.35),

$$\begin{aligned}
S[z] &= \frac{1}{1+P[z]F[z]\frac{Q[z]}{1-P[z]F[z]Q[z]}}\\
&= \frac{1-P[z]F[z]Q[z]}{1-P[z]F[z]Q[z]+P[z]F[z]Q[z]}\\
&= 1-P[z]F[z]Q[z]. && (2.37)
\end{aligned}$$

Substituting the expression for $S[z]$ given by (2.37) into the H_∞ norms given in Table 1.1 from the feedback control column for S results in

$$\begin{aligned} \|W_2 S\|_\infty &= \|W_2 - W_2 PFQ\|_\infty && (2.38)\\ &\geq \inf_{Q\in\mathcal{S}} \|W_2 - W_2 PFQ\|_\infty = \beta_n && (2.39)\\ &\geq \inf_{Q\in\mathcal{S}} \|W_2 - FQ\|_\infty = \underline{\beta}_n, && (2.40) \end{aligned}$$

and similarly, since $T_{dy}[z] = S[z]$,

$$\begin{aligned} \|W_3 T_{dy}\|_\infty &= \|W_3 - W_3 PFQ\|_\infty && (2.41)\\ &\geq \inf_{Q\in\mathcal{S}} \|W_3 - W_3 PFQ\|_\infty = \gamma_n && (2.42)\\ &\geq \inf_{Q\in\mathcal{S}} \|W_3 - FQ\|_\infty = \underline{\gamma}_n. && (2.43) \end{aligned}$$

The argument for removing W_2P and W_3P in (2.40) and (2.43) is based on interpolation theory, which forms the basis for a solution to the model-matching problem, as described in Section 2.2.2. Specifically, the presence of W_2P or W_3P can never decrease the optimal model-matching cost since extra factors in the T_2 term only increase the optimal cost by adding extra interpolation constraints. To verify this, consider an interpolation problem with data points $\{x_i : i = 1,2,...,k\}$, giving an optimal error of y_{opt}. Then consider the same interpolation problem with the same points except with an extra point added on, i.e., $\{x_i : i = 1,2,...,k+1\}$, resulting in an optimal error of z_{opt}. Now, since at best the optimal solution to the original problem contains the point x_{k+1}, clearly, $z_{opt} \geq y_{opt}$ must hold. □

Bounds (2.40) and (2.43) do not depend on the plant, but only depend on the delay and the weighting function, which makes them useful for characterizing the performance degradation caused by the sensor time delay. These bounds show that for any specified weight, a sensor time delay results in a plant-independent (subject to the plant being stable) performance limitation for disturbance rejection and sensitivity to plant perturbations.

2.3.2 What happens to performance as the sensor time delay is increased?

We can argue that γ_n, $\underline{\gamma}_n$, β_n and $\underline{\beta}_n$ are non-decreasing function of the delay, n. For simplicity, we will only deal with the $\underline{\gamma}_n$ and $\underline{\beta}_n$ to illustrate why this is the case, but essentially the same argument can be made for γ_n and β_n. Both (2.40) and (2.43) are posed as model-matching problems, with $T_1 = W_2$ or $T_1 = W_3$ and $T_2 = F$. As such, using the same argument as at the end of the proof for Theorem 2.1 (that adding points to an interpolation problem will produce an optimal error that is greater than or equal to the previous optimal error), it is clear that increasing the delay (which adds extra points to the interpolation problem since $\frac{1}{z^n}$ becomes $(\frac{s-1}{s+1})^n$ after application of the bilinear

transformation (1.14)), cannot reduce the error. This can be presented formally as follows for any admissible W_1 and W_2:

$$\begin{aligned} \underline{\gamma}_n &\leq \underline{\gamma}_{n+1} \quad \forall n \geq 1 \\ \underline{\beta}_n &\leq \underline{\beta}_{n+1} \quad \forall n \geq 1. \end{aligned}$$

Similar arguments apply to the expressions in (2.39) and (2.42). Consequently, we can say that the performance limitations $\underline{\gamma}_n$ and $\underline{\beta}_n$ are non-decreasing functions of n, and that for a given plant P, the optimal performance does not get better as n increases.

However, despite $\underline{\gamma}_n$ and $\underline{\beta}_n$ being non-decreasing functions of n, they do not tend to ∞. This is easily shown using the expressions for $\underline{\gamma}_n$ and $\underline{\beta}_n$ in (2.40) and (2.43). Substituting in $Q = 0$, which is stable and minimum phase (i.e., it is an admissible value of Q), we conclude that $\underline{\gamma}_n$ and $\underline{\beta}_n$ are no more than $\|W_3\|_\infty$ and $\|W_2\|_\infty$ respectively. Since $\|W_2\|_\infty$ and $\|W_3\|_\infty$ are defined as having an infinity norm equal to one, it is clear that:

$$\begin{aligned} \underline{\gamma}_n &\leq \gamma_n \leq 1 \quad \forall n \geq 1 \\ \underline{\beta}_n &\leq \beta_n \leq 1 \quad \forall n \geq 1. \end{aligned}$$

Unfortunately, no proof has been developed showing that the limit of $\underline{\gamma}_n$ and $\underline{\beta}_n$ as n approaches ∞ equals one. But as will be seen in the examples, it appears that this is indeed the case; in this sense, the performance limitations in Theorem 2.1 are tight.

2.3.3 Can tracking performance be recovered?

Given a stabilizing controller for the standard feedback control setup of Figure 1.11, can a controller be designed for the setup with a sensor time delay shown in Figure 1.8 that will mimic the tracking performance of the undelayed setup? The answer is that tracking performance can indeed be recovered with a time delay in the feedback loop, as outlined in the following theorem:

Theorem 2.2 Consider a stable plant, P, and a given stabilizing controller, C^b, with transfer function from r to e denoted T_{re}^b as shown in Figure 1.11. Then, given the same plant P for the 1-DOF setup of Figure 1.8, with a transfer function from r to e denoted T_{re}, the controller

$$C = \frac{C^b}{1 + PC^b(1-F)} \tag{2.44}$$

is stabilizing and recovers tracking, i.e., $T_{re} = T_{re}^b$. □

Proof: Equation (2.44) follows from straightforward algebra and the 1-DOF Youla parameterization. Using the simplified stable version of Youla (2.22), the stabilizing controller C^b can be constructed as

$$C^b = \frac{Q^b}{1 - PQ^b} \tag{2.45}$$

$$\tag{2.46}$$

where $Q^b \in \mathcal{S}$. Moreover,

$$\begin{aligned} T_{re}^b &= \frac{1}{1+PC^b} \\ &= \frac{1}{1+P\frac{Q^b}{1-PQ^b}} \\ &= 1-PQ^b. \end{aligned} \tag{2.47}$$

Again by Youla, any stabilizing controller for Figure 1.8 can be written as

$$C = \frac{Q}{1-PQ}, \tag{2.48}$$

$$\tag{2.49}$$

and defining $e \equiv r-y$ for the setup in Figure 1.8,

$$\begin{aligned} T_{re} &= \frac{1}{1+PFC} + \frac{PC(F-1)}{1+PCF} \\ &= \frac{1}{1+PF\frac{Q}{1-PFQ}} + \frac{\frac{P(F-1)Q}{1-PFQ}}{1+\frac{PFQ}{1-PFQ}} \\ &= 1-PFQ+PFQ-PQ \\ &= 1-PQ. \end{aligned} \tag{2.50}$$

Force $T_{re} = T_{re}^b$ in (2.47) and (2.50) to get

$$Q = Q^b, \tag{2.51}$$

which is stable since $Q^b \in \mathcal{S}$. Therefore, by Corollary 2.5, we know that a recovering controller exists. To get (2.44), rearrange (2.45) to solve for Q^b in terms of C^b:

$$Q^b = \frac{C^b}{1+PC^b}. \tag{2.52}$$

Then substitute (2.52) into (2.48),

$$Q = \frac{C^b}{1+PC^b}, \tag{2.53}$$

and then substitute (2.53) into (2.48):

$$\begin{aligned} C &= \frac{Q}{1-PFQ} \\ &= \frac{\frac{C^b}{1+PC^b}}{1-PF\frac{C^b}{1+PC^b}} \\ &= \frac{C^b}{1-PC^b(1-F)} \quad \square \end{aligned} \tag{2.54}$$

Based on the above theorem, adding a delay to the feedback loop has no fundamental penalty in terms of tracking performance, in the sense that performance of the undelayed system in Figure 1.11 can be recovered. Also of note is that (2.51) shows that the same Youla parameter Q recovers the tracking of the original system for the 1-DOF, stable plant case, except it must be applied to the augmented plant, PF.

2.3.4 Examples

Two example calculations will be performed on a plant related to the radiotherapy problem outlined in the introduction. The plant is given by

$$P[z] = \frac{0.044332}{z - 0.9704}, \tag{2.55}$$

and is taken from [8]. The first calculation entails finding the bound (2.31) for various delays given a frequency-varying weighting function, W_3. The second problem involves constructing the recovering controller (2.44) for the given plant. For all examples, the sensor time delay is represented by $F[z] = \frac{1}{z^n}$.

Example 1: For the radiotherapy plant given above, we can compute γ_n from bound (2.31) for a given weighting function, W_3. So, using the discrete-time weighting function (which is a discretized first order low pass filter)

$$W_3[z] = \frac{z\tan(\frac{\Omega_b}{2}) + \tan(\frac{\Omega_b}{2})}{z(\tan(\frac{\Omega_b}{2}) + 1) + \tan(\frac{\Omega_b}{2}) - 1}, \tag{2.56}$$

with $\Omega_b \in (0, \pi)$, it is possible to compute the performance limitations for various delays and for various values of Ω_b. To see how $W_3[z]$ varies with Ω_b, consider Figure 2.1, which shows the magnitude Bode plot of $W_3[z]$ for various values of Ω_b; Ω_b can be thought of as the "bandwidth" of $W_3[z]$. Figure 2.2 shows the fundamental performance limitation, γ_n, for the best achievable weighted sensitivity for various values of the delay, n.

Figure 2.2 clearly shows the worsening effect of the time delay. For a given weighting function (i.e., for a fixed value of Ω_b), Figure 2.2 shows an increase in the best achievable performance as the delay, n, increases, consistent with the discussion in Section 2.3.2. Figure 2.2 also shows the upper bound of $||W||_\infty = 1$ for large values of Ω_b (which corresponds to weighting almost all frequencies equally), as discussed in Section 2.3.2.

Example 2: This example explores the performance of the "recovering" controller, which is described by (2.44). Consider the same radiotherapy plant (2.55) with a stabilizing controller, $C^b[z] = 10$, designed without knowledge of the sensor time delay, as shown by Figure 1.11. Then, given a sensor time delay, $F[z] = \frac{1}{z^3}$, for the setup of Figure 1.8, a "recovering controller" can be designed through use of (2.44). For the given problem, this "recovering" controller is given by

$$C[z] = \frac{10z^3(z - 0.9704)}{(z - 0.9875)(z + 0.7102)(z^2 - 0.2499z + 0.6321)}. \tag{2.57}$$

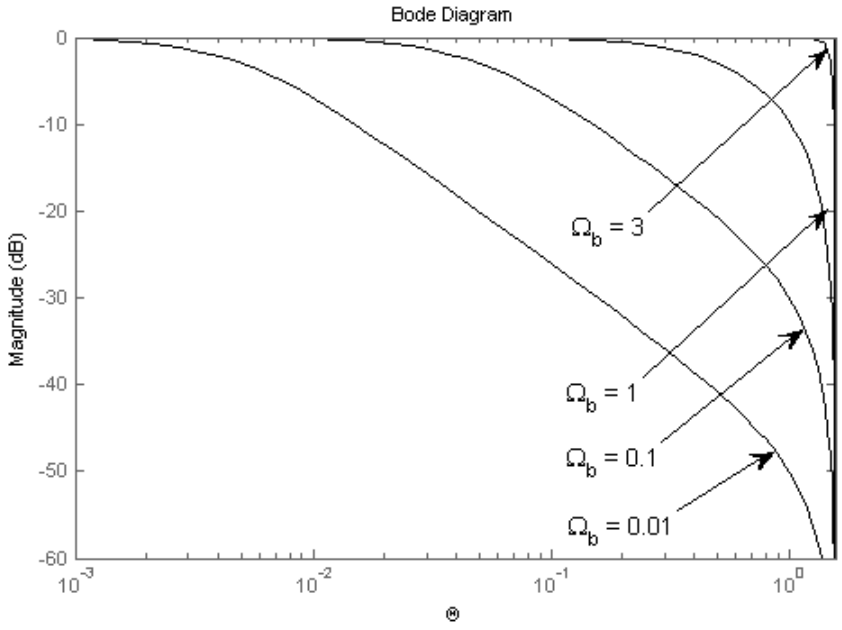

Figure 2.1: A magnitude Bode plot of $W_3[z] = \frac{z\tan(\frac{\Omega_b}{2})+\tan(\frac{\Omega_b}{2})}{z(\tan(\frac{\Omega_b}{2})+1)+\tan(\frac{\Omega_b}{2})-1}$ for various values of Ω_b.

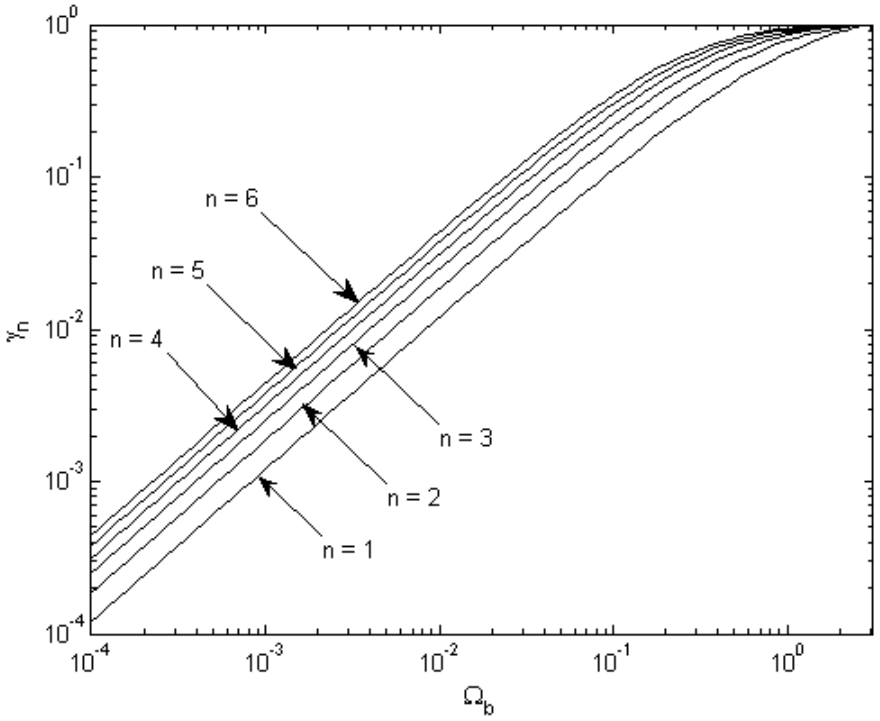

Figure 2.2: The weighted performance limitation for various values of n and Ω_b.

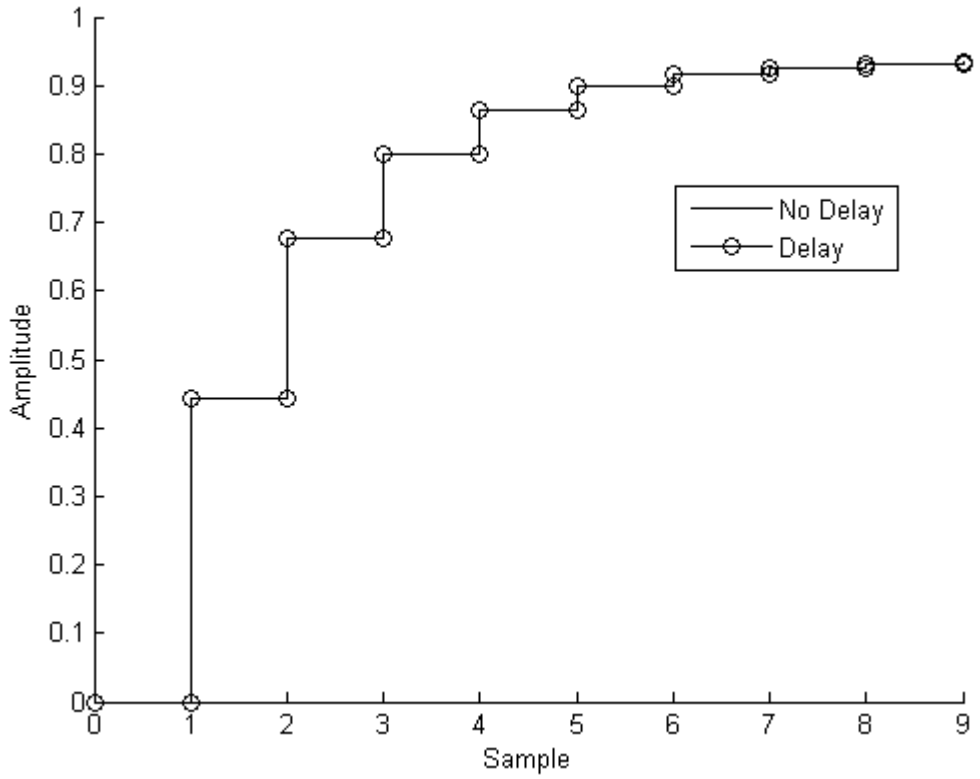

Figure 2.3: The step response from the input, r, to the output, y, for both the undelayed system of Figure 1.11, with controller $C^b[z] = 10$, and the delay system of Figure 1.8, with controller $C[z] = \frac{10z^3(z-0.9704)}{(z-0.9875)(z+0.7102)(z^2-0.2499z+0.6321)}$.

The step responses for the delayed and undelayed feedback systems are shown in Figure 2.3, and as expected, both systems show identical performance in the tracking domain. However, the sensor time delay does degrade performance in other areas, despite the ability to recover tracking performance. Consider the same systems, except with a unit step disturbance, instead of a unit step reference. The output, y, for both systems under the effect of the disturbance is shown in Figure 2.4. The effect of the time delay is now quite clear, as the time-delayed system rejects the disturbance three samples behind the undelayed system. Due to bounds (2.40) and (2.43), this result is not surprising, since the time delay creates a fundamental performance limitation for disturbance rejection. In essence, the sensor time delay delays the effect of the feedback, creating a quasi-feedforward control structure for the first n samples for an n sample sensor time delay.

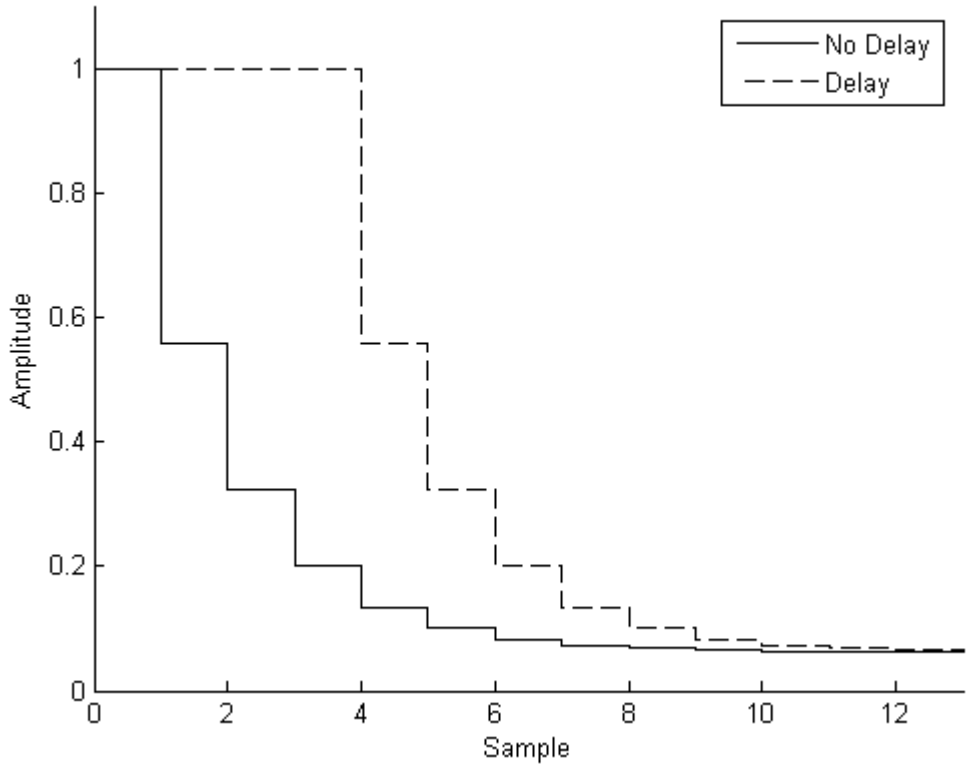

Figure 2.4: The step response for a disturbance, d, to the output, y, for both the undelayed system of Figure 1.11, with controller $C_b[z] = 10$, and the delay system of Figure 1.8, with controller $C[z] = \frac{10z^3(z-0.9704)}{(z-0.9875)(z+0.7102)(z^2-0.2499z+0.6321)}$.

2.4 Unstable Plant Case

For the unstable plant case, two different approaches are taken. The first is equivalent to the path taken for the stable plant case, using Youla Parameterization. Unfortunately, while this can provide a computational tool for determining optimal performance for a known plant and delay, the resulting expression is too complex to ascertain any trends or gain any insight into the effect of the delay. This motivated a second approach, using the Francis-Zames bound given in Lemma 2.4. While the resulting bound is not tight like the Youla derived bound, it is simple to calculate and provides a clear picture of the effect of the time delay. Also unlike in the stable case, a fundamental performance limitation exists for noise rejection. Questions 1-3 from Chapter 1 are answered below, just as for the stable plant case, and then followed with some examples.

2.4.1 Is there a fundamental performance limitation?

The short answer is that for all four metrics in Table 1.1, there is a fundamental performance limitation for the unstable plant case. First, an insightful lower bound on performance is presented, followed by an exact method for calculating optimal performance. The insightful lower bound is based on the Francis-Zames bound in Section 2.2.3, and is presented in the following theorem:

Theorem 2.3 Assume $P[z]$ has $k \geq 1$ possibly repeated unstable poles; denote these poles by $p_i, i = 1,...,k$. If the closed-loop system in Figure 1.8 is stable, then the performance metrics given in the feedback control column of Table 1.1 are bounded from below as follows:

$$\|W_1 T_{re}\|_\infty^{DT} \geq \max_{i=1,...,k} |W_1(p_i) \cdot p_i^n| - \|W_1\|_\infty^{DT} \tag{2.58}$$

$$\|W_2 S\|_\infty^{DT} \geq \max_{i=1,...,k} |W_2(p_i) \cdot p_i^n| - \|W_2\|_\infty^{DT} \tag{2.59}$$

$$\|W_3 T_{dy}\|_\infty^{DT} \geq \max_{i=1,...,k} |W_3(p_i) \cdot p_i^n| - \|W_3\|_\infty^{DT} \tag{2.60}$$

$$\|W_4 T_{we}\|_\infty^{DT} \geq \max_{i=1,...,k} |W_4(p_i) \cdot p_i^n| . \tag{2.61}$$

□

Proof: Let $\tilde{P}(s)$, $\tilde{C}(s)$, and $\tilde{F}(s)$ denote $P[z]$, $C[z]$, and $F[z]$ after the applying the bilinear transformation (1.14). Let $\tilde{p}_i$, $i = 1,\ldots,k$ denote the values of p_i mapped to the s-plane, also using (1.14). Also let $\tilde{z}_j$, $j = 1,\ldots,m$ denote all zeros of $\tilde{P}\tilde{C}\tilde{F}$ with positive real parts; note that there are at least n such zeros located at $s = 1$ due to the presence of $\tilde{F}$. Let the n zeros associated with $\tilde{F}$ be the first n zeros, i.e., $\tilde{z}_j = 1$ for $j = 1,\ldots,n$.

Let's start by proving (2.60). The key element of the proof is to apply Lemma 2.4 with

$$\tilde{R} = \frac{\tilde{P}\tilde{C}\tilde{F}}{1 + \tilde{P}\tilde{C}\tilde{F}}. \tag{2.62}$$

By the assumption of closed-loop stability, $\tilde{R}(\tilde{p}_i) = 1, i = 1,\ldots,k$ and $\tilde{R}(\tilde{z}_j) = 0, j = 1,\ldots,m$. The proof of (2.60) starts by using the fact that $\|\cdot\|_\infty$ norms are preserved under mapping (1.14), recognizing that $\tilde{T}_{dy} = 1 - \tilde{R}$, applying the triangle inequality, and exploiting Lemma 2.4:

$$\begin{aligned}
\|W_3 T_{dy}\|_\infty^{DT} &= \|\tilde{W}_3 \tilde{T}_{dy}\|_\infty^{CT} \\
&= \|\tilde{W}_3 - \tilde{W}_3 \tilde{R}\|_\infty^{CT} \\
&\geq \|\tilde{W}_3 \tilde{R}\|_\infty^{CT} - \|\tilde{W}_3\|_\infty^{CT} \\
&\geq \max_{i=1,\ldots,k} \left| \tilde{W}_3(\tilde{p}_i) \prod_{j=1}^{m} \left(\frac{\bar{\tilde{z}}_j + \tilde{p}_i}{\tilde{z}_j - \tilde{p}_i} \right) \right| - \|\tilde{W}_3\|_\infty^{CT}. \qquad (2.63)
\end{aligned}$$

Next, use the fact that at least n of the $\tilde{z}_j$ values are 1, and use (1.14) to convert back to discrete time, as follows:

$$\begin{aligned}
\|W_3 T_{dy}\|_\infty^{DT} &\geq \max_{i=1,\ldots,k} \left| \tilde{W}_3(\tilde{p}_i) \left(\frac{1+\tilde{p}_i}{1-\tilde{p}_i} \right)^n \prod_{j=n+1}^{m} \left(\frac{\bar{\tilde{z}}_j + \tilde{p}_i}{\tilde{z}_j - \tilde{p}_i} \right) \right| - \|\tilde{W}_3\|_\infty^{CT} \qquad (2.64) \\
&\geq \max_{i=1,\ldots,k} \left| \tilde{W}_3(\tilde{p}_i) \left(\frac{1+\tilde{p}_i}{1-\tilde{p}_i} \right)^n \right| - \|\tilde{W}_3\|_\infty^{CT} \\
&= \max_{i=1,\ldots,k} |W_3(p_i) \cdot p_i^n| - \|W_3\|_\infty^{DT}.
\end{aligned}$$

This proves (2.60); because $S = T_{dy}$, as shown by (2.35)-(2.36), it also proves (2.59).

The proof of (2.61) is very similar, except the triangle inequality step is not needed since $\tilde{T}_{we}$ equals $\tilde{R}$:

$$\begin{aligned}
\|W_4 T_{we}\|_\infty^{DT} &= \|\tilde{W}_4 \tilde{T}_{we}\|_\infty^{CT} \\
&= \|\tilde{W}_4 \tilde{R}\|_\infty^{CT} \\
&\geq \max_{i=1,\ldots,k} |W_4(p_i) \cdot p_i^n|.
\end{aligned}$$

The proof of (2.58) is again similar, except an extra step is needed to deal with the final $\tilde{F}$ term in the relationship

$$\tilde{T}_{re} = 1 - \frac{\tilde{P}\tilde{C}}{1 + \tilde{P}\tilde{C}\tilde{F}} = 1 - \frac{\tilde{R}}{\tilde{F}}.$$

The extra term is easily managed since $|\tilde{F}(j\omega)| = 1 \; \forall \; \omega$:

$$\begin{aligned}
\|W_1 T_{re}\|_\infty^{DT} &= \|\tilde{W}_1 \tilde{T}_{re}\|_\infty^{CT} \\
&= \left\| \tilde{W}_1 - \frac{\tilde{W}_1 \tilde{R}}{\tilde{F}} \right\|_\infty^{CT} \\
&\geq \left\| \frac{\tilde{W}_1 \tilde{R}}{\tilde{F}} \right\|_\infty^{CT} - \|\tilde{W}_1\|_\infty^{CT} \\
&= \|\tilde{W}_1 \tilde{R}\|_\infty^{CT} - \|\tilde{W}_1\|_\infty^{CT} \\
&\geq \max_{i=1,\ldots,k} |W_1(p_i) \cdot p_i^n| - \|\tilde{W}_1\|_\infty^{CT}. \square
\end{aligned}$$

The ramifications of Theorem 2.3 are discussed after the next theorem, and are highlighted in the examples at the end of this chapter. The next theorem presents a method for calculating the exact optimal performance using a model-matching approach:

Theorem 2.4 Consider the control setup of Figure 1.8 where $P[z]$ is possibly unstable. Perform a coprime factorization on the plant and delay, i.e., $P[z]F[z]$, resulting in $N[z]$, $M[z]$, $X[z]$, and $Y[z]$ as given by Corollary 2.1. Then, assuming closed loop stability,

$$\begin{aligned}
\|W_1 T_{re}\|_\infty &\geq \inf_{Q\in\mathcal{S}} \|W_1 MPX - W_1 M^2 PQ\|_\infty && (2.65)\\
\|W_2 S\|_\infty &\geq \inf_{Q\in\mathcal{S}} \|W_2 MY - W_2 MNQ\|_\infty && (2.66)\\
\|W_3 T_{dy}\|_\infty &\geq \inf_{Q\in\mathcal{S}} \|W_3 MY - W_3 MNQ\|_\infty && (2.67)\\
\|W_4 T_{we}\|_\infty &\geq \inf_{Q\in\mathcal{S}} \|W_4 NX - W_4 MNQ\|_\infty. && (2.68)
\end{aligned}$$

□

Proof: Only the result for T_{dy} is derived. The remaining three expressions can all be derived in a similar fashion. The derivation starts with the expression for T_{dy}, and then substitutes for the controller with its Youla parameterization, as follows:

$$\begin{aligned}
T_{dy} &= \frac{1}{1+PFC}\\
&= \frac{1}{1+\frac{N}{M}\frac{X+MQ}{Y-NQ}}\\
&= \frac{MY-MNQ}{MY+NX+MNQ-MNQ}\\
&= MY-MNQ.
\end{aligned}$$

Now, multiply by the weighting function, resulting in:

$$\begin{aligned}
W_3 T_{dy} &= W_3 MY - W_3 MNQ\\
\Rightarrow \|W_3 T_{dy}\|_\infty &\geq \inf_{Q\in\mathcal{S}} \|W_3 MY - W_3 MNQ\|_\infty
\end{aligned}$$

□

Unfortunately, both the T_1 and T_2 terms of the model-matching problems (2.65)-(2.68) depend on the delay (since M, X, and Y depend on F), and therefore the bounds of Theorem 2.4 provide almost no insight into the effect of the delay. However, they can be used to compute the optimal performance, which is done in the examples at the end of this section. The results of Theorem 2.3, on the other hand, provide great insight into the effect of the delay, at the cost of introducing conservativeness. There are four sources of conservativeness in (2.58)-(2.61):

- Use of the triangle inequality in deriving (2.58)-(2.60) results in conservativeness (reflected in the presence of the $-\|W\|_\infty$ terms).

- The bounds involve calculating a result for each unstable pole and then taking the maximum over all unstable poles. The consequence is that only one pole affects the resulting bounds, resulting in some conservativeness for systems with multiple unstable poles.
- The dropping of any extra plant zeros with magnitude greater than one in (2.58)-(2.61) to isolate the effect of the time delay results in conservativeness. This can be overcome by converting (2.64) to discrete time and keeping the remaining plant zeros, but at the expense of clarity on the effect of the delay.
- In the derivation in Lemma 2.4, specifically, (2.28), additional conservativeness may be introduced.

The examples at the end of this section illustrate these sources of conservativeness.

2.4.2 What happens to performance as the sensor time delay is increased?

The bounds in Theorem 2.3 increase exponentially as the delay increases; however, since the bounds are not tight, all that can be said is that the lower bounds get worse as the delay gets worse. The results of Theorem 2.4, on the other hand, provide little insight into system behaviour as n increases. Take for example (2.66), and compare it to the stable case, (2.39). For the stable case, when the time delay is increased, the only term that changes is F, and the result is an extra interpolation condition that can only make the optimal performance worse. However, for the unstable case, an increase in the time delay not only affects F, but it also affects X and Y through the coprime factorization. The effects of the change on X and Y are unclear and problem dependent, making it impossible to say for certain that the optimal performance is a non-decreasing function on n as it is for the stable plant case.

However, it is simple to see that the limit of (2.58)-(2.61) as the delay, n, approaches infinity is also infinity. Since (2.58)-(2.61) are lower bounds on performance, and they tend to infinity as the delay tends to infinity, it is safe to say that system performance gets arbitrarily bad for an arbitrarily long delay. It should be noted that this result is fairly intuitive. An infinite delay in the feedback loop is essentially the same thing as not having a feedback loop at all. Since the results of Theorem 2.3 are for open loop unstable plants, it is hardly surprising that in the absence of a feedback loop the various performance measures blow up.

2.4.3 Can tracking performance be recovered?

Inequality (2.58) proves that tracking performance cannot always be recovered, since for a long enough delay tracking performance becomes arbitrarily poor. This conclusion can also be reached using Youla parameterization, except instead of finding a stable Q as in

Theorem 2.2, the Q for the unstable case that would recover tracking performance is not stable and therefore not admissible. This is outlined in the following theorem:

Theorem 2.5 Given an unstable plant, P, consider a stabilizing controller, C^b, with transfer function from r to e denoted T_{re}^b as shown in Figure 1.11. Then, given the same unstable plant P for the 1-DOF, time-delayed setup of Figure 1.8, with a transfer function from r to e denoted T_{re}, in general, no recovering controller exists (i.e., $T_{re} \neq T_{re}^b$). □

Proof: Using the same procedure as the proof of Theorem 2.2, the recovering Youla parameter is given by:

$$Q = \frac{1 + M_2 N_2 Q_2 - M_2 Y_2 - PMX}{PM^2}. \tag{2.69}$$

The unstable plant poles appear in the denominator of this expression, making it unstable barring a fluke cancellation from the numerator. □

2.4.4 Examples

This subsection illustrates the effect of the intuitive bounds (2.58)-(2.61) for a plant with one unstable pole, and for a plant with two unstable poles. These bounds are compared to the tighter model-matching bounds given by (2.65)-(2.68), to show the conservativeness penalty for the intuition gained in (2.58)-(2.61). In both examples, the weighting function used is the same as for the stable example (2.56), except with varying subscripts for W, i.e.,

$$W_1[z] = W_2[z] = W_3[z] = W_4[z] = \frac{z\tan(\frac{\Omega_b}{2}) + \tan(\frac{\Omega_b}{2})}{z(\tan(\frac{\Omega_b}{2}) + 1) + \tan(\frac{\Omega_b}{2}) - 1}.$$

This is a simple first-order filter with cutoff frequency Ω_b, as introduced in Example 1.

Example 3: Consider an unstable plant,

$$P[z] = \frac{(z+0.5)^2}{(z+2)(z+0.25)}, \tag{2.70}$$

which is biproper and has one pole with magnitude greater than one. For the sensor time delay setup of Figure 1.8, bounds (2.58)-(2.61) can be computed. The first three of these bounds, for tracking, disturbance rejection and sensitivity to plant perturbations, are shown far various sensor time delays in Figure 2.5, and the bound for noise rejection is shown in Figure 2.6. The main difference between the two figures is the lack of the $-||W_i||_\infty$ term for the noise rejection bound. The difference is especially relevant at lower values of Ω_b, where the bounds in Figure 2.5 become negative. As a result, these bounds are not shown on the logarithmic scale below these frequencies. The conclusion is that bounds (2.58)-(2.60) do not provide meaningful information when both of n and Ω_b are "small". The noise rejection bound does not suffer from this problem, and it shows a

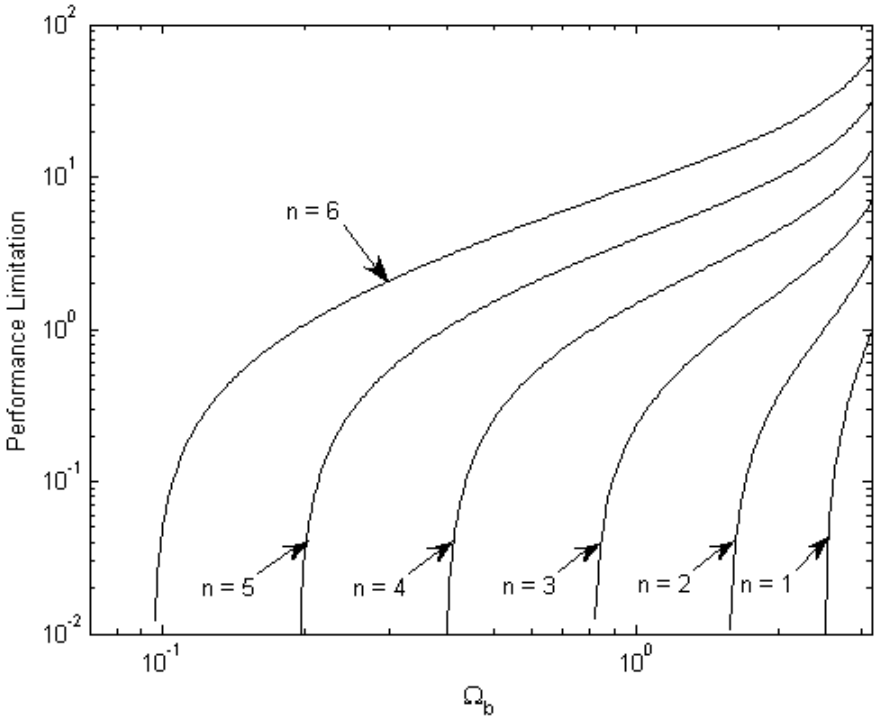

Figure 2.5: Bounds (2.58)-(2.60) for various values of n and Ω_b with P given by (2.70).

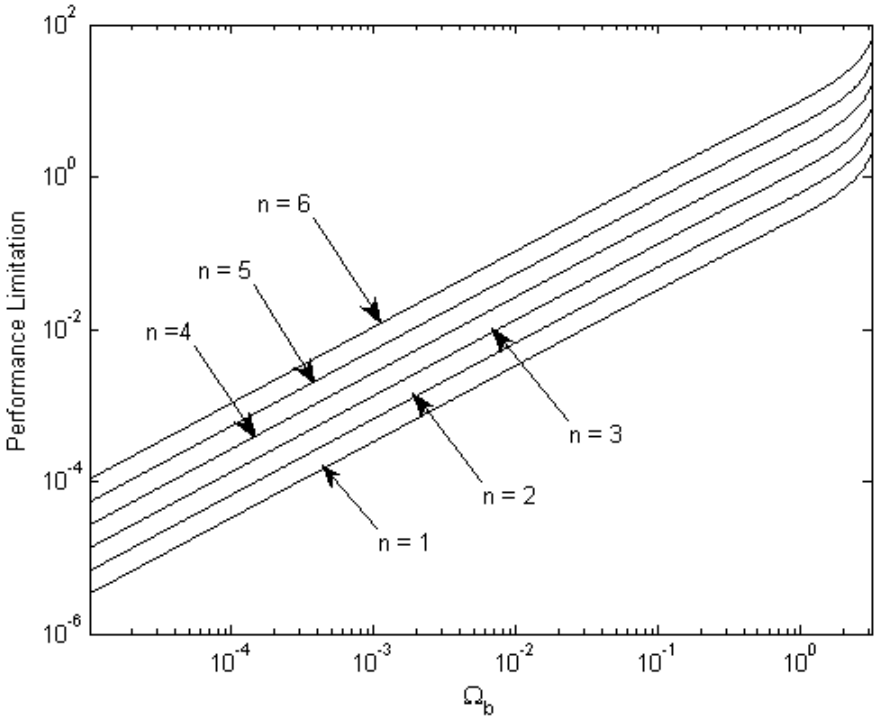

Figure 2.6: Bound (2.61) for various values of n and Ω_b with P given by (2.70).

fundamental performance limitation for all values of Ω_b. In both cases, as the delay, n, increases, so too does the bound.

Now, the question of the conservativeness of the bounds in Figures 2.5 and 2.6 arises. For this example, the degree of conservativeness is best shown by calculating bounds (2.65)-(2.68) (which are tight) and comparing them to bounds (2.58)-(2.61). This will be done for $n = 3$, in order to clearly illustrate the results. Figure 2.7 shows the result for disturbance rejection and sensitivity to plant perturbations, while Figure 2.8 shows the result for tracking.

Figures 2.7 and 2.8 are extremely similar, and effectively show the same thing. At low values of Ω_b, the $-\|W_i\|_\infty$ term dominates, resulting in a negative bound (and hence the sharp drop off of the Francis-Zames curve). At higher values of Ω_b, a non-trivial bound ensues, but one that is still conservative compared to the tight model-matching bound. Despite the conservative nature of (2.58)-(2.60) when compared to the tight bounds (2.65)-(2.67), they are still quite useful. The major source of conservativeness is the $-||W_i||_\infty$ term for these equations, which at small values of n and Ω_b produce a trivial bound. However, the same trends are illustrated by the Francis-Zames bounds in the region where a non-trivial bound is produced, and the conclusions reached by a designer would be very similar.

Figure 2.9 shows the result for noise rejection. When compared to the previous cases, the biggest difference is the lack of the $-\|W_i\|_\infty$ term. The result is that (2.61), interestingly, is exactly the same as (2.68). For this example, the only possible source of conservativeness is from the derivation of the Francis-Zames bound in Lemma 2.4 (see (2.28) for details); it appears that Lemma 2.4 is in fact tight for this example. However, consider the strictly proper plant

$$P[z] = \frac{z+0.5}{(z+2)(z+0.25)}, \tag{2.71}$$

which is the same as (2.70) except for the omission of one of the zeros. The new plant (2.71) now has a non-zero relative degree, which adds conservativeness to (2.61) due to the creation of a non-minimum-phase zero when mapped to continuous time. This conservativeness is clearly demonstrated in Figure 2.10, which also shows a modified version of (2.61), based on (2.64), which, just as for the biproper plant case, recreates the tight model-matching bound (2.68). The conclusion is that for cases with only one unstable plant pole, the Francis-Zames bound can produce a tight bound on the best achievable performance for noise rejection.

Example 4: This example further explores the conservative nature of (2.58)-(2.61), particularly as it applies to plants with multiple poles with magnitude greater than one. Consider

$$P[z] = \frac{(z+0.5)^2}{(z+2)(z+3)}, \tag{2.72}$$

with the same weighting functions as before. As in the previous example, bounds can be calculated for various values of the delay, n, and the weighting function cutoff frequency,

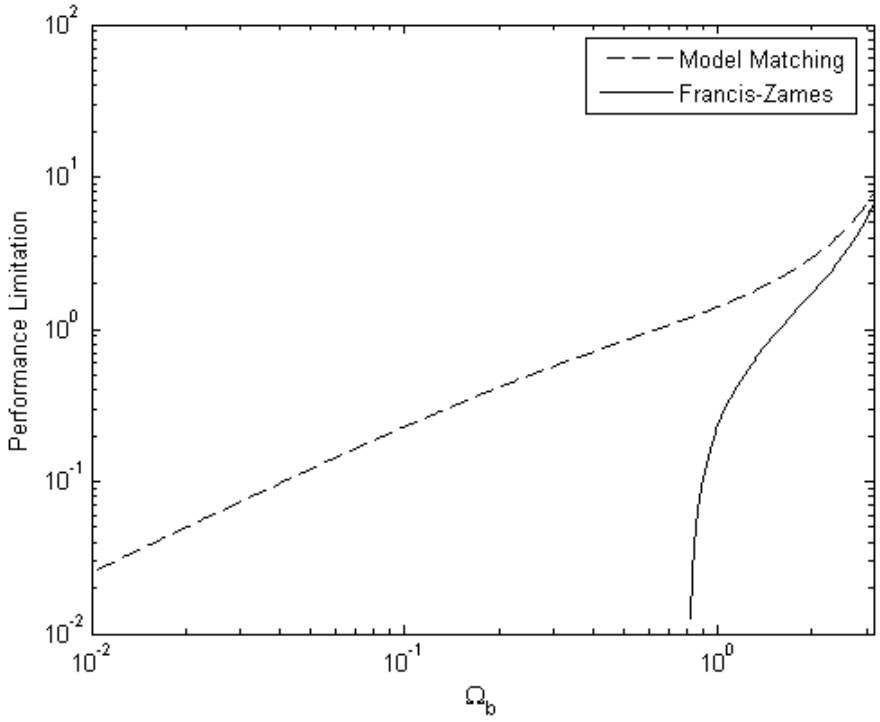

Figure 2.7: Comparing (2.59)-(2.60) to (2.66)-(2.67) for $n = 3$ and one unstable pole at $p = -2$.

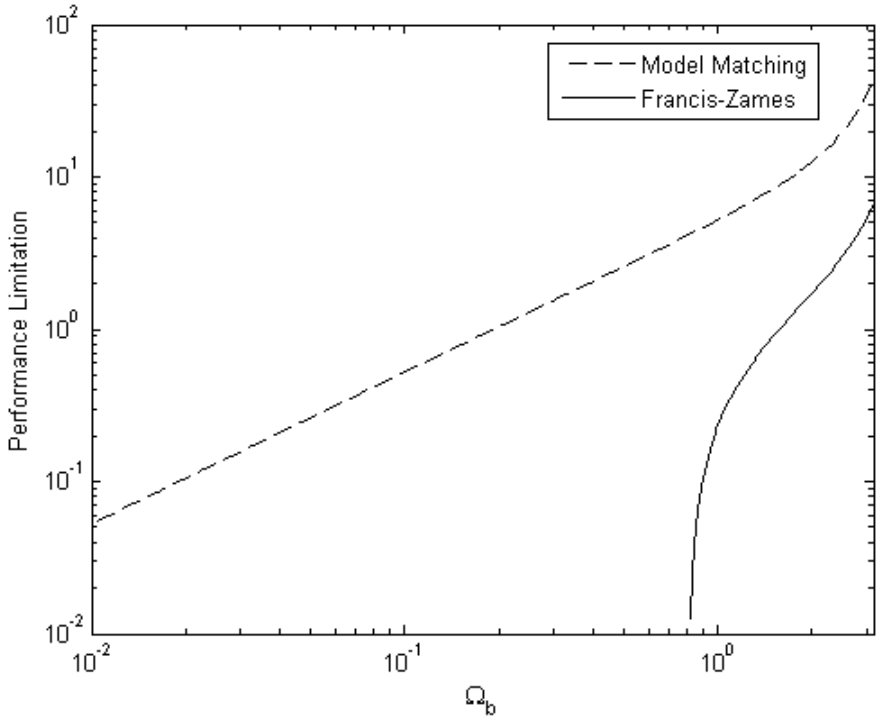

Figure 2.8: Comparing (2.58) to (2.65) for $n = 3$ and one unstable pole at $p = -2$.

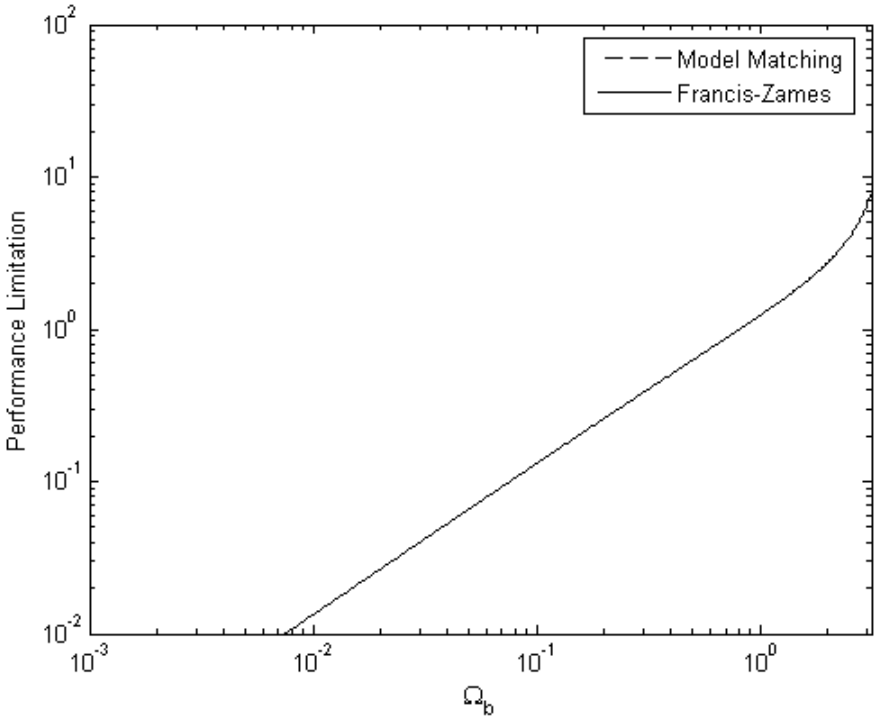

Figure 2.9: Comparing (2.61) to (2.68) for $n = 3$ and for the plant (2.70) which is biproper with one unstable pole at $p = -2$. Note that the dashed curve is the same as the solid curve.

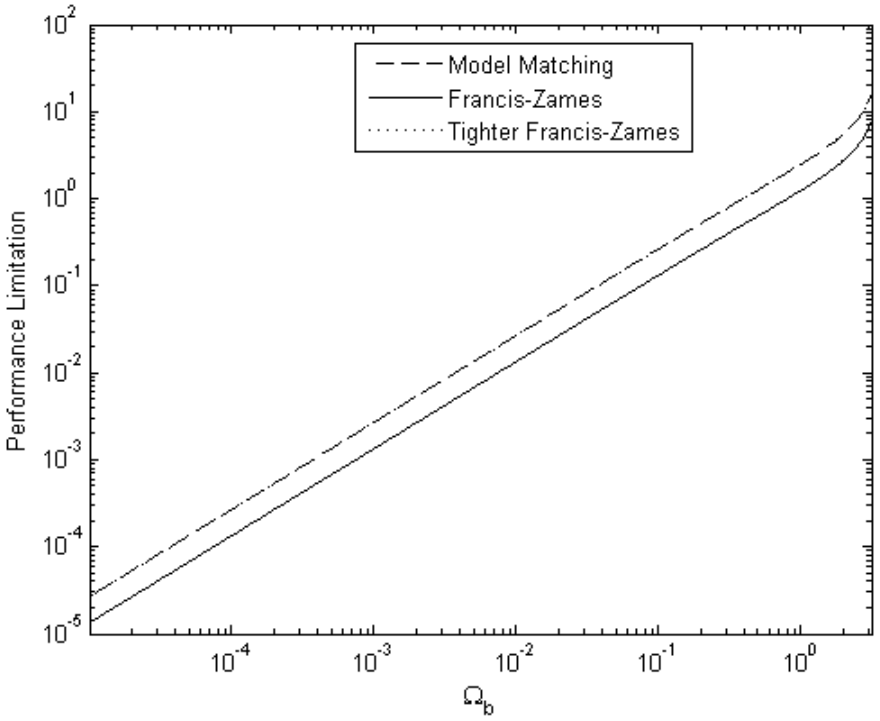

Figure 2.10: Comparing (2.61) to (2.68) for $n = 3$ and for the plant (2.71) which is strictly proper with one unstable pole at $p = -2$. Note that the dotted curve is the same as the dashed curve.

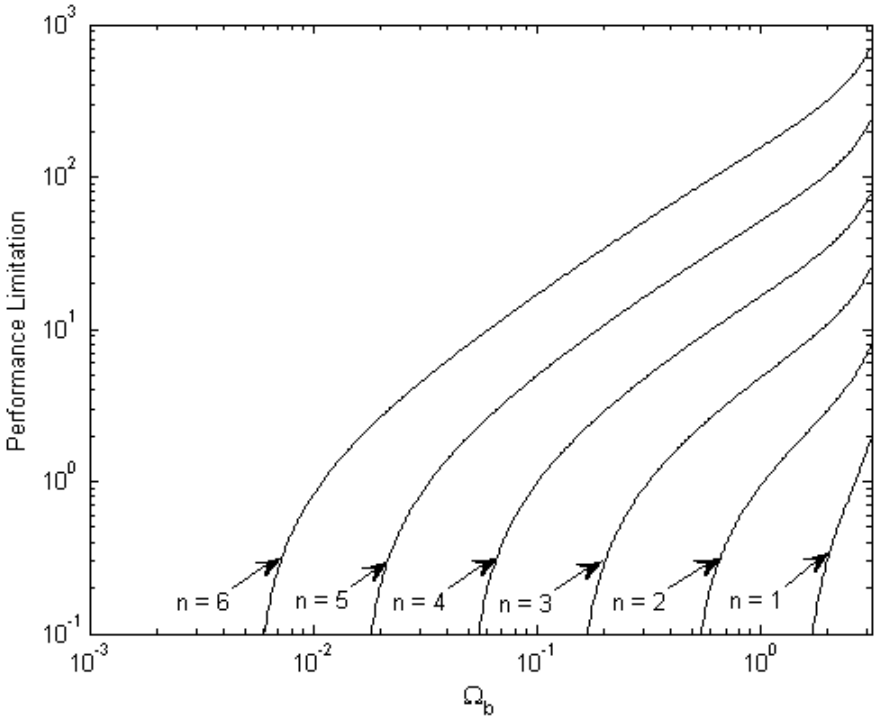

Figure 2.11: Bounds (2.58)-(2.60) for various values of n and Ω_b with P given by (2.72).

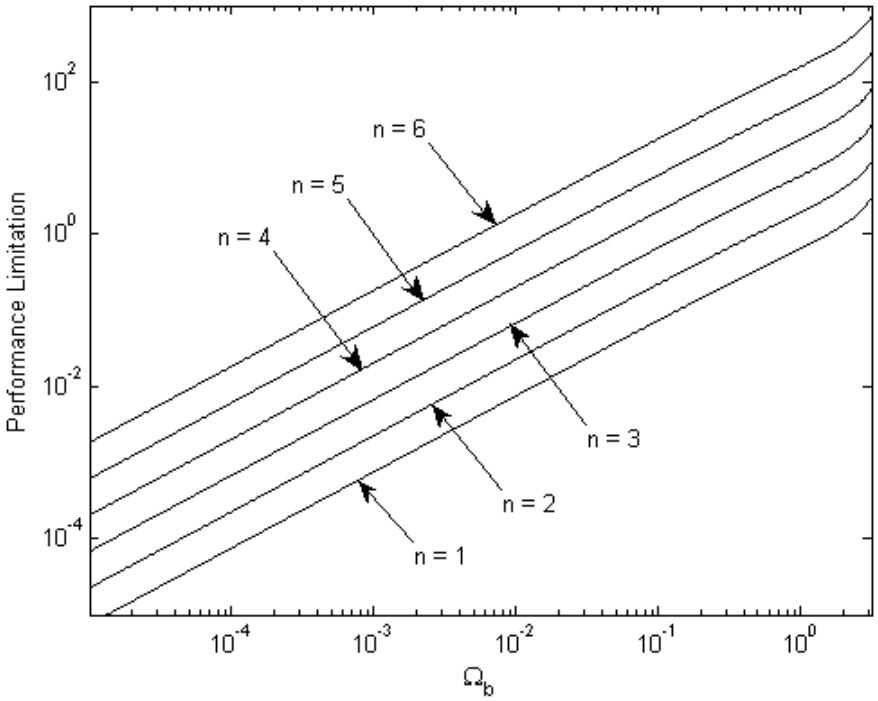

Figure 2.12: Bound (2.61) for various values of n and Ω_b with P given by (2.72).

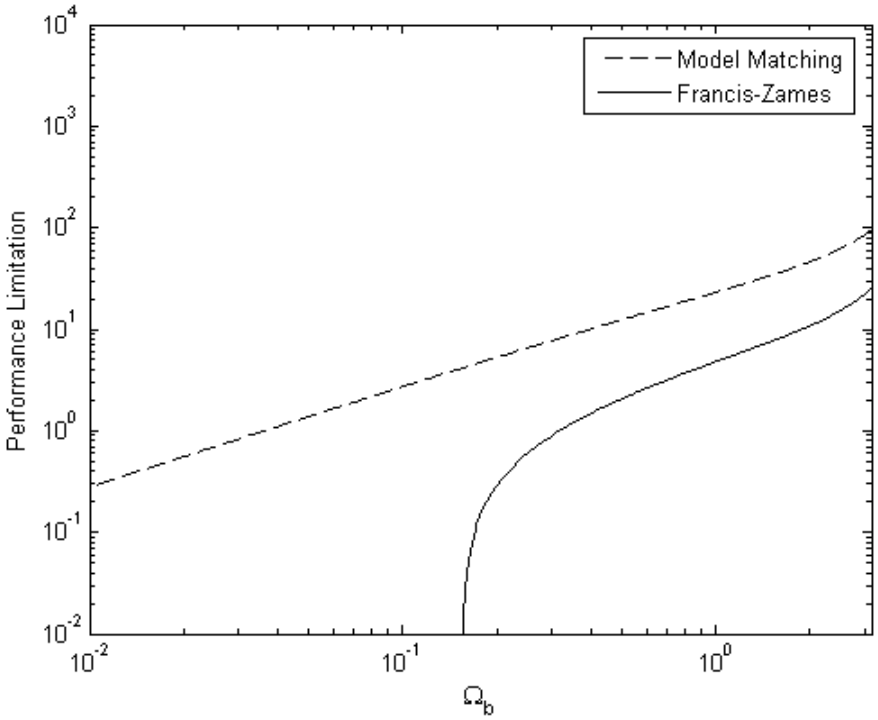

Figure 2.13: Comparing (2.59)-(2.60) to (2.66)-(2.67) for $n = 3$ and two unstable poles at $p = -2, -3$.

Ω_b. Results for tracking, disturbance rejection and sensitivity to plant perturbations are shown in Figure 2.11, and those for noise rejection in Figure 2.12.

As for their conservativeness, again, using the same technique as the previous example, a comparison can be made, again using a delay of three samples ($n = 3$). Figure 2.13 shows the result for disturbance rejection and sensitivity to plant perturbations, Figure 2.14 shows the result for tracking and Figure 2.15 shows the result for noise rejection. In contrast to the previous example, the Francis-Zames bounds are more conservative then for the one-unstable-pole case. This is not surprising since bounds (2.58)-(2.61) are based on only one of the unstable poles, and in effect, ignore the performance degradation caused by the other unstable pole. The lines corresponding to the Francis-Zames bounds would be the same for a plant with only one unstable pole at $p = -3$. This limitation can be seen extremely well for the noise rejection bound shown in Figure 2.15. For the one-unstable-pole case, shown in Figure 2.9, the Francis-Zames bound produces the same curve as the tight model-matching bound. With the addition of a second unstable pole, this is no longer the case, and even the noise rejection bound shows some conservativeness. However, the shape of the curve is correct, and a designer would reach a similar conclusion based on the Francis-Zames bound as with the model-matching derived bound.

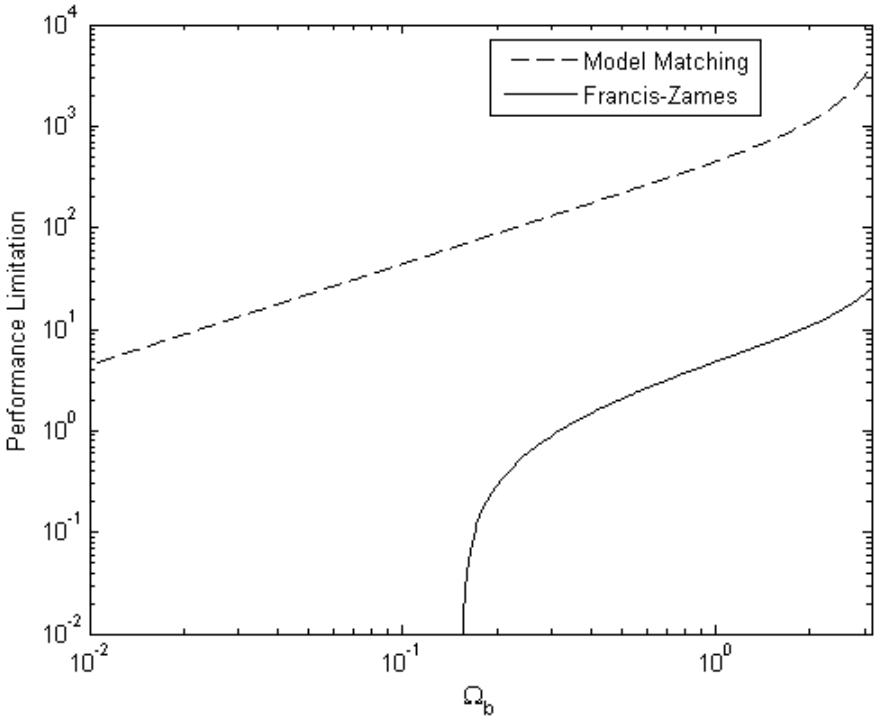

Figure 2.14: Comparing (2.58) to (2.65) for $n = 3$ and two unstable poles at $p = -2, -3$.

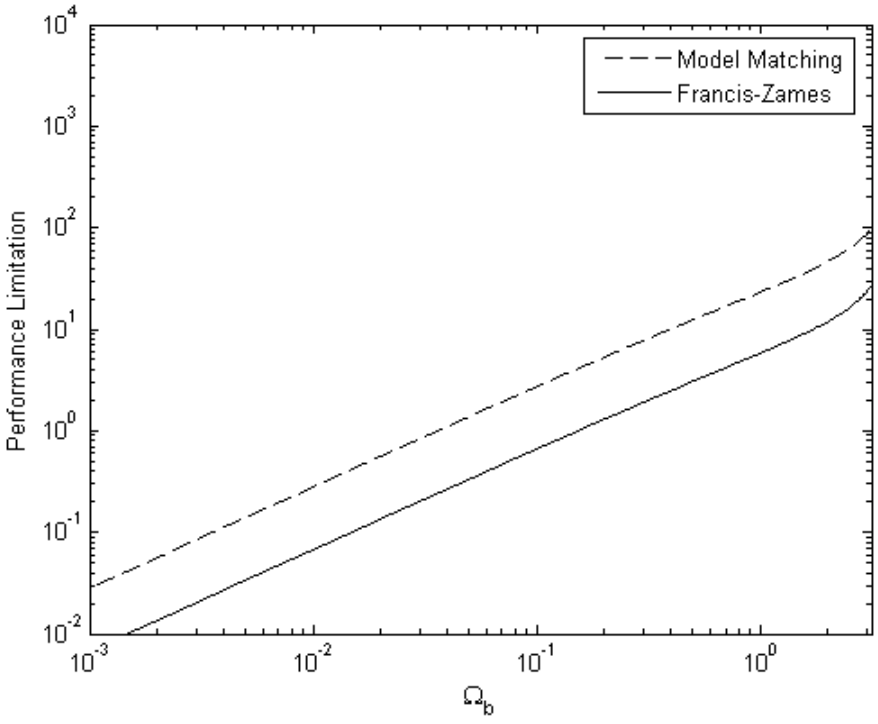

Figure 2.15: Comparing (2.61) to (2.68) for $n = 3$ and two unstable poles at $p = -2, -3$.

Chapter 3

Discrete-Time SISO Estimation

3.1 Overview

The motivation for this research is again the radiotherapy control problem described in Section 1.1. This chapter concerns itself with the estimation subsystem at the top of Figure 1.4. Figure 3.1 (which is a copy of Figure 1.9, repeated here for convenience) shows a two-degree-of-freedom (2-DOF) generalized estimator scheme, with the delayed output generated by passing the output signal through $F[z] = \frac{1}{z^n}$. The estimator's role is to estimate the current output, y, with only the input, u, and a delayed version of the output, y_d, being available. The estimate is denoted by $\hat{y}$.

For the estimation problem, only Q1-Q2 from page 11 are dealt with, since a "recovering" controller does not make sense in the estimation setting. This chapter focuses on answering those two questions, and is laid out in a similar fashion as Chapter 2. The next section presents a new method for parameterizing all asymptotic estimators, resulting in a Youla-esque parameterization for estimators instead of controllers. An "asymptotic estimator" is simply an estimator that estimates perfectly as time goes to ∞ with no noise or disturbances and with a known, nominal plant. After that, Q1 and Q2 are answered for the estimation problem, first for a stable plant, and then for an unstable plant. Commentary on the results (in particular, how they relate to the feedback control results of Chapter 2) are also provided.

Unless specifically noted otherwise, all systems in this chapter are taken as discrete-time, SISO linear time invariant, causal, with proper and rational transfer functions.

3.2 A Parameterization of all Asymptotic Estimators

This section outlines a Youla-esque parameterization of all asymptotic estimators for the estimation problem shown in Figure 3.1. An *asymptotic estimator* is a pair (G_1, G_2) that satisfies the following (for $d = w = 0$):

$$\lim_{k\to\infty} (\hat{y}[k] - y[k]) = 0 \quad \forall u, \forall \text{initial conditions.} \tag{3.1}$$

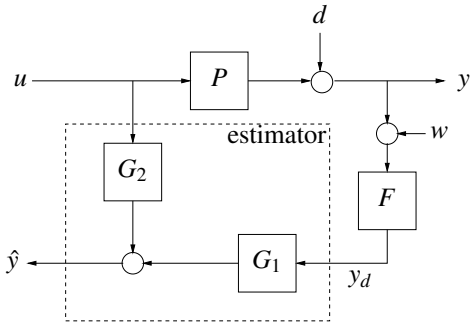

Figure 3.1: A block diagram of the estimation problem with a sensor time delay.

By using the parameterization provided below, performance limitations similar to those derived in Chapter 2 can be found. The parameterization was developed independently in [5] using a state-space approach, and by us in [6] using a transfer function approach. The work in [6] required an extension to account for cases with repeated poles, as well as an extension for MIMO systems, which can be found in [24]. The SISO result with the extension to repeated poles is given by the following theorem:

Theorem 3.1 Consider the estimation scheme in Figure 3.1 with $d = w = 0$. Let $\mathcal{S}$ denote the set of all stable transfer functions and let $p_1, \ldots, p_m$ denote the unstable poles of P, if any exist, with multiplicities $r_1, .., r_m$. Perform a coprime factorization of the system PF, as per Corollary 2.1, resulting in stable proper transfer functions N,M,X, and Y.

Finally, define

$$T_{y\hat{y}} \equiv \frac{\hat{Y}[z]}{Y[z]} = \frac{\hat{Y}[z]}{U[z]} \div \frac{Y[z]}{U[z]} = \frac{G_2 + FG_1P}{P}, \tag{3.2}$$

and the following four sets:

$$\mathcal{A} \equiv \{(G_1, G_2) : (3.1) \text{ is satisfied}\} \tag{3.3}$$

$$\mathcal{B} \equiv \{(G_1, G_2) : G_1 \in \mathcal{S}, G_2 \in \mathcal{S}, T_{y\hat{y}} = 1\} \tag{3.4}$$

$$\begin{aligned} \mathcal{C} \equiv \{&(G_1, G_2) : G_1 \in \mathcal{S} \text{ with} \\ &\text{for } \; i = 1, ..., m \\ &\quad \text{for } \; j = 1, ..., r_{i-1} \\ &\quad\quad \frac{d^j}{dz^i} G_1[z]|_{z=p_i} = \frac{d^j}{dz^i} \frac{1}{F[z]}|_{z=p_i}, \\ &\text{and } G_2 = P(1 - G_1F)\} \end{aligned} \tag{3.5}$$

$$\begin{aligned} \mathcal{D} \equiv \{&(G_1, G_2) : G_1 = MPX + MQ \text{ and} \\ &G_2 = MPY - NQ \text{ for } Q \in \mathcal{S}\}. \end{aligned} \tag{3.6}$$

Then, $\mathcal{A} = \mathcal{B} = \mathcal{C} = \mathcal{D}$. □

Proof: The proof involves showing that the above four sets are equivalent. In order to do this, two pairs will be shown to be the same ($\mathcal{A} = \mathcal{B}$, $\mathcal{B} = \mathcal{C}$), and then $\mathcal{D}$ is shown to be a subset of $\mathcal{B}$ and a superset of $\mathcal{C}$ (i.e., $\mathcal{D} \subseteq \mathcal{B}$ and $\mathcal{D} \supseteq \mathcal{C}$).

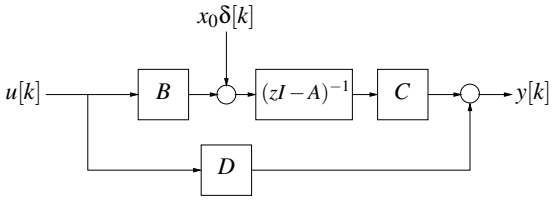

Figure 3.2: Decomposition of a system with state-space realization (A,B,C,D), initial condition $x[0] = x_0$, input $u[k]$, and output $y[k]$. In the diagram, $\delta[k]$ is the unit pulse function.

Step 1: Show $\mathcal{A} \supseteq \mathcal{B}$

To show this, first fix $(G_1,G_2) \in \mathcal{B}$, and introduce minimal state-space realizations for each element in Figure 3.1:

$$\begin{aligned} P &= (A_P,B_P,C_P,D_P) \text{ (with initial state } x_{P0}), \\ F &= (A_F,B_F,C_F,D_F) \text{ (with initial state } x_{F0}), \\ G_1 &= (A_1,B_1,C_1,D_1) \text{ (with initial state } x_{10}), \text{and} \\ G_2 &= (A_2,B_2,C_2,D_2) \text{ (with initial state } x_{20}). \end{aligned}$$

Now, by superposition, the zero-input response and the zero-initial-condition response of a linear system with input u, output y, state x, initial condition x_0, and state-space matrices (A,B,C,D) can be separated, as shown in Figure 3.2.

That is, the output can be decomposed as

$$Y[z] = H[z] \cdot U[z] + C(zI-A)^{-1}X_0[z],$$

where $H[z] \equiv D + C(zI-A)^{-1}B$ and $X_0[z]$ is the Z-transform of $x_0\delta$, i.e., $X_0[z] = x_0$. Apply this decomposition to each element in Figure 3.1, to obtain

$$Y[z] = P[z]U[z] + C_P(zI-A_P)^{-1}x_{P0} \tag{3.7}$$

$$\begin{aligned} \hat{Y}[z] &= (G_2[z] + G_1[z]F[z]P[z]) \cdot U[z] \\ &\quad + C_2(zI-A_2)^{-1}x_{20} + C_1(zI-A_1)^{-1}x_{10} \\ &\quad + G_1[z]C_F(zI-A_H)^{-1}x_{F0} \\ &\quad + G_1[z]F[z]C_P(zI-A_P)^{-1}x_{P0}. \end{aligned} \tag{3.8}$$

Define $e \equiv \hat{y} - y$ and use (3.7)–(3.8) to obtain

$$\begin{aligned} E[z] &= (G_2[z] + G_1[z]F[z]P[z] - P[z]) \cdot U[z] \\ &\quad + C_2(zI-A_2)^{-1}x_{20} + C_1(zI-A_1)^{-1}x_{10} \\ &\quad + G_1[z]C_F(zI-A_F)^{-1}x_{F0} \\ &\quad + (G_1[z]F[z]-1)C_P(zI-A_P)^{-1}x_{P0}. \end{aligned} \tag{3.9}$$

Next, use the facts that $G_2 + G_1FP = P$ and $G_1F - 1 = -G_2/P$ (both which follow from $T_{y\hat{y}} = 1$) to obtain

$$\begin{aligned} E[z] &= C_2(zI - A_2)^{-1}x_{20} + C_1(zI - A_1)^{-1}x_{10} \\ &\quad + G_1[z]C_F(zI - A_F)^{-1}x_{H0} \\ &\quad - \frac{G_2[z]}{P[z]}C_P(zI - A_P)^{-1}x_{P0}. \end{aligned} \tag{3.10}$$

Due to the stability assumptions on G_1, G_2, and F, each of the first three terms in (3.10) has stable poles. The last term in (3.10) also has stable poles; this can be argued by writing the term as

$$\frac{G_2[z]}{P[z]}\frac{C_P\text{Adj}(zI - A_P)x_{P0}}{\det(A_P)},$$

and recognizing that unstable poles can arise from exactly three sources:

- unstable roots of $\det(A_P)$ (but all such roots are canceled by poles in $P[z]$),
- unstable zeros of $P[z]$ (but, since $T_{y\hat{y}} = 1$, all such zeros are canceled by zeros of $G_2[z]$), and
- unstable poles of $G_2[z]$ (but there are none since G_2 is stable).

We conclude that the poles of each term in (3.10) are stable, and therefore, for any x_{P0}, x_{F0}, x_{10}, and x_{20}, and any signal u, $e[k] \to 0$ as $k \to \infty$. Hence, $(G_1, G_2) \in \mathcal{A}$ and $\mathcal{A} \supseteq \mathcal{B}$.

Step 2: Show $\mathcal{A} \subseteq \mathcal{B}$

Fix $(G_1, G_2) \in \mathcal{A}$. The expression (3.9) for $E[z]$ still holds. Since, for any x_{P0}, x_{F0}, x_{10}, and x_{20}, and any signal u, $e[k] \to 0$ as $k \to \infty$, we conclude that:

- the coefficient of $U[z]$ in (3.9) must be zero (i.e., $G_2 + G_1FP - P = 0$, which is equivalent to $T_{y\hat{y}} = 1$),
- the coefficient of x_{20} in (3.9) must have no unstable poles (i.e., G_2 must be stable), and
- the coefficient of x_{10} in (3.9) must have no unstable poles (i.e., G_1 must be stable).

These three conclusions imply that $(G_1, G_2) \in \mathcal{B}$; hence, $\mathcal{A} \subseteq \mathcal{B}$, and therefore $\mathcal{A} = \mathcal{B}$.

Next, we will show that $\mathcal{B} = \mathcal{C}$ for the special case of non-repeated poles (i.e., $r_i = 1 \forall i$). To see the repeated pole case, refer to [24].

Step 3: Show $\mathcal{B} \subseteq \mathcal{C}$

Fix $(G_1, G_2) \in \mathcal{B}$, i.e., $G_1 \in \mathcal{S}$, $G_2 \in \mathcal{S}$ and $T_{y\hat{y}} = 1$. Then,

$$\begin{aligned} T_{y\hat{y}} &= \frac{G_2 + FG_1P}{P} = 1 \\ \Rightarrow G_2 + FG_1P &= P \\ \Rightarrow G_2 &= P(1 - FG_1). \end{aligned} \tag{3.11}$$

Since $G_2 \in \mathcal{S}$ it follows from (3.11) that $1 - FG_1$ cancels out any unstable poles of P, i.e.,

$$\begin{aligned} 1 - F(p_i)G_1(p_i) &= 0 \\ \Rightarrow G_1(p_i) &= \frac{1}{F(p_i)}. \end{aligned}$$

which is the form of G_1 and G_2 for $\mathcal{C}$. Therefore, $\mathcal{B} \subseteq \mathcal{C}$.

Step 4: Show $\mathcal{B} \supseteq \mathcal{C}$

Fix $(G_1, G_2) \in \mathcal{C}$, i.e., $G_1 \in \mathcal{S}$ with $G_1(p_i) = \frac{1}{F(p_i)}$, $G_2 = P(1 - FG_1)$. Then it follows that, $G_2 \in \mathcal{S}$ since:

- $F \in \mathcal{S}$, $G_1 \in \mathcal{S}$ implies that $1 - FG_1 \in \mathcal{S}$
- $1 - F(p_i)G_1(p_i) = 0$ implies that p_i is a zero of $1 - FG_1$, giving $P(1 - FG_1) \in \mathcal{S}$.

Finally to see that $T_{y\hat{y}} = 1$ simply substitute G_1, G_2 into (3.2), resulting in:

$$\begin{aligned} T_{y\hat{y}} &= \frac{G_2 + PFG_1}{P} \\ &= \frac{P - PFG_1 + PFG_1}{P} \\ &= 1. \end{aligned}$$

Therefore, $\mathcal{C} \subseteq \mathcal{B}$ and $\mathcal{B} = \mathcal{C}$ for the non-repeated pole case.

Step 5: Show $\mathcal{D} \subseteq \mathcal{B}$

First, fix $(G_1, G_2) \in \mathcal{D}$. Hence, there is a $Q \in \mathcal{S}$ such that

$$G_1 = MPX + MQ \tag{3.12}$$
$$G_2 = MPY - NQ. \tag{3.13}$$

Note the following:

- G_1 in (3.12) is stable and proper since X, M, Q, and $MP = N/F$ are stable and proper.
- Similarly, G_2 in (3.13) is stable and proper.
- Use (3.12), (3.13), (3.2) and Corollary 2.1 to calculate

$$\begin{aligned} T_{y\hat{y}} &= \frac{G_2}{P} + FG_1 \\ &= MY - \frac{NQ}{P} + FMPX + HMQ \\ &= 1 - NX - \frac{NQ}{P} + FMPX + HMQ \\ &= 1 - (N - FMP)X - \left(\frac{N}{P} - FM\right)Q = 1. \end{aligned}$$

We conclude that $(G_1, G_2) \in \mathcal{B}$, and therefore $\mathcal{D} \subseteq \mathcal{B}$.

Step 6: Show $\mathcal{D} \supseteq \mathcal{C}$

Fix $(G_1, G_2) \in \mathcal{C}$. It is claimed that (G_1, G_2) also lies in $\mathcal{D}$ with the following particular value of Q:

$$Q_0 \equiv \frac{G_1 - MPX}{M}. \tag{3.14}$$

To verify the claim, observe that:

- $G_1 = MPX + MQ_0$ holds (trivially).
- $G_2 = MPY - NQ_0$ holds because

$$\begin{aligned} G_2 &= P(1 - G_1 F) \\ &= P(NX + MY - G_1 F) \\ &= P(FMPX + MY - G_1 F) \\ &= PMY - PF(G_1 - MPX) \\ &= MPY - \frac{N}{M}(G_1 - MPX) \\ &= MPY - NQ_0. \end{aligned}$$

- Q_0 is proper because both $G_1 - MPX$ and $1/M$ are proper.
- Q_0 is stable because
  - $(G_1 - MPX)$ is stable (which follows because $MP = N/F$ is stable), and
  - the unstable zeros of M, i.e., the values $p_1, \ldots, p_m$, are also zeros of $G_1 - MPX$; this last fact follows since

$$\begin{aligned} G_1(p_i) &= \frac{1}{F(p_i)} = \frac{P(p_i)M(p_i)X(p_i)}{N(p_i)X(p_i)} \\ &= \frac{P(p_i)M(p_i)X(p_i)}{1 - M(p_i)Y(p_i)} = P(p_i)M(p_i)X(p_i). \end{aligned}$$

We conclude that $(G_1, G_2) \in \mathcal{D}$; hence, $\mathcal{D} \supseteq \mathcal{C}$ and $\mathcal{A} = \mathcal{B} = \mathcal{C} = \mathcal{D}$. □

Note from (3.4) that every asymptotic estimator satisfies $T_{y\hat{y}} = 1$; hence, unlike in the feedback control framework, there is no sense in considering performance limitations on "tracking". For the remainder of this chapter, the parameterization in Theorem 3.1 is used to characterize the performance of the time-delayed estimation problem. For stable plants, a simpler form for $\mathcal{D}$ can be found, and this is given in the following corollary:

Corollary 3.1 Given a stable plant P, $\mathcal{D}$ from Theorem 3.1 can be written as:

$$\begin{aligned} \mathcal{D} \equiv \{&(G_1, G_2) : G_1 = Q \text{ and} \\ &G_2 = P - PFQ \text{ for } Q \in \mathcal{S}\}. \end{aligned} \tag{3.15}$$

□

Proof: To get the result, substitute into (3.6) the stable coprime terms given by Corollary 2.2 for M, N, X, and Y. □

3.3 Stable Plant Case

This section answers Q1-Q2 from the end of Chapter 1 for the estimation problem of Figure 3.1 assuming a stable plant. The results in this section were first reported in [6], and use the results of Theorem 3.1, along with the model-matching solution from Section 2.2.2. Q3 will not be answered for the estimation problem, as the idea of a "recovering" controller no longer makes sense.

Just like the stable-plant case for the feedback control problem in Section 2.3, there is no fundamental performance limitation for noise rejection. Choosing $G_2 = P$ and $G_1 = 0$ results in an asymptotic estimator that exhibits perfect noise rejection (i.e., $T_{we} = 0$ where $e = y - \hat{y}$). Also of note is the similarity of the results of the estimation problem to the results of the feedback control problem; this similarity will be discussed in more detail after the results have been presented.

3.3.1 Is there a fundamental performance limitation?

It turns out that the answer is the same as for the feedback control case of the previous chapter: there exists a fundamental performance limitation for disturbance rejection and sensitivity to plant perturbations for any asymptotic estimator. This result is given by the following theorem:

Theorem 3.2 Assume $P[z]$ is stable for the 2-DOF estimation setup shown in Figure 3.1. For the sensor time delay $F[z] = \frac{1}{z^n}$ with $n \geq 1$, define

$$\alpha_n \equiv \inf_{Q \in \mathcal{S}} \|W_5 - FQ\|_\infty > 0 \tag{3.16}$$

$$\kappa_n \equiv \inf_{Q \in \mathcal{S}} \|W_6 - FQ\|_\infty > 0. \tag{3.17}$$

Then, for any asymptotic estimator,

$$\|W_5 S\|_\infty \geq \alpha_n \tag{3.18}$$

$$\|W_6 T_{de}\|_\infty \geq \kappa_n. \tag{3.19}$$

□

Proof: The proof is similar to the proof of Theorem 2.1, with the primary difference being the use of Corollary 3.1 instead of Youla parameterization (Corollary 2.5). Start by calculating the two required transfer functions (T_{de} and S):

$$\begin{aligned} T_{de} &= 1 - FG_1 \\ &= 1 - FQ, \end{aligned} \tag{3.20}$$

and, beginning with (1.19) and using (3.2),

$$\begin{aligned} S &= \frac{\partial T_{y\hat{y}}[z]}{\partial P[z]} \frac{P[z]}{T_{y\hat{y}}[z]} \\ &= \frac{PFG_1 - G_2 - PFG_1}{P^2} \frac{P^2}{G_2 + PFG_1} \\ &= \frac{-G_2}{G_2 + PFG_1} \\ &= \frac{-1}{1 + PF\frac{G_1}{G_2}} \\ &= \frac{-1}{1 + \frac{PFQ}{P - PFQ}} \\ &= \frac{-P + PFQ}{P - PFQ + PFQ} \\ &= -1 + FQ. \end{aligned} \tag{3.21}$$

$$\tag{3.22}$$

Using (3.20) and (3.22), multiply by their respective weighting functions from Table 1.1, and take their H_∞ norms:

$$\begin{aligned} \|W_5 S\|_\infty &= \| - W_5 + W_5 FQ\|_\infty & (3.23) \\ &= \|W_5 - W_5 FQ\|_\infty & (3.24) \\ \|W_6 T_{de}\|_\infty &= \|W_6 - W_6 FQ\|_\infty. & (3.25) \end{aligned}$$

By minimizing the norms over all stable Q, the desired bounds (3.18) and (3.19) can be found. Weights W_5 and W_6 can be dropped from the T_2 term of the model-matching problem since they can only make the optimal norm worse (see the proof of Theorem 2.1 for a more detailed discussion). □

Comparing the results from the estimation problem given by Theorem 3.2 to the feedback control problem given by Theorem 2.1, an interesting observation can be made: the sensor time delay leads to the same fundamental performance limitations for both the estimation problem (**??**)-(**??**) and the control problem (2.29)-(2.31). Given that the estimation and control problems are only related by the sensor time delay, this is quite surprising. However, there is a subtle difference between the two results, and that involves the effect of the plant. For the estimation problem, the actual weighted disturbance rejection H_∞-norm is given by (3.25), whereas for the feedback control case, it is given by (see (2.41)):

$$\|W_3 T_{dy}\|_\infty = \|W_3 - W_3 PFQ\|_\infty \tag{3.26}$$

If it was desired to calculate the actual best achievable performance, we would simply find the infimum over all stable Q of (3.26) and (3.25). However, for the same plant and weighting function ($W_3 = W_6$),

$$\inf_{Q\in\mathcal{S}} \|W_3 - W_3PFQ\|_\infty \geq \inf_{Q\in\mathcal{S}} \|W_6 - W_6FQ\|_\infty. \tag{3.27}$$

Inequality (3.27) implies that the feedback control bounds found in Section 2.3 are more conservative than the estimation bounds found in this section. Any plant zeros with magnitude greater than one or any plant that is not biproper will degrade the best achievable performance of the feedback control system, but will have no effect for the estimation problem. Moreover, from (3.24)-(3.25), we see that for the estimation problem all stable plants have identical disturbance rejection and sensitivity to plant perturbations.

3.3.2 What happens to performance as the sensor time delay is increased?

Due to the similarities between Theorem 3.2 and Theorem 2.1, the same trends occur for the estimation problem as for the feedback control problem. As a result, the discussion in Section 2.3.2 also applies for the estimation problem, meaning that α_n and κ_n are non-decreasing functions of n and are bounded above by $\|W_5\|_\infty$ and $\|W_6\|_\infty$ respectively. Formally, this means that

$$\begin{aligned} \alpha_n &\leq \alpha_{n+1}\ \forall n \geq 1 \\ \kappa_n &\leq \kappa_{n+1}\ \forall n \geq 1, \end{aligned}$$

and

$$\begin{aligned} \alpha_n &\leq 1\ \forall n \geq 1 \\ \kappa_n &\leq 1\ \forall n \geq 1. \end{aligned}$$

3.3.3 Example

Since the bounds of Theorem 3.2 are the same as those for Theorem 2.1, this section will not repeat their calculation. Instead, in one example we compare the performance of two different estimators to the optimal performance, and in a second example we clarify the effect of plant non-minimum phase zeros.

Example 5: Using

$$P[z] = \frac{0.044332}{z-0.9704} \tag{3.28}$$

$$W_6[z] = \frac{z\tan(\frac{\Omega_b}{2}) + \tan(\frac{\Omega_b}{2})}{z(\tan(\frac{\Omega_b}{2})+1) + \tan(\frac{\Omega_b}{2}) - 1}, \tag{3.29}$$

consider a standard Luenberger observer for a delay of three samples (i.e., $F[z] = \frac{1}{z^3}$), as well as an estimator designed for optimal weighted disturbance rejection with $\Omega_b = 0.1$ for the given weighting function (3.29). The Luenberger observer has its poles placed at $z = 0.15, 0.2, 0.25,$ and 0.3, which is then mapped over to the 2-DOF estimator setting of Figure 3.1, resulting in:

$$\begin{aligned} G_1[z] &= \frac{0.044332(z+0.5204)(z^2-0.45z+0.6)}{(z-0.3)(z-0.25)(z-0.2)(z-0.15)} \\ G_2[z] &= \frac{0.30525(z+2.241x10^{-6})(z^2-2.241x10^{-6}z+5.021x10^{-12})}{(z-0.3)(z-0.25)(z-0.2)(z-0.15)}. \end{aligned} \quad (3.30)$$

The optimal estimator constructed for $\Omega_b = 0.1$ results in the following G_1 and G_2:

$$\begin{aligned} G_1[z] &= \frac{3.4324z^3}{(z+1)(z^2+0.7693z+0.2877)} \\ G_2[z] &= \frac{0.044332(z-0.9047)(z^2+2.674z+3.476)}{(z-0.9704)(z+1)(z^2+0.7693z+0.2877)}. \end{aligned} \quad (3.31)$$

Note that the pole at $z = -1$ arises due to the improperness of the optimal Q found in the model-matching solution. This unstable pole can be eliminated using a proper approximation of the improper Q. For the purposes of keeping this example simple, this step was not carried out.

With these two estimators, we can now plot their weighted disturbance rejection performance over a wide range of Ω_b for the given delay of $n = 3$. The performance of the two estimators is compared to the optimal disturbance rejection (**??**) in Figure 3.3. Of note is that the standard Luenberger observer performs worse than optimal at all frequencies, and is substantially worse than the estimator designed with $\Omega_b = 0.1$, except at large values of Ω_b.

Example 6: This example compares, for a given plant and weighting function, the optimal disturbance rejection for the estimation problem of Figure 3.1 (**??**) with that for the feedback control problem of Figure 1.8 (2.42). Utilizing the same weighting function as Example 5 (3.29), and the following plant, which contains a non-minimum-phase zero at $z = 5$,

$$P[z] = \frac{z-5}{z-0.9704}, \quad (3.32)$$

the optimal disturbance rejection can be computed. The results are shown in Figure 3.4, where it is clear that the optimal performance for the estimation problem is lower (i.e., better) than for the feedback control problem. In essence, the non-minimum-phase zero of the plant has no effect on the optimal performance of the estimation problem, but does have an effect for the feedback control problem. The end result is that the performance bounds given by Theorem 3.2 are tighter than the bounds given by Theorem 2.1. It should also be noted that the disturbance rejection bound given by (2.31) in Theorem 2.1 would generate the same curve as for the estimation problem.

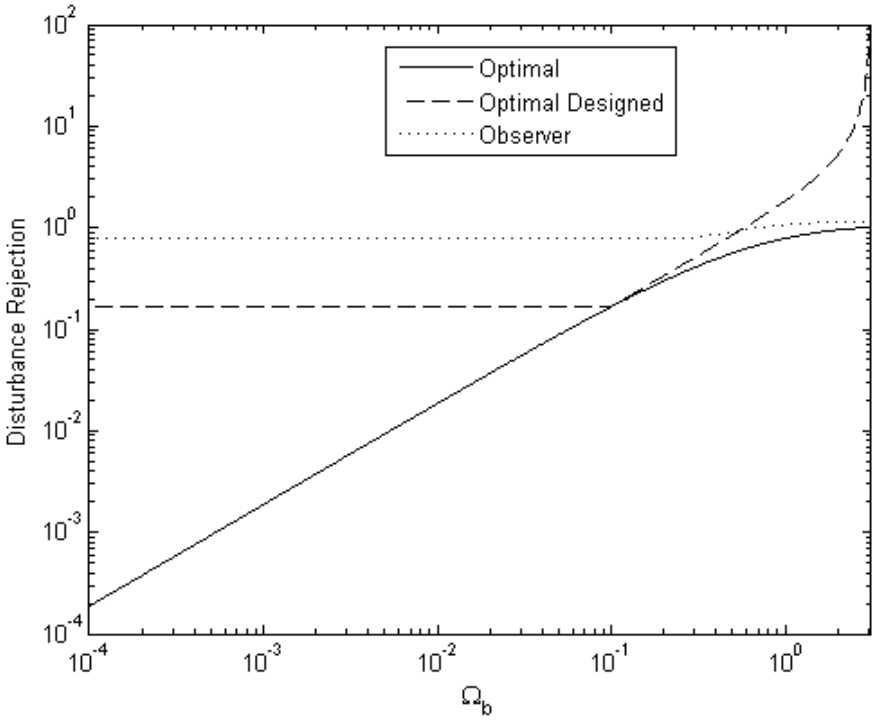

Figure 3.3: Comparing the performance of a Luenberger observer (3.30) to an estimator designed optimally for $\Omega_b = 0.1$ (3.31) and to the optimal performance for all values of Ω_b.

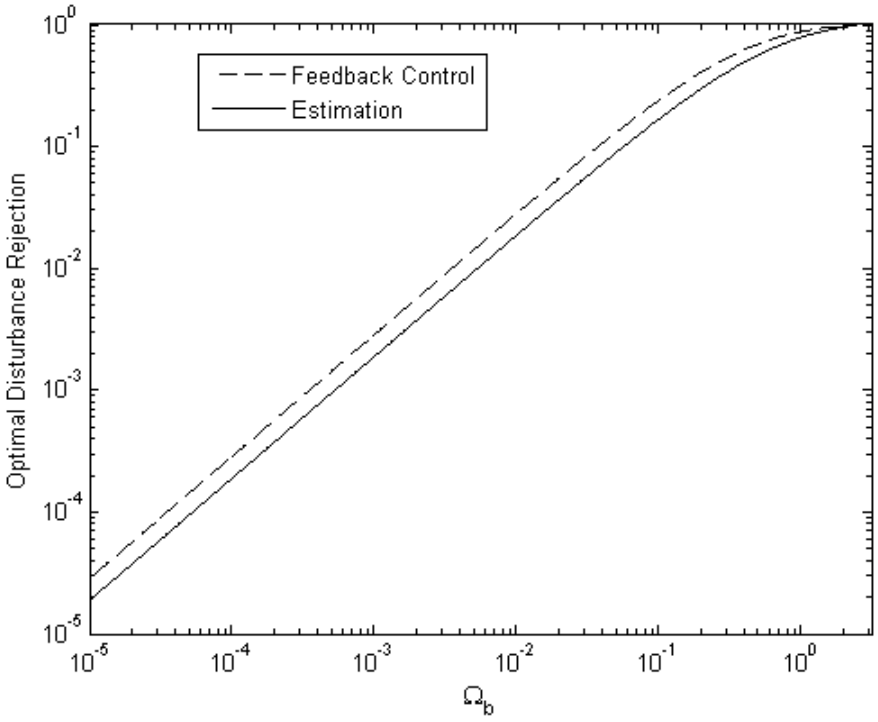

Figure 3.4: Optimal disturbance rejection for the estimation and feedback control problems for the plant given by (3.32).

3.4 Unstable Plant Case

This section answers Q1-Q2 from the end of Chapter 1 for the unstable plant case. Just as for the feedback control situation, two forms of performance limitations are presented: first, an insightful bound based on the Francis-Zames bound of Section 2.2.3, and then a non-insightful bound based on model-matching techniques. In another parallel between the feedback control problem and the estimation problem, there is a fundamental performance limitation on noise rejection for the estimation problem.

3.4.1 Is there a fundamental performance limitation?

The answer is a resounding yes, as shown by the following two theorems. Theorem 3.3 presents insightful, but conservative, bounds for weighted disturbance rejection, sensitivity to plant perturbations, and noise rejection. Theorem 3.4 presents tight, but less insightful, bounds for the same three metrics. As in the results for the feedback control problem, due to a $-\|W\|_\infty$ term for weighted disturbance rejection and sensitivity to plant perturbations, the insightful bound is trivial for systems with small delays and "generous" weighting functions. This term does not appear in the model-matching bounds, which are positive for any delay and any weighting function.

The following technical lemma simplifies the proofs to follow:

Lemma 3.1 For an unstable plant P in Figure 3.1 with an asymptotic estimator, with M, N, X, and Y a coprime factorization of PF given by Corollary 2.1, the following holds:

$$\begin{aligned} S &= -MY + MFQ &&= -1 + NX + MFQ && (3.33)\\ T_{de} &= MY - MFQ &&= 1 - NX - MFQ && (3.34)\\ T_{we} &= NX + MFQ &&= 1 - MY + MFQ. && (3.35) \end{aligned}$$

□

Proof: The proof follows using simple algebra on the various transfer functions after substituting G_1 and G_2 as given by (3.6) and using the coprime factorization identity (2.4). The technique will be demonstrated for S with the remaining two left to the reader. The proof starts from the simplest form of S, given by (3.21):

$$
\begin{aligned}
S &= \frac{-1}{1+PF\frac{G_1}{G_2}} \\
&= \frac{-1}{1+\frac{N}{M}\frac{MPX+MQ}{MPY-NQ}} \\
&= \frac{-MPY+NQ}{MPY+NPX-NQ+NQ} \\
&= \frac{-MPY+MPFQ}{P(MY+NX)} \\
&= -MY+MFQ \\
&= -1+NX+MFQ.
\end{aligned}
$$

□

And now for the two main results, starting with the insightful performance limitations based on the Francis-Zames bound:

Theorem 3.3 Assume that P in Figure 3.1 is unstable, with possibly repeated unstable poles, denoted p_i, $i = 1,\ldots,m$. Then, for any asymptotic estimator, the performance measures in the estimation column of Table 1.1 are bounded from below as follows:

$$\|W_5 S\|_\infty^{DT} \geq \max_{i=1,\ldots,m} |W_5(p_i)\cdot p_i^n| - \|W_5\|_\infty^{DT} \tag{3.36}$$

$$\|W_6 T_{de}\|_\infty^{DT} \geq \max_{i=1,\ldots,m} |W_6(p_i)\cdot p_i^n| - \|W_6\|_\infty^{DT} \tag{3.37}$$

$$\|W_7 T_{we}\|_\infty^{DT} \geq \max_{i=1,\ldots,m} |W_7(p_i)\cdot p_i^n|. \tag{3.38}$$

□

Proof: The proof is similar to that of Theorem 2.3, and is based on Lemma 2.4. We will start by proving (3.36).

First, use the bilinear transformation (1.14) on $1+S$, resulting in $1+\tilde{S}$. Define $\tilde{p}_i$, $i = 1,...,a$, to be any poles of $\tilde{P}\tilde{F}$ with positive real parts, and $\tilde{z}_j$, $j = 1,...,b$, to be any zeros of $\tilde{F}$ with positive real parts. Note that only the plant poles are used; plant zeros with positive real parts have no effect on the result. Also note that for $F[z] = \frac{1}{z^n}$, $\tilde{F}(s)$ has n zeros at $s = 1$. Choose, for the purposes of applying Lemma 2.4,

$$\tilde{R} = 1+\tilde{S},$$

where $\tilde{p}_i$ and $\tilde{z}_j$ are defined above. We need to show that $\tilde{R}(\tilde{p}_i) = 1$ and $\tilde{R}(\tilde{z}_i) = 0$. To this end, note that

$$
\begin{aligned}
\tilde{M}(\tilde{p}_i) &= 0 \\
\tilde{N}(\tilde{z}_j) &= 0 \\
\tilde{F}(\tilde{z}_i) &= 0.
\end{aligned}
$$

Now, apply Lemma 3.1 to $\tilde{S}$, giving

$$\begin{aligned} 1+\tilde{S} &= 1-\tilde{M}\tilde{Y}+\tilde{M}\tilde{F}\tilde{Q} && (3.39)\\ &= \tilde{N}\tilde{X}+\tilde{M}\tilde{F}\tilde{Q}. && (3.40)\end{aligned}$$

From (3.39),

$$\begin{aligned} 1+\tilde{S} &= 1-\tilde{M}\tilde{Y}+\tilde{M}\tilde{F}\tilde{Q}\\ \Rightarrow 1+\tilde{S}(\tilde{p}_i) &= 1-\tilde{M}(\tilde{p}_i)\tilde{Y}(\tilde{p}_i)+\tilde{M}(\tilde{p}_i)\tilde{F}(\tilde{p}_i)\tilde{Q}(\tilde{p}_i)\\ \Rightarrow \tilde{R}(\tilde{p}_i) &= 1 && (3.41)\end{aligned}$$

and then from (3.40),

$$\begin{aligned} 1+\tilde{S} &= \tilde{N}\tilde{X}+\tilde{M}\tilde{F}\tilde{Q}\\ \Rightarrow 1+\tilde{S}(\tilde{z}_j) &= \tilde{N}(\tilde{z}_j)\tilde{X}(\tilde{z}_j)+\tilde{M}(\tilde{z}_j)\tilde{F}(\tilde{z}_j)\tilde{Q}(\tilde{z}_j)\\ \Rightarrow \tilde{R}(\tilde{z}_i) &= 0. && (3.42)\end{aligned}$$

The proof from this point is exactly the same as for Theorem 2.3, and will not be repeated here.

For the remaining two bounds, using Lemma 3.1, it is easy to show that:

$$\begin{aligned} 1+S &= 1-T_{de}\\ 1+S &= T_{we}.\end{aligned}$$

As a result, we can also apply Lemma 2.4 to $1-T_{de}$ and to T_{we}, and then continue exactly as before. □

Just as in the stable plant case, the asymptotic estimator bounds (in Theorem 3.3) are identical to those for the feedback control problem (in Theorem 2.3). However, there is a subtle difference in conservativeness between the asymptotic estimator bounds and the feedback control bounds. Specifically, for the feedback control problem, an extra term dealing with the non-minimum-phase zeros of $\tilde{P}$ arises, and is eliminated, in (2.64), but this term does not arise in the estimator problem. Consequently, the bounds are more conservative for the feedback control problem than for the estimator problem. This is discussed in more detail with the help of an example at the end of this section. We now turn to Theorem 3.4 which provides tight bounds for the estimator problem and sheds more light on the above discussion:

Theorem 3.4 Consider the estimation setup of Figure 3.1 where $P[z]$ is possibly unstable. Perform a coprime factorization on the plant and delay, i.e., $P[z]F[z]$, resulting in $N[z]$, $M[z]$, $X[z]$, and $Y[z]$ as given by Corollary 2.1. Then for any asymptotic estimator,

$$\begin{aligned} \|W_5S\|_\infty &\geq \inf_{Q\in\mathcal{S}}\|W_5MY-W_5MFQ\|_\infty && (3.43)\\ \|W_6T_{de}\|_\infty &\geq \inf_{Q\in\mathcal{S}}\|W_6MY-W_6MFQ\|_\infty && (3.44)\\ \|W_7T_{we}\|_\infty &\geq \inf_{Q\in\mathcal{S}}\|W_7NX+W_7MFQ\|_\infty. && (3.45)\end{aligned}$$

□

Proof: Use Lemma 3.1 as a starting point, and then simply follow the same procedure as that used in the proof of Theorem 2.4. □

The lack of performance degradation from the non-minimum-phase zeros of $\tilde{P}$ is made even more clear in Theorem 3.4. Consider the noise rejection bound for the feedback control problem given by Theorem 2.4, that is,

$$\|W_4 T_{we}\|_\infty \geq \inf_{Q \in \mathcal{S}} \|W_4 NX - W_4 MNQ\|_\infty, \tag{3.46}$$

and compare it to the noise rejection bound for the estimation problem (3.45). The only difference appears in the T_2 term of the model-matching problem. For the estimation bounds, the T_2 term contains M and F, so interpolation constraints arise from the unstable poles of $\tilde{P}\tilde{F}$ and the non-minimum-phase zeros of $\tilde{F}$, whereas for the feedback control bounds, the T_2 term contains M and N, so interpolation constraints arise from the unstable poles of $\tilde{P}\tilde{F}$ and the non-minimum-phase zeros of $\tilde{P}\tilde{F}$. However, both Theorem 3.4 and Theorem 2.4 provide tight bounds, and the conclusion is that plant non-minimum-phase zeros do not affect the optimal performance for the estimation problem whereas they do affect the optimal performance for the feedback control problem. This is further explored in the example at the end of this section.

3.4.2 What happens to performance as the sensor time delay is increased?

The conclusions drawn in Section 2.4.2 apply to the estimation problem as well. As the delay gets arbitrarily bad, performance gets arbitrarily bad (for all three metrics). Due to the complicated nature of the coprime factorization problem, it is not possible to say that an increase in the sensor time delay must cause a degradation of the best achievable performance, which is the same conclusion reached for the feedback control problem.

3.4.3 Example

The two examples in this section are the same as the examples in Section 3.3.3 except the plant is now unstable.

Example 7: Using the same weighting function (3.29), and using the plant

$$P[z] = \frac{1}{z-10}, \tag{3.47}$$

we construct a Luenberger observer and an estimator designed for optimal weighted disturbance rejection when $\Omega_b = 0.1$, and compare their performance to the optimal performance over a wide range of Ω_b. The Lueneberger observer has its poles placed at $z = -0.05, -0.1, -0.15,$ and -0.2, and produces the following equivalent G_1 and G_2:

$$\begin{aligned} G_1[z] &= \frac{(z+10.25)(z^2+0.25z+102.5)}{(z+0.2)(z+0.15)(z+0.1)(z+0.05)} \\ G_2[z] &= \frac{10508.8127(z+6.215\times10^{-5})(z^2-6.215\times10^{-5}z+3.863\times10^{-9})}{(z+0.2)(z+0.15)(z+0.1)(z+0.05)} \end{aligned} \tag{3.48}$$

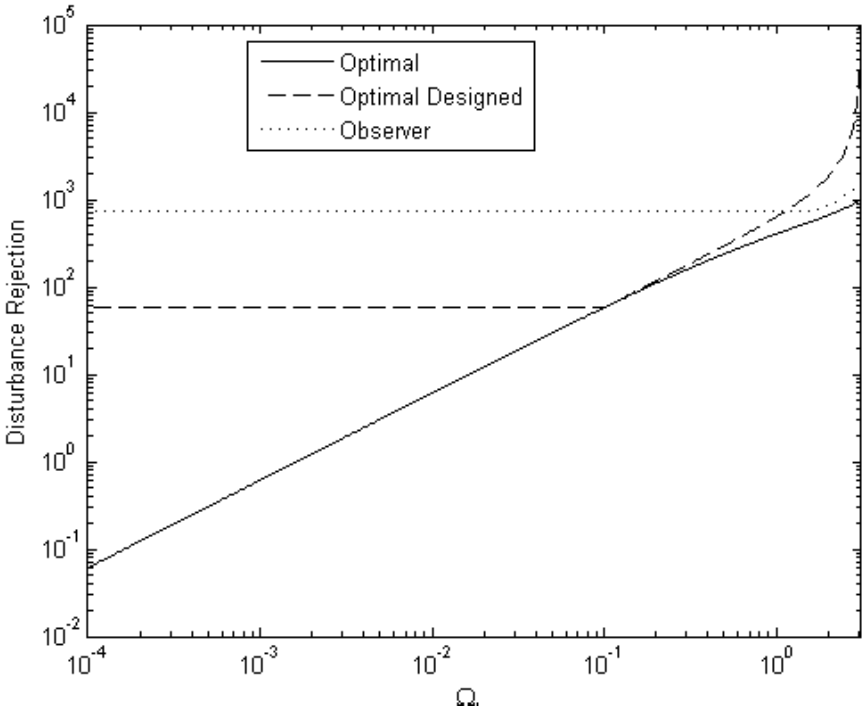

Figure 3.5: Comparing the performance of a Luenberger observer (3.48) to an estimator optimized for $\Omega_b = 0.1$ (3.49) and to the optimal performance for all values of Ω_b.

The optimal estimator produces the following G_1 and G_2:

$$\begin{aligned} G_1[z] &= 1209.068(z+0.7923)(z+0.8091)(z+0.6147)(z+0.5893)(z+0.3987)\times \\ &\quad (z+0.3935)(z-0.9035)(z+3.263\times 10^{-5})(z^2-3.263\times 10^{-5}z+1.065\times 10^{-9})\times \\ &\quad \frac{(z^2+0.8079z+0.1632)(z^2+1.599z+0.639)(z^2+1.196z+0.3577)}{(z+0.8)^4(z+1)(z+0.6)^4(z+0.4)^4(z-0.1)(z^2+0.09858z+0.008281)} \\ G_2[z] &= (z+0.8642)(z+0.3856)(z-0.9047)(z^2+0.38z+0.03617)(z^2+0.4186z+0.044)\times \\ &\quad (z^2+0.7172z+0.1309)(z^2+1.67z+0.7018)(z^2+0.9146z+0.2192)\times \\ &\quad \frac{(z^2+1.465z+0.5506)(z^2+1.185z+0.3698)(z^2+11.9z+120.8)}{(z+0.8)^4(z+1)(z+0.6)^4(z+0.4)^4(z+0.2)^4(z-0.1)(z^2+0.099z+0.0083)}. \end{aligned} \quad (3.49)$$

As before, note that the pole at $z=-1$ arises due to the improper nature of the continuous-time optimal Q, and can be eliminated by using a proper approximation for Q. The weighted disturbance rejection for both estimators is shown in Figure 3.5, along with the the optimal disturbance rejection given by (3.44). Figure 3.5 shows a similar trend to the stable case, where the optimal estimator gives optimal performance at $\Omega_b = 0.1$, and outperforms the Luenberger observer for most values of Ω_b, only falling off at higher values of Ω_b. It should also be noted that the optimal performance is much worse for this unstable plant than for the stable plant case.

Example 8: This example demonstrates the differing impact of plant non-minimum-phase zeros on the optimal performance. Given the same weighting function (3.29) and

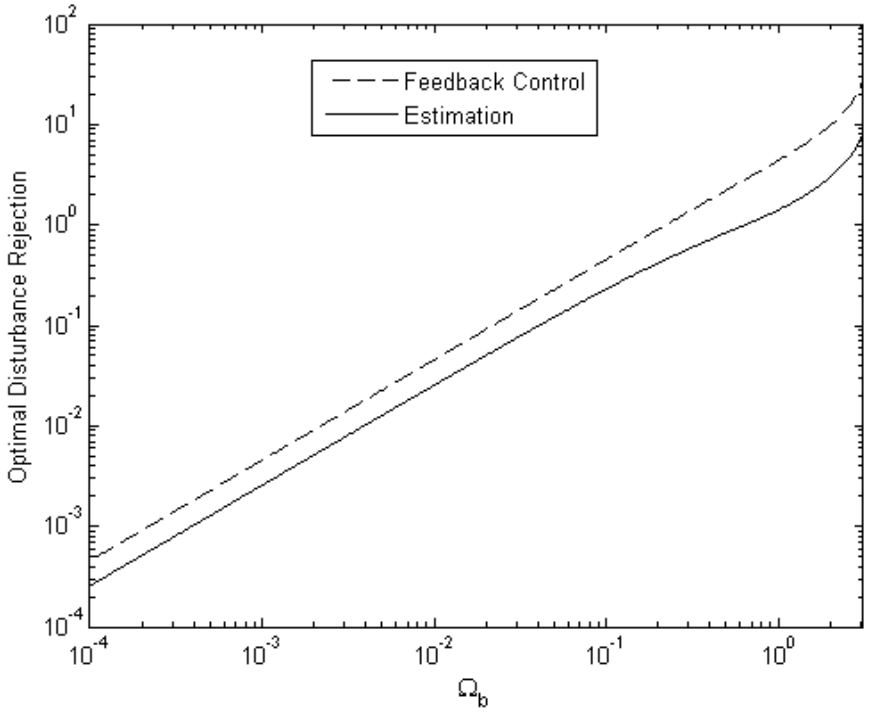

Figure 3.6: Optimal disturbance rejection for the estimation and feedback control problems for the plant given by (3.50).

the plant

$$P[z] = \frac{z+2}{z+4}, \tag{3.50}$$

the optimal disturbance rejection for both the estimation problem given by Figure 3.1, with corresponding bound (3.44), and the feedback control problem given by Figure 1.8, with corresponding bound (2.67), are calculated for a wide range of Ω_b. The results are shown in Figure 3.6, and clearly show a lower (i.e., better) optimal performance for the estimation problem than for the feedback control problem. The source of the difference is the plant non-minimum-phase zero which adds an extra interpolation constraint to the feedback control problem with everything else being the same for the two problems.

Chapter 4

Continuous-Time SISO Extensions

4.1 Overview

This chapter deals with both the delayed control and delayed estimation problems in a continuous-time setting. Unlike a discrete-time delay, a continuous-time delay is an infinite-dimensional system. The end result is that in order to address Q1-Q3 from Chapter 1, new approaches are required. For some problems, using a finite approximation and then taking limits leads to a solution to the problem. For others, new tools that deal explicitly with the continuous-time delay must be used. Unfortunately, as will be seen later, many of the infinite-dimensional tools are extremely complex, making them difficult to calculate, and are nearly impossible to gain intuition from.

Figure 4.1 shows the feedback control problem (and is repeated from Chapter 1 for convenience). However, in this chapter, P, C and F are all continuous-time systems, with F no longer being rational, but instead having the form

$$F(s) = e^{-sT}. \tag{4.1}$$

When infinite-dimensional tools are used, C is also not necessarily rational. Figure 3.1 shows the estimation problem, and again, P, F, G_1 and G_2 are all continuous-time systems. The delay F has the same form as for the feedback control problem (4.1), and G_1 and G_2 are not necessarily rational.

This chapter starts by introducing some of the tools that we used, specifically, an introduction to a rational, finite approximations of a continuous-time delay, and an infinite-dimensional Youla-esque parameterization. Unfortunately, extending the parameterization of asymptotic estimators to the infinite-dimensional case has not been worked out, and would be an excellent candidate for future work. The chapter then continues with the unstable-plant case, where an approximation method yields a similar result to those in Chapters 2 and 3, followed by the stable-plant case. Two approaches are taken for the stable-plant case, one using a finite approximation of the delay, and the other using the various infinite-dimensional tools. Unfortunately, neither technique produces desirable results.

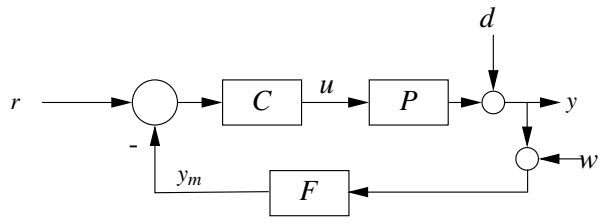

Figure 4.1: A block diagram of the feedback control problem with a sensor time delay.

4.2 Background Results

4.2.1 Approximating e^{-sT}

One common technique for handling a continuous-time delay is to use an approximation. There are many different approximations that are available, but this thesis concerns itself with one of the simplest, taken from [29]. Start with

$$e^{-sT} = \lim_{m\to\infty} \left(\frac{1 - \frac{Ts}{2m}}{1 + \frac{Ts}{2m}} \right)^m \tag{4.2}$$

to arrive at the approximation

$$e^{-sT} \approx \left(\frac{1 - \frac{Ts}{2m}}{1 + \frac{Ts}{2m}} \right)^m . \tag{4.3}$$

This approximation has two properties that lead to the "approximation conjecture" that is explored later in the chapter. These two properties are outlined in the following lemmas.

Lemma 4.1 Let $H_m(s)$ denote the mth order approximation of a time delay, i.e.,

$$H_m(s) = \left(\frac{1 - \frac{Ts}{2m}}{1 + \frac{Ts}{2m}} \right)^m , \tag{4.4}$$

and let $H(s)$ denote the actual time delayed system, i.e., $H(s) = e^{-sT}$. Then,

$$\angle H_m(j\omega) \geq \angle H_{m+1}(j\omega) \quad \forall T, \omega > 0 \quad \forall m \geq 1 \text{ and} \tag{4.5}$$

$$\angle H_m(j\omega) \geq \angle H(j\omega) \quad \forall T, \omega > 0 \quad \forall m \geq 1. \tag{4.6}$$

□

Proof: The proof starts by showing (4.5). The phase can be written as

$$\angle H_m(j\omega) = -m \tan^{-1}(\frac{T\omega}{2m}), \tag{4.7}$$

so (4.5) is equivalent to

$$-m\tan^{-1}(\frac{T\omega}{2m}) \geq -(m+1)\tan^{-1}\left(\frac{T\omega}{2(m+1)}\right) \quad \forall T,\omega > 0 \;\&\; m \geq 1. \tag{4.8}$$

To show (4.8), introduce

$$f(x) = x\tan^{-1}(\frac{1}{x}). \tag{4.9}$$

The left side of (4.8) can be written in terms of $f(x)$ by choosing

$$x = x_1 \equiv \frac{2m}{T\omega}, \tag{4.10}$$

resulting in

$$\begin{aligned} -m\tan^{-1}(\frac{T\omega}{2m}) &= -\frac{T\omega x_1}{2}\tan^{-1}(\frac{1}{x_1}) \\ &= -0.5T\omega f(x_1). \end{aligned}$$

The right side of (4.8) can be written in a similar form, choosing

$$x = x_2 = \frac{2(m+1)}{T\omega}, \tag{4.11}$$

resulting in

$$-(m+1)\tan^{-1}\left(\frac{T\omega}{2(m+1)}\right) = -0.5T\omega f(x_2). \tag{4.12}$$

We can then rewrite (4.8) as:

$$\begin{aligned} -0.5T\omega f(x_1) &\geq -0.5T\omega f(x_2) \\ \Leftrightarrow f(x_1) &\leq f(x_2) \quad . \end{aligned}$$

We conclude that, since $0 < x_1 < x_2$, (4.8) holds if $f(x)$ is a non-decreasing function for $x > 0$.

To show that $f(x)$ is non-decreasing $\forall x > 0$, it will be shown that $f'(x) \geq 0 \quad \forall x > 0$. In order to show that $f'(x) \geq 0 \;\; \forall x > 0$, we show that $f'(x)$ starts off non-negative, i.e.,

$$\lim_{x\to 0^+} f'(x) \geq 0$$

and ends at zero, i.e.,

$$\lim_{x\to\infty} f'(x) = 0$$

and that $f''(x) \leq 0$, i.e., $f(x)$ is concave, implying that the function has no local minima or maxima $\forall x > 0$.

Start by writing $f'(x)$ as:

$$\begin{aligned} f'(x) &= \tan^{-1}(\frac{1}{x}) + \left(\frac{x}{1+\frac{1}{x^2}}\right)\left(\frac{-1}{x^2}\right) \\ &= \tan^{-1}(\frac{1}{x}) - \frac{x}{x^2+1}, \end{aligned}$$

and then computing

$$\lim_{x\to 0^+} f'(x) = \tan^{-1}(\infty) - 0 = \frac{\pi}{2},$$

which is clearly ≥ 0. Next, we show that $\lim_{x\to\infty} f'(x) = 0$:

$$\lim_{x\to\infty} f'(x) = \tan^{-1}(0) - 0 = 0.$$

So, all that remains is showing that $f''(x) \leq 0$:

$$f''(x) = \frac{-2}{(x^2+1)^2} \leq 0 \quad \forall x \in \mathcal{R}.$$

As a result $f(x)$ is a non-decreasing function $\forall x > 0$, and therefore, (4.5) holds.

Now, to prove (4.6), we start by writing the phase of $H(j\omega)$ as

$$\angle H(j\omega) = -\omega T \tag{4.13}$$

allowing us to rewrite (4.6) as

$$-m\tan^{-1}(\frac{T\omega}{2m}) \geq -\omega T \tag{4.14}$$

Using (4.10), and $f(x)$ as defined by (4.9), we can rewrite (4.14) as

$$\begin{aligned} -0.5T\omega f(x_1) &\geq -\omega T & (4.15)\\ \Leftrightarrow f(x_1) &\leq 2. & (4.16) \end{aligned}$$

But, since $f(0) = \frac{\pi}{2}$, and $f(x)$ is non-increasing, (4.16) must hold. Therefore, (4.6) holds as well. □

Lemma 4.2 Let $H_m(s)$ denote the mth order approximation of a time delay, i.e.,

$$H_m(s) = \left(\frac{1-\frac{T}{2m}}{1+\frac{T}{2m}}\right)^m, \tag{4.17}$$

and let $H(s)$ denote the actual time delay, i.e., $H(s) = e^{-sT}$. Then,

$$\begin{aligned} \frac{\partial \angle H_m(j\omega)}{\partial\omega} &\geq \frac{\partial \angle H_{m+1}(j\omega)}{\partial\omega} \quad \forall\omega, \forall m \geq 1 \text{ and} & (4.18)\\ \frac{\partial \angle H_m(j\omega)}{\partial\omega} &\geq \frac{\partial \angle H(j\omega)}{\partial\omega} \quad \forall\omega, \forall m \geq 1. & (4.19) \end{aligned}$$

□

Proof: We start by proving (4.18). Using (4.7), we can find the required derivatives allowing us to write (4.18) as:

$$\frac{-2Tm^2}{4m^2+T^2\omega^2} \geq \frac{-2T(m+1)^2}{4(m+1)^2+T^2\omega^2} \quad \forall T,\omega>0 \;\&\; m\geq 1. \tag{4.20}$$

Re-arranging (4.20), we get

$$\begin{aligned} -8Tm^2(m+1)^2-2T^3m^2\omega^2 &\geq -8T(m+1)^2m^2-2T^3(m)^2\omega^2 \\ \Leftrightarrow -m^2 &\geq -(m+1)^2 \end{aligned} \tag{4.21}$$

which is true for all m, and therefore, (4.18) is true for all $T,\omega\in\mathcal{R}$ and for all integers $m\geq 1$.

The proof of (4.19) is similar. We need to show that

$$\frac{-2Tm^2}{4m^2+T^2\omega^2} \geq -T \quad \forall T,\omega>0 \;\&\; m\geq 1. \tag{4.22}$$

Re-arrange the terms in (4.22) as follows:

$$\begin{aligned} -2m^2 &\geq -4m^2-T^2\omega^2 \\ \Leftrightarrow 0 &\geq -2m^2-T^2\omega^2, \end{aligned} \tag{4.23}$$

which holds for any $T,\omega\in\mathcal{R}$ and for any integer m. Therefore, (4.19) holds. □

Lemma 4.1 implies that there is more phase lag at all frequencies for higher-order approximations, and that the actual time delay has more phase lag than any approximation. Lemma 4.2 implies that the rate of change of phase lag with respect to frequency is faster for a higher-order approximation, and fastest for the actual time delay. Figure 4.2 shows the phase plots for various delays, demonstrating the properties of Lemmas 4.1 and 4.2. Note that the curve for $m=1$ is always higher than that for $m=2$, and that the slope of the $m=1$ curve is less severe than for the $m=2$ case. These two properties are exploited in more detail later on in the chapter.

4.2.2 Time-Delay Youla Parameterization

Unfortunately, when dealing with a continuous-time delay, standard Youla parameterization does not work. Fortunately, this problem can be overcome, and Youla-esque factorizations do exist for delayed systems, for example, see [26]. The result in [26] is an extension of Youla, and has a very similar form, including the use of a coprime factorization for delay systems, again found in [26]. Both results are presented below without proof. The interested reader is encouraged to consult [26] for further details, including a procedure for performing the coprime factorization.

Lemma 4.3 [26] Define z as a delay operator of duration T, i.e., $zx(t)=x(t-T)$. Note that the transfer function of z is e^{-sT}. Then, given a strictly proper $P(s,z)$, there exist

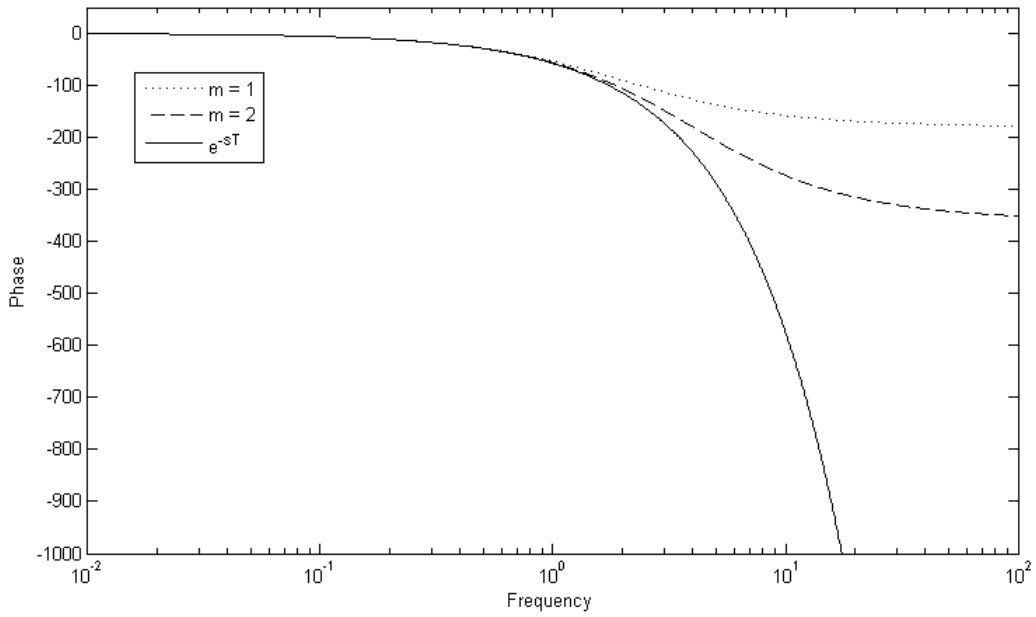

Figure 4.2: Phase plot for a first and second order delay approximation (4.3) and the actual delay.

stable, possibly irrational transfer function matrices N, $\tilde{N}$, M, $\tilde{M}$, X, $\tilde{X}$, Y, and $\tilde{Y}$ such that:

$$P(s,z) = N(s,z)M^{-1}(s,z) = \tilde{M}(s,z)\tilde{N}^{-1}(s,z) \tag{4.24}$$

and

$$\begin{bmatrix} Y(s,z) & X(s,z) \\ -\tilde{N}(s,z) & \tilde{M}(s,z) \end{bmatrix} \begin{bmatrix} M(s,z) & -\tilde{X}(s,z) \\ N(s,z) & \tilde{Y}(s,z) \end{bmatrix} = \begin{bmatrix} I & 0 \\ 0 & I \end{bmatrix}. \tag{4.25}$$

□

Lemma 4.4 [26] Using z as a delay operator, as in Lemma 4.3, and given any system $P(s,z)$ with a coprime factorization given by Lemma 4.3, for the feedback setup shown in Figure 1.11, the set of all stabilizing controllers, $C(s,z)$, is given by:

$$\left\{(Y(s,z) - Q(s,z)\tilde{N}(s,z))^{-1}(X(s,z) + Q(s,z)\tilde{M}(s,z)) : Q \text{ stable}\right\} \tag{4.26}$$

$$\text{or} \quad \left\{(\tilde{X}(s,z) + M(s,z)Q(s,z))(\tilde{Y}(s,z) - N(s,z)Q(s,z))^{-1} : Q \text{ stable}\right\}. \tag{4.27}$$

Note that $C(s,z)$ will in general be infinite dimensional. □

4.3 Unstable Plant Case

This section presents a result based on Lemma 2.4. By using (4.2), a nice, simple bound on the optimal performance can be found for both the feedback control problem and the estimation problem. These results are presented in the following theorems:

Theorem 4.1 Assume $P(s)$ has $k \geq 1$ possibly repeated unstable poles; denote these poles by p_i, $i = 1, ..., k$. If the closed-loop system in Figure 4.1 is stable, with the delay given by $F(s) = e^{-sT}$, then the performance metrics given in the feedback control column of Table 1.1 are bounded from below as follows:

$$\|W_1 T_{re}\|_\infty \geq \max_{i=1,...,k} \left| W_1(p_i) \cdot e^{p_i T} \right| - \|W_1\|_\infty \tag{4.28}$$

$$\|W_2 S\|_\infty \geq \max_{i=1,...,k} \left| W_2(p_i) \cdot e^{p_i T} \right| - \|W_2\|_\infty \tag{4.29}$$

$$\|W_3 T_{dy}\|_\infty \geq \max_{i=1,...,k} \left| W_3(p_i) \cdot e^{p_i T} \right| - \|W_3\|_\infty \tag{4.30}$$

$$\|W_4 T_{we}\|_\infty \geq \max_{i=1,...,k} \left| W_4(p_i) \cdot e^{p_i T} \right|. \tag{4.31}$$

□

Proof: The proof follows by using (4.2) for the delay, then using the approximation (4.3) to satisfy the interpolation constraints required for the use of Lemma 2.4, and then using (4.2) again to get to the desired form. We focus on proving (4.30), with the remaining results derived using a similar approach.

To start, define

$$\tilde{F}(s) = \left(\frac{1 - \frac{Ts}{2m}}{1 + \frac{Ts}{2m}} \right)^m \text{ and} \tag{4.32}$$

$$\tilde{T}_{dy}(s) = \frac{1}{1 + PC \left(\frac{1 - \frac{Ts}{2m}}{1 + \frac{Ts}{2m}} \right)^m} \tag{4.33}$$

and note that

$$\lim_{m \to \infty} \tilde{F}(s) = F(s) \text{ and} \tag{4.34}$$

$$\lim_{m \to \infty} \tilde{T_{dy}} = T_{dy}(s). \tag{4.35}$$

Let $\tilde{z}_j$, $j = 1, \ldots, m$ denote all zeros of $\tilde{F}$ with positive real parts, i.e., $\tilde{z}_j = \frac{2m}{T}$. Now, to use Lemma 2.4, set $\tilde{R} = 1 + \tilde{T}_{dy}$, with $\tilde{p}_i = p_i$ and the defined $\tilde{z}_j$, resulting in:

$$\begin{aligned}
\|W_3 T_{dy}\|_\infty &= \lim_{m\to\infty} \|W_3 \tilde{T}_{dy}\|_\infty \\
&= \lim_{m\to\infty} \|W_3 - W_3\tilde{R}\|_\infty \\
&\geq \lim_{m\to\infty} \|W_3\tilde{R}\|_\infty - \|W_3\|_\infty \\
&\geq \lim_{m\to\infty} \max_{i=1,\ldots,k} \left| W_3(\tilde{p}_i) \prod_{j=1}^{m} \left(\frac{\tilde{\tilde{z}}_j + \tilde{p}_i}{\tilde{z}_j - \tilde{p}_i} \right) \right| - \|W_3\|_\infty \\
&= \lim_{m\to\infty} \max_{i=1,\ldots,k} \left| W_3(p_i) \prod_{j=1}^{m} \left(\frac{\frac{2m}{T} + p_i}{\frac{2m}{T} - p_i} \right) \right| - \|W_3\|_\infty \\
&= \max_{i=1,\ldots,k} \left| W_3(p_i) \lim_{m\to\infty} \prod_{j=1}^{m} \left(\frac{\frac{2m}{T} + p_i}{\frac{2m}{T} - p_i} \right) \right| - \|W_3\|_\infty \\
&= \max_{i=1,\ldots,k} \left| W_3(p_i) \cdot e^{p_i T} \right| - \|W_3\|_\infty .
\end{aligned}$$

The remaining bounds can be found using the same technique. □

Theorem 4.2 Assume that $P(s)$ in Figure 3.1 is unstable, with possibly repeated unstable poles, denoted p_i, $i = 1, \ldots, k$. Then, for any asymptotic estimator, the performance measures in the estimation column of Table 1.1 are bounded from below as follows:

$$\|W_5 S\|_\infty \geq \max_{i=1,\ldots,k} |W_5(p_i) \cdot e^{p_i T}| - \|W_5\|_\infty \tag{4.36}$$

$$\|W_6 T_{de}\|_\infty \geq \max_{i=1,\ldots,k} |W_6(p_i) \cdot e^{p_i T}| - \|W_6\|_\infty \tag{4.37}$$

$$\|W_7 T_{we}\|_\infty \geq \max_{i=1,\ldots,k} |W_7(p_i) \cdot e^{p_i T}|. \tag{4.38}$$

□

Proof: The proof is essentially the same as for Theorem 4.1, and is left to the reader. □

Theorems 4.1 and 4.2 provide extremely intuitive bounds into the performance of a continuous-time delay system. As shown in the next section, most of the results that work directly with e^{-sT} require complex calculations and are difficult to use, whereas the above results are easy to calculate and clearly show the worsening of performance as the delay is increased. In fact, just like in the discrete-time case, an arbitrarily bad delay produces arbitrarily poor performance for any unstable plant, for both the estimation and control problems.

4.4 Stable Plant Case

In this section, two approaches to deal with the stable plant case are briefly explored. The first approach is to consider infinite-dimensional tools that can handle the continuous-time delay, while the second involves using the delay approximation (4.3) to compute

various performance bounds. Unfortunately, neither approach leads to meaningful performance limitations.

4.4.1 Exact Computational Approaches

Unfortunately, the techniques available in the literature to solve model-matching problems involving time delays either heavily restrict the class of weighting functions for which a result applies, or are extremely complex. Two results are presented here, one from [13], and the other from [23]. The result from [13] restricts the weighting function, but in doing so, leads to a relatively useful bound. The other result, [23], applies for an arbitrary weighting function, and re-derives the result from [13] for a first-order low-pass filter weighting function. However, for a more complex weighting function, the problem devolves into computing the maximum root of a extremely complex function which makes solving the problem difficult, and destroys any possibility of gaining meaningful insight into the problem. At this time we deal only with the control problem, since an extension of the parameterization of asymptotic estimators to infinite-dimensional systems is required to get continuous-time results.

Both [13] and [26] assume a pure time delay plant. However, since dropping extra plant information can only lower the optimal performance, the results still produce meaningful bounds, and in essence, mimic the results in Chapter 2 where we drop the plant to isolate the delay. Using Lemma 4.4, the various transfer functions can be written in terms of a Youla parameter, for example, $T_{dy} = \frac{1}{1-PFQ}$, which has a weighted infinity norm of $\|W_3 - W_3PFQ\|_\infty$. Since removing the plant produces a smaller optimal norm, we can say

$$\inf_{Q\in\mathcal{S}} \|W_3 - W_3PFQ\|_\infty \geq \inf_{Q\in\mathcal{S}} \|W_3 - e^{-sT}Q\|_\infty. \tag{4.39}$$

Hence, for simplicity, $\inf_{Q\in\mathcal{S}} \|W_3 - e^{-sT}Q\|_\infty$ is the problem that we focus on here. Both [13] and [23] solve this problem, and their solutions are outlined in the following two lemmas (the interested reader is encouraged to consult the sources for the required proofs):

Lemma 4.5 [13] Assuming $W(s) = \frac{1}{as+1}$, then

$$\inf_{Q\in\mathcal{S}} \|W - e^{-Ts}Q\|_\infty = \frac{1}{\sqrt{1+\frac{a^2y_{aT}^2}{T^2}}} \tag{4.40}$$

where y_{aT} is the unique root of

$$\tan y + \frac{ay}{T} = 0. \tag{4.41}$$

□

Lemma 4.6 [23] Let A, B, C and D be a minimal state-space representation of a stable, minimum phase weighting function $W_3(s)$, and let $\phi(s) = e^{sT}$. Defining:

$$F_\lambda \equiv \begin{bmatrix} A + D(\lambda^2 - D^2)^{-1}BC & \lambda(\lambda^2 - D^2)^{-1}BB' \\ -\lambda(\lambda^2 - D^2)^{-1}C'C & -(A + D(\lambda^2 - D^2)BC') \end{bmatrix}, \tag{4.42}$$

then

$$\inf_{Q\in\mathcal{S}} \|W - e^{-sT}Q\|_\infty = \sup\{|D|, \lambda : \det([\phi^*(F_\lambda)]_{(2,2)}) = 0\} \tag{4.43}$$

where $\phi^*(s) = e^{sT}$ and $[H]_{(2,2)}$ denotes the (2,2) block of the block matrix H. □

Lemma 4.6 is a nightmare to work with, and drawing any conclusions is virtually impossible. On the other hand, Lemma 4.5 is far more manageable, and drawing conclusions is in fact possible. Namely, while the proof is omitted here, it is possible to show that the optimal performance for a pure time delay plant necessarily gets worse as the delay T increases. Unfortunately, Lemma 4.5 applies only to first-order weighting functions.

4.4.2 "Approximation Conjecture" Approach

This section details a conjecture dealing with the model-matching problem and the time delay approximation (4.3). The conjecture is built on the two phase properties of the time-delay approximation given in Lemmas 4.1 and 4.2. The conjecture (and the counterexample that shows the conjecture does not apply to all weighting functions and plants) is outlined below.

Conjecture 1 Given two all-pass functions, $H_1(s)$ and $H_2(s)$, with

$$\angle H_1(j\omega) \geq \angle H_2(j\omega) \tag{4.44}$$

$$\frac{\partial \angle H_1(j\omega)}{\partial \omega} \geq \frac{\partial \angle H_2(j\omega)}{\partial \omega} \tag{4.45}$$

and any stable, minimum-phase weighting function $W(s)$, then

$$\inf_{Q_1\in\mathcal{S}} \|W - WH_1Q_1\|_\infty \leq \inf_{Q_2\in\mathcal{S}} \|W - WH_2Q_2\|_\infty. \tag{4.46}$$

□

If Conjecture 1 holds, it follows that any approximation of the form (4.3) results in a model matching bound that is lower than the actual performance, i.e., a fundamental performance limitation could be computed using (4.3) for any m. At first, the conjecture appeared to be correct, since for any standard looking weighting function (i.e., a standard low-pass or high-pass filter), simulation results supported the conjecture. In an attempt to prove the conjecture, it was first decided to solve the model-matching problem using the $m = 1$ and $m = 2$ time-delay approximations (4.3) to show the conjecture holds for a specific $H_1(s)$ and $H_2(s)$, i.e.,

$$H_1(s) = \frac{1 - \frac{Ts}{2}}{1 + \frac{Ts}{2}} \tag{4.47}$$

$$H_2(s) = \left(\frac{1 - \frac{Ts}{4}}{1 + \frac{Ts}{4}}\right)^2. \tag{4.48}$$

An explicit solution to the model-matching problem was found for $H_1(s)$ and $H_2(s)$ using [35]. The result for $H_1(s)$ was solved explicitly in [35], while the solution for $H_2(s)$ was constructed using the technique for repeated poles provided in [35]. After much tedious algebra, and letting $\frac{4}{T} = a$, we get

$$\inf_{Q_1 \in \mathcal{S}} \|W - WH_1Q_1\|_\infty = W(\frac{a}{2}) \tag{4.49}$$

$$\inf_{Q_2 \in \mathcal{S}} \|W - WH_2Q_2\|_\infty = W(a) \left| \frac{\frac{-W(a)}{W'(a)} + \sqrt{\left(\frac{W(a)}{W'(a)}\right)^2 + a^2} + a}{\frac{-W(a)}{W'(a)} + \sqrt{\left(\frac{W(a)}{W'(a)}\right)^2 + a^2} - a} \right|. \tag{4.50}$$

For Conjecture 1 to hold, we then require

$$W(a) \left| \frac{\frac{-W(a)}{W'(a)} + \sqrt{\left(\frac{W(a)}{W'(a)}\right)^2 + a^2} + a}{\frac{-W(a)}{W'(a)} + \sqrt{\left(\frac{W(a)}{W'(a)}\right)^2 + a^2} - a} \right| \geq W(\frac{a}{2}), \tag{4.51}$$

which, after more tedious algebra, can be shown to hold anytime $W(a) \geq W(\frac{a}{2})$ or anytime both $W(a) \leq W(\frac{a}{2})$ and

$$W(\frac{a}{2})^2 \leq W(a)^2 + 2a|W'(a)|W(\frac{a}{2}). \tag{4.52}$$

It can be shown that any first-order weighting function satisfies (4.52). Unfortunately, higher-order weights need not satisfy (4.52). A counter-example is

$$W(s) = \frac{101(s+0.001793)(s^2+0.315s+0.1104)}{(s+10)(s+1)(s+0.1)(s+0.01)}, \tag{4.53}$$

with associated Bode plot shown in Figure 4.3 (note that the Bode plot required is quite bizarre and would be a very odd choice for a weighting function). The optimal performance of $H_1(s)$ and $H_2(s)$ is shown in Figure 4.4. Note that (4.46) is violated for some values of T.

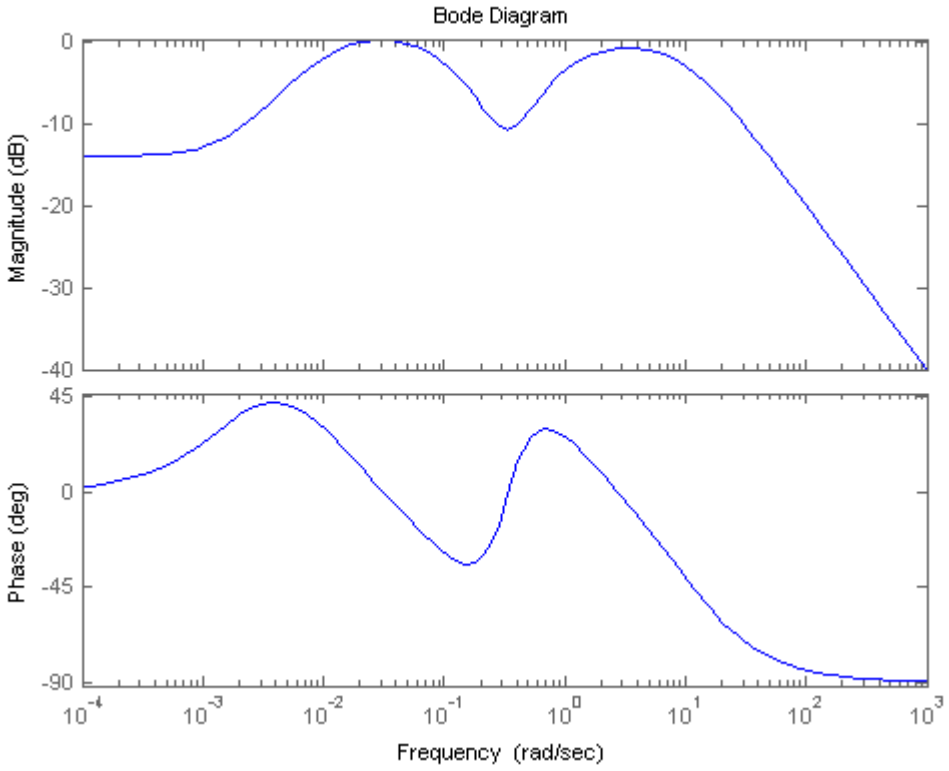

Figure 4.3: Bode plot of a weighting function that violates the conjecture.

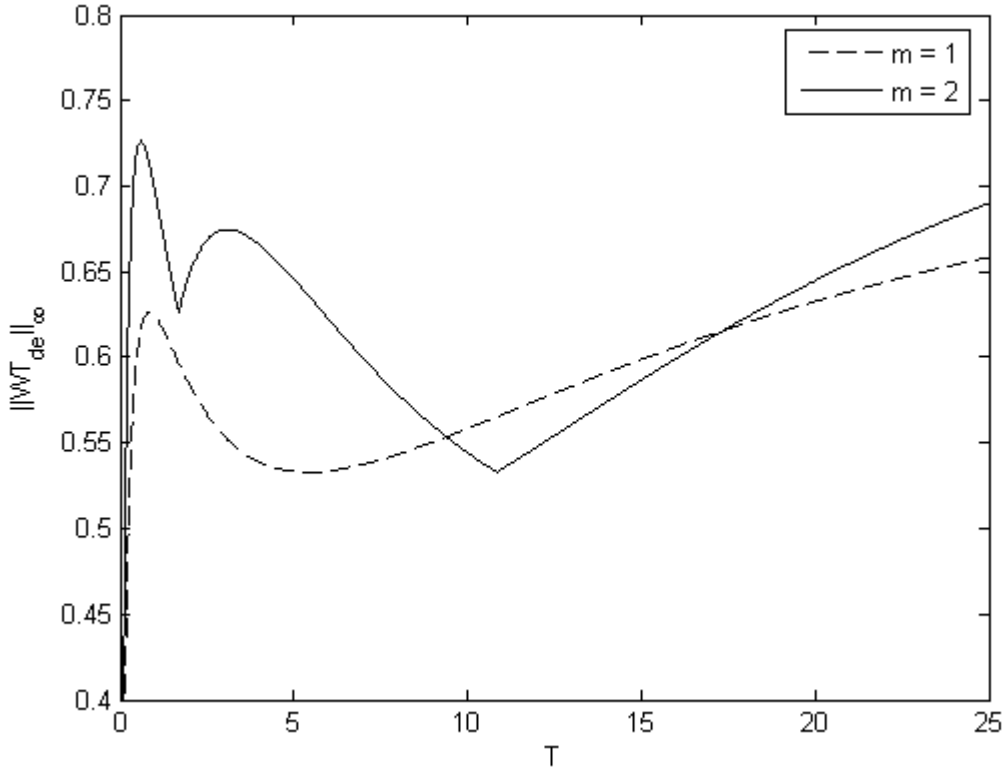

Figure 4.4: Optimal performance using the weighting function given by (4.53) and $H_1(s)$ and $H_2(s)$.

Chapter 5

Other Extensions

This section outlines a few other extensions to the work in Chapters 2 and 3. The first extension is for a two-degree-of-freedom (2-DOF) feedback control setup, as shown in Figure 5.1. It should be noted that the primary advantage to a 2-DOF controller is for tracking performance. The second extension is for an alternative 1-DOF topology, as shown in Figure 5.2, which again, only affects tracking performance. The final extension is for MIMO systems, where a few numerical solution techniques are briefly discussed. Further extensions to MIMO systems is an area for future work.

5.1 Alternative Topologies

5.1.1 2-DOF Feedback Control Topology

A 2-DOF topology with a sensor time delay, as shown in Figure 5.1, accomplishes two important things. First, as is shown later in this section, it is possible to recover tracking performance for an unstable plant. Second, it separates the tracking performance from the other three aspects of performance (disturbance rejection, sensitivity and noise rejection). This is best seen through the 2-DOF Youla parameterization, taken from [32], which has two free parameters, one for the controller in the feedback loop, C_2, and one for the feedforward controller, C_1. This section primarily focuses on the first point, but, the idea of the second point is that one can design $C_2[z]$ for optimal wighted disturbance

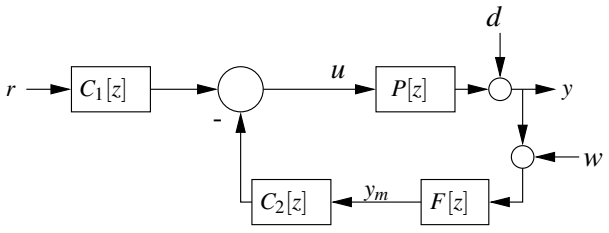

Figure 5.1: A block diagram of a 2-DOF control setup with a sensor time delay .

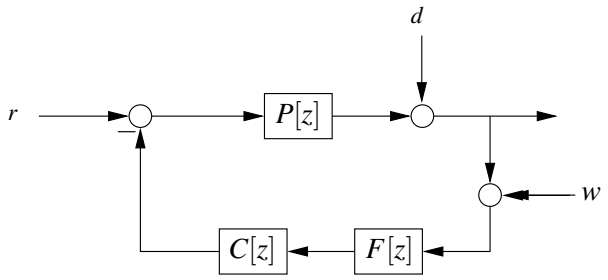

Figure 5.2: A block diagram of the alternative 1-DOF feedback control problem with a sensor time delay.

rejection and then design $C_1[z]$ to recover tracking, leading to much better "overall" performance than for a standard 1-DOF setup.

The 2-DOF Youla parameterization for SISO systems is presented below, without proof:

Lemma 5.1 [32] Given a SISO system P, with a coprime factorization given by Corollary 2.1, for the feedback setup shown in Figure 5.1, the set of all stabilizing controllers, $C_1[z]$ and $C_2[z]$, is given by:

$$C_1[z] = \left\{ \frac{R[z]}{Y[z]-N[z]Q[z]} : Q,R \in \mathcal{S}, Y-NQ \neq 0 \right\} \tag{5.1}$$

$$C_2[z] = \left\{ \frac{X[z]+M[z]Q[z]}{Y[z]-N[z]Q[z]} : Q \in \mathcal{S}, Y-NQ \neq 0 \right\}. \tag{5.2}$$

□

Note that in particular, the parameterization for $C_2[z]$ has the same form as the standard 1-DOF Youla parameterization.

Using Lemma 5.1, it is possible to construct a "recovering" controller, as in Theorem 2.2. This is shown in the following theorem:

Theorem 5.1 Consider a possibly unstable plant, P, and a given stabilizing controller, C^b, with transfer function from r to e denoted T_{re}^b as shown in Figure 1.11. Then, given the same plant P for the 2-DOF setup of Figure 5.1, with a transfer function from r to e denoted T_{re}, the tracking performance of the baseline system in Figure 1.11 can be recovered, i.e., $T_{re} = T_{re}^b$. In particular, perform coprime factorizations on both P and F:

$$P = \frac{N_1}{M_1},\ N_1X_1 + M_1Y_1 = 1$$
$$F = \frac{N_2}{M_2},\ N_2X_2 + M_2Y_2 = 1.$$

Let Q^b denote the 1-DOF Youla parameter corresponding to stabilizing controller C^b, i.e.,

$$Q^b = \frac{C^bY_1 - X_1}{C^bN_1 + M_1}.$$

Then, using any controller for the 2-DOF setup of Figure 5.1 whose Youla parameters satisfy

$$R = \frac{X_1 + M_1 Q^b}{M_2}, \quad Q \in \mathcal{S}. \tag{5.3}$$

recovers the baseline tracking performance. Note that $R \in \mathcal{S}$ sinceX_1, M_1, M_2 and Q are stable, and M_2 has the poles of F, but F is stable and therefore, M_2 has no non-minimum-phase zeros (which would make R unstable).

Note that unlike many earlier results in this thesis, the stability of the sensor dynamics is important. A recovering controller only exists for "stable" sensor dynamics (due to the M_2 term in the denominator of R). Since a sensor time delay of $\frac{1}{z^n}$ is stable, the recovering controller does exist. □

Proof: The proof is left up the reader, but it is essentially the same as for Theorem 2.2. □

It should also be mentioned that all the non-tracking bounds for a 1-DOF control setup in Chapter 2 apply to the 2-DOF setup as well. The only gain from the second degree of freedom is the separation of tracking from disturbance rejection, sensitivity and noise rejection, and the ability to recover tracking performance for an unstable plant.

5.1.2 Limitations in the Alternative 1-DOF Setup

The alternative 1-DOF topology of Figure 5.2 behaves the same as the standard 1-DOF topology of Figure 1.8 except in terms of tracking performance. In short, for the stable plant case, a recovering controller is not guaranteed to exist. This is shown in the following lemma:

Lemma 5.2 Consider a stable plant, P, and a given stabilizing controller, C^b, with transfer function from r to e denoted T_{re}^b as shown in Figure 1.11. Then, given the same plant P for the 1-DOF setup of Figure 5.2, with transfer function from r to e denoted T_{re}, no stabilizing controller is guaranteed to exist. □

Proof: Details are again left to the reader. The end result is an unstable Youla parameter, Q, is required to recover tracking performance. That Q is shown below,

$$Q = \frac{1 + PC^b - C^b}{PF(1 + PC^b)}, \tag{5.4}$$

which is improper in general. □

This result is not surprising, as the controller is only receiving a delayed signal. In the normal topology, the controller has access to the current input and can use feedforward to recover tracking. By putting the controller in the feedback loop after the delay, the controller has access to only the delayed output, eliminating the feedforward element, and thereby not allowing a recovering controller to exist.

5.2 MIMO Systems

We attempted to extend the results of Chapters 2 to discrete-time MIMO systems (a MIMO extension of Theorem 3.1 would be required before solving MIMO estimation problems). Using Lemma 2.3, we can write the various MIMO metrics in the form of a MIMO model-matching problem. MIMO model-matching is a problem in the form

$$\inf_{Q\in\mathcal{S}} \|W_1 T_{de} W_2\|_\infty = \inf_{Q\in\mathcal{S}} \|W_1 T_1 W_2 - W_1 T_2 Q T_3 W_2\|_\infty, \tag{5.5}$$

where W_1 and W_2 are stable, minimum-phase weighting function matrices and T_1, T_2 and T_3 are stable transfer function matrices. Using Lemma 2.3, with a coprime factorization of PF given by Lemma 2.1, we can write our various transfer functions in the form of a MIMO model-matching problem, for example, for disturbance rejection,

$$\inf_{Q\in\mathcal{S}} \|W_1 T_{de} W_2\|_\infty = \inf_{Q\in\mathcal{S}} \|W_1 \tilde{Y}\tilde{M} W_2 - W_1 N Q \tilde{M} W_2\|_\infty. \tag{5.6}$$

There are numerous tools for solving the MIMO model-matching problem, see [11, 12, 15, 21, 3]. The most progress was made with [3]. Unfortunately, even the simplest approach is complex and virtually destroys any insight into the effect of the delay. One re-occurring problem is handling the repeated zeros in T_2 and T_3 that arise from the discrete-time delay, as many of the tools do not work with repeated zeros. One other approach was attempted, based on [4]; unfortunately, this runs into the same repeated-zero problem as before.

One final complication with MIMO systems is simply the form of the time delay. Delays can be the same for each output, they can be different between various output channels, and there can even be delayed cross-channel interactions. Their are numerous problems that can be studied, and specifying a particular trend for a generalized time-delay is virtually impossible.

Chapter 6

Conclusions

A discrete-time sensor time delay imposes a fundamental performance limitation for:

- Weighted disturbance rejection and sensitivity for both feedback control and estimation for both stable and unstable plants.
- Noise rejection for both control and estimation and tracking for a 1-DOF controller with an unstable plant.

If a performance limitation exists, it is:

- Bounded from above for a stable plant.
- Unbounded for an unstable plant (i.e., an arbitrarily long delay produces an arbitrarily large bound).

A recovering controller exists if:

- The plant is stable.
- The plant is unstable and a 2-DOF controller is used.

Table 6.1 summarizes the various conclusions for discrete-time systems.

A continuous-time sensor time delay imposes a fundamental performance limitation for weighted disturbance rejection, sensitivity, noise rejection, and tracking for feedback control with an unstable plant, and for weighted disturbance rejection, sensitivity, and noise rejection for estimation with an unstable plant.

The following are items for future work:

- For $F[z] = \frac{1}{z^n}$, and a stable, minimum phase W_2 with $\|W_2\|_\infty = 1$, show that

$$\lim_{n\to\infty} \inf_{Q\in\mathcal{S}} \|W_2 - FQ\|_\infty = 1.$$

	Feedback Control		Estimation	
	Stable Plant	Unstable Plant	Stable Plant	Unstable Plant
Tracking Recovery	Unique 1-DOF Controller	Many 2-DOF Controllers	N/A	N/A
Sensitivity	Bounded Bound	Unbounded Bound	Bounded Bound	Unbounded Bound
Disturbance Rejection	Bounded Bound	Unbounded Bound	Bounded Bound	Unbounded Bound
Noise Rejection	No Bound Exists	Unbounded Bound	No Bound Exists	Unbounded Bound

Table 6.1: Summary of the conclusions for discrete-time systems.

- Extend the parameterization of asymptotic estimators to include infinite-dimensional systems (i.e., a continuous-time delay).
- Complete the work dealing with continuous-time delays, especially for the stable plant case.
- Extend the results to multivariable systems.
- Explore other application areas involving sensor time delays.

List of References

[1] J. A. Ball, I. Gohberg, and L. Rodman. *Interpolation of Rational Matrix Functions*, volume 45 of *Operator Theory: Advances and Applications*. Basel:Birkhauser, 1990.

[2] Hendrik W. Bode. *Network Analysis and Feedback Amplifier Design*. Van Nostrand, Princeton, NJ, 1945.

[3] Bor-Chin Chang and Jr. J. Boyd Pearson. Optimal disturbance rejection in linear multivariable systems. *IEEE Transactions on Automatic Control*, 29(10):880–887, October 1984.

[4] Jie Chen. Logarithmic integrals, interpolation bounds, and performance limitations in MIMO feedback systems. *IEEE Transactions on Automatic Control*, 45(6):1098–1115, June 2000.

[5] M. Darouach. Linear functional observers for systems with delays in state variables: The discrete-time case. *IEEE Transactions on Automatic Control*, AC-50(2):228–233, feb 2005.

[6] D. E. Davison and D. Gaudette. Tumor-tracking in radiotherapy: Parameterizaton of a sensor time delay compensators and associated performance limitations. In *Conference on Control Applications*, Toronto, August 2005. IEEE.

[7] D. E. Davison and E. S. Hwang. Automating radiotherapy cancer treatment: Use of multirate observer-based control. In *Proceedings of the American Control Conference*, Denver, CO, June 2003. AACC.

[8] Daniel E. Davison, Eui Seong Hwang, and Xiaomei Li. Generalization of the separation principle beyond constant-gain state-feedback control. In *Proceedings of the American Control Conference*, Denver, CO, June 2003. AACC.

[9] Daniel E. Davison and Robert Tonita. Performance limitations in control systems with sensor time delays. In *IFAC World Congress*, Prague, July 2005. IFAC.

[10] John C. Doyle, Bruce A. Francis, and Allen R. Tannenbaum. *Feedback Control Theory*, chapter 5. Macmillan, New York, NY, 1992.

[11] John C. Doyle, Keith Glover, Pramod P. Khargonekar, and Bruce A. Francis. State-space solutions to standard $\mathcal{H}_2$ and $\mathcal{H}_\infty$ control problems. *IEEE Transactions on Automatic Control*, 34(8):831–847, August 1989.

[12] A. Feintuch and B. A. Francis. Uniformly optimal control of linear feedback systems. *Automatica*, 21(5):563–574, 1985.

[13] Ciprian Foias, Allen Tannenbaum, and George Zames. Weighted sensitivity minimization for delay systems. *IEEE Transactions on Automatic Control*, AC-31(8):763–766, Aug 1986.

[14] Bruce Francis. *A course in H_∞ Control Theory*, volume 88 of *Lecture Notes in Control and Information Sciences*. Springer-Verlag, New York, 1987.

[15] Bruce A. Francis, J. William Helton, and George Zames. H_∞-optimal feedback controller for linear multivariable systems. *IEEE Transactions on Automatic Control*, 29(10):888–900, October 1984.

[16] Bruce A. Francis and George Zames. On H^∞-optimal sensitivity theory for siso feedback systems. *IEEE Transactions on Automatic Control*, 29(1):9–16, January 1984.

[17] J.S. Freudenberg, R.H. Middleton, and A. Stefanopoulou. A survey of inherent design limitations. In *Proceedings of the American Control Conference*, Chicago, IL, June 2000. AACC.

[18] D. Gaudette and D. E. Davison. Performance limitations imposed by sensor time delays in a general 2-DOF control scheme. In *American Control Conference*, Minneapolis, June 2006. IEEE.

[19] Princess Margeret Hospital. IGRT education course. http://www.radiationatpmh.com/body.php?id=153, September 2007.

[20] Sheridan Memorial Hospital. Multileaf collimator (mlc). http://welchcancercenter.org/Radiation%20Therapy%20Equip/multileaf%20-collimator.htm, September 2007.

[21] Edmond A. Jonckheere and Jyh-Ching Juang. Fast computation of achievable feedback performance in mixed sensitivity H_∞ design. *IEEE Transactions on Automatic Control*, 32(10):896–906, October 1987.

[22] F. M. Khan. *The Physics of Radiation Therapy*. Lippincott Williams & Wilkins, Baltimore, 3rd ed edition, 2003.

[23] Pramrod P. Khargonekar and Kemin Zhou. Weighted sensitivity minimization for delay systems. In *Proceedings of the 25th Conference on Decision and Control*, pages 1950–1952, Athens, Greece, December 1986. IEEE.

[24] Wilfred Wai-Fung Kwok. Automating radiotherapy: Parameterizations of sensor time delay compensators and the separation principle. Master's thesis, University of Waterloo, April 2006.

[25] Samantha Morris. *Radiotherapy Physics and Equipment*. Churchill Livingstone, London, 2001.

[26] Eitaku Nobuyama and Toshiyuki Kitamori. Spectrum assignment and parameterization of all stabilizing compensators for time-delay systems. In *Proceedings of the 29th Conference on Decision and Control*, pages 3629–3634, Honolulu, Hawaii, December 1990. IEEE.

[27] Charles L. Phillips and Jr H. Troy Nagle. *Digital Control System Analysis and Design*, page 337. Prentice Hall, Englewood Cliffs, NJ, 1984.

[28] María M. Seron, Julio H. Braslavsky, and Graham C. Goodwin. *Fundamental Limitations in Filtering and Control*. Communications and Control Engineering. Springer, London, 1997.

[29] Sigurd Skogestad and Ian Postlethwaite. *Multivariable Feedback Control: Analysis and Design*. Wiley, Chichester, UK, 1999.

[30] A. Tannenbaum. *Invariance and System Theory: Algebraic and Geometric Aspects*, volume 845 of *Lecture Notes Mathmatics*. Springer-Verlag, Berlin, 1980.

[31] unknown. http://static.sws.bfh.ch/diplom/t38/t38_01/Image74.gif, September 2007.

[32] M. Vidyasagar. *Control System Synthesis: A Factorization Approach*. MIT Press Series in Signal Processing, Optimization, and Control. MIT Press, Cambridge, MA, 1985.

[33] D. Youla, H. Jabr, and J. Bongiorno Jr. Modern wiener–hopf design of optimal controllers part II: The multivariable case. *IEEE Transactions on Automatic Control*, 21(3):319–338, 1976.

[34] D. Youla, J. Bongiorno Jr., and H. Jabr. Modern wiener–hopf design of optimal controllers part I: The single-input-output case. *IEEE Transactions on Automatic Control*, 21(1):3–13, 1976.

[35] George Zames and Bruce A. Francis. Feedback, minimax sensitivity, and optimal robustness. *IEEE Transactions on Automatic Control*, 28(5):585–601, May 1983.